2018

# EFFECT OF ETHANOL ON GASTROINTESTINAL TIGHT JUNCTIONS AND P-GLYCOPROTEIN EXPRESSION AND FUNCTIONALITY

Armin Sadighi
*University of Rhode Island*, arminsadighi@uri.edu

# EFFECT OF ETHANOL ON GASTROINTESTINAL TIGHT JUNCTIONS AND P-GLYCOPROTEIN EXPRESSION AND FUNCTIONALITY

BY

ARMIN SADIGHI

A DISSERTATION SUBMITTED IN PARTIAL FULFILLMENT OF THE

REQUIREMENTS FOR THE DEGREE OF

DOCTOR OF PHILOSOPHY

IN

BIOMEDICAL AND PHARMACEUTICAL SCIENCES

UNIVERSITY OF RHODE ISLAND

2018

DOCTOR OF PHILOSOPHY DISSERTATION

OF

ARMIN SADIGHI

APPROVED:

Dissertation Committee:

Major Professor: Fatemeh Akhlaghi

Ingrid Lofgren

Jie Shen

Noah Daniels

Nasser H. Zawia
DEAN OF THE GRADUATE SCHOOL

UNIVERSITY OF RHODE ISLAND

2018

## ABSTRACT

Alcoholism, alcohol abuse or alcohol use disorder (AUD) is considered as a major untreated epidemic health concerns in modern societies. According to the 2014 report of World Health Organization (WHO), alcoholism causes approximately 6% of all cases of death every year. It has been evident that chronic alcohol consumption leads to organ damage, and in some cases, it progresses to cirrhosis and carcinoma. Some pharmacotherapy strategies have been proposed during decades to treat AUD; however, the efficacy of these medications to reduce drinking or alcohol abstinence remained controversial. Naltrexon, acamprosate, desulfiram, and nalmefen have been approved by the US Food and Drug Administration (FDA) and the European Medicines Agency (EMEA) for alcohol abstinence. However, clinical studies show that the efficiency of these medications in AUD treatment is limited. As a result, finding a targetable biomarker in alcoholic patients to decrease alcohol craving and prevent organ damage remained as a major health challenge. According to the literatures, paracellular tight junction proteins are highly affected by ethanol (EtOH). In this work, the effect of EtOH on the expression of paracellular proteins as well as efflux transporters (mainly P-glycoprotein) was investigated. The effects of EtOH on paracellular route of drug permeation as well as P-glycoprotein-mediated drug efflux provide more insights onto how pharmacokinetic characteristics are impacted in alcoholic individuals. Understanding of the pharmacokinetic changes will lead to dose-adjustment for drugs that are administered to alcoholic patients. Moreover, finding novel biomarkers to treat different stages of alcoholism would be another beneficial outcome of this research.

Gastrointestinal (GI) tract is considered as the first organ to be affected by alcohol. The highest EtOH concentration reaches to GI tract right after each alcohol drink. Due to propensity of GI tract epithelium with the highest EtOH concentration entering the body, more harmful effects would be predicted in GI tract after alcohol ingestion. Hence, estimating the actual concentration of EtOH in GI lumen after each alcohol intake and subsequently other organs seems to be beneficial. To address this question, a full physiologically based pharmacokinetic (PBPK) model was developed for EtOH as described in Manuscript I (to be submitted to the *European Journal of Pharmaceutics and Biopharmaceutics*). This manuscript describes development of an advanced dissolution, absorption, and metabolism (ADAM) model integrated into the Simcyp Simulator® 15 for alcohol. In this work, three common alcoholic beverages including beer (325 mg/kg body weight), wine (300 mg/kg body weight), and whisky (400 mg/kg body weight) were selected to be investigated. After simulation of beverages ingestion, the concentration-time profile of EtOH in stomach and duodenum as well as plasma and peripheral tissues was predicted. According to the results, the highest EtOH concentration was observed in stomach right after beverage ingestion and the concentration significantly decline during a 3-hour period. Eventually after stomach, duodenal concentration was the highest. The theoretical concentrations of EtOH in our model were validated according to the experimentally reported results. Moreover, EtOH concentration-time profile in well- and poorly-perfused tissues was estimated. Results present that liver and muscle showed the highest and the lowest rate of EtOH absorption, respectively.

**Manuscript II** (to be submitted to *the Journal of Molecular Pharmaceutics*) outlines the effect of clinically relevant EtOH concentrations on the expression and functionality of P-glycoprotein (P-gp) in Caco-2 cell monolayer. EtOH did not show significant alteration in cell viability at concentrations found in GI tract. To investigate the EtOH effect on P-gp, expression of P-gp was induced by treating normal cells with vinblastine (10 nM). Immunofluorescent (IF) images of normal and P-gp induced Caco-2 showed that the abundance of P-gp decreased by increasing EtOH concentration and treatment time. Moreover, the effect of EtOH on the abundance of xenobiotic transporters in normal and P-gp induced Caco-2 cells was analyzed. Sequential Windowed data independent Acquisition of the Total High-resolution Mass Spectra (SWATH-MS) proteomics approach showed that the abundance of P-gp polypeptides was decreased after treatment of normal and P-gp induced Caco-2 cells with EtOH for 4 and 24 h. Moreover, Calcein-AM assay showed that by increasing concentration of EtOH to 25 mM, the efflux activity of P-gp was reduced in P-gp induced Caco-2 cells. Increasing EtOH concentration more than 25 mM did not show significant effect on P-gp functionality. Furthermore, EtOH effect on transport parameters of talinolol (Tal, a P-gp substrate) and PF-5190457 (PF-57), an alcohol craving treatment currently undergoing clinical trials) was investigated in the presence and absence of verapamil (P-gp inhibitor). According to the results, EtOH showed significant decrease in efflux ratio (ER) of Tal in Caco-2 cells treated with 50 mM EtOH for 24 h in the presence of verapamil (200 µM). However, EtOH did not show significant effect on ER of PF-57 in the presence or absence of verapamil.

**Manuscript III** (to be submitted to *Biochimica et Biophysica Acta (BBA) Biomembranes*) outlines the effect of clinically relevant EtOH concentrations on the organization of paracellular membrane proteins in Caco-2 cell monolayer. Neither EtOH, nor its metabolite, acetaldehyde (AA), showed significant alteration in cell viability at concentrations found in GI tract. Transepithelial electrical resistance (TEER) assay showed that the paracellular hyper permeability of Caco-2 cells induced by EtOH and AA was reversible. Fluorescent Lucifer yellow (LY) permeation showed that paracellular transport of LY was enhanced after treatment of Caco-2 cells with EtOH. Transmission electron microscopy (TEM) images of EtOH-treated Caco-2 cells showed the disintegration of membrane proteins including tight junctions (TJs), adherent junctions (AJs), and desmosomes (DS). Moreover, the Sequential Windowed data independent Acquisition of the Total High-resolution Mass Spectra (SWATH-MS) proteomics was used to analyze the EtOH effects on paracellular proteins. SWATH-MS showed that the abundance of TJs, AJs, and DS were diminished after treatment of Caco-2 cells with EtOH for 4 and 24 h.

**Manuscript IV** (to be submitted to the *Journal of Proteomics–clinical applications*) outlines the proteome of sigmoid colon obtained from human subjects using label-free quantification proteomics. The sigmoid colon of healthy human subjects was compared to alcoholic patients with and without liver disease. Moreover, the proteome of GI tract in chronic-binge rat model was investigated and compared to that in control rats. SWATH-MS proteomics exhibits as a prominent technique in quantitative analysis of proteins from limited biopsy samples. In this work, the proteome of human sigmoid colon biopsies as well as alcoholic rat GI tracts were

studied. Results show that the expression level of some proteins in sigmoidal colon samples of alcoholic patients was altered compared to the healthy subjects. Significant differences were observed in expression of proteins in AWLDLQ subjects compare to the HC. No significant difference was observed in the expression of any investigated protein in ALD patients. Moreover, the effect of chronic EtOH consumption on proteins of different parts of GI tracts was examined in rat models. Vimentin and desmin showed a significant induction in pCol of binge-chronic rat models compare to the control group. The power of SWATH-MS proteomics in analysis of clinical biopsies might be helpful in identification of biomarkers to cure different stages of alcoholism.

In summary, analyzing the proteome of Caco-2 cell monolayer treated by EtOH revealed alteration in efflux transporters (e.g., P-gp) as well as paracellular barrier proteins (i.e., TJs, AJs, and DS). Mainly, EtOH-treatment showed decrease in the expression level of paracellular barriers and efflux transporters. The proteomics evidence were confirmed with immunofluorescent assay, transmission electron microscopy (TEM) images, Calcein-AM assay, and transport behavior of talinolol (a P-gp probe). Furthermore, analyzing the proteome of binge-chronic rat models as well as human alcoholic patients with or without liver disease were accomplished. We anticipate that proteomic analyses of GI tract from alcoholic patients would be beneficial to explore protein biomarkers for early detection and treatment of alcohol-related diseases in liver and GI tract. In this way, the power of mass spectrometry proteomics (i.e., SWATH-MS) in analysis of clinical biopsies might be helpful in identification of novel biomarkers to cure different stages of alcoholism.

## ACKNOWLEDGMENTS

I take this opportunity to extend my sincere thanks and gratitude to all those who made this Ph.D. dissertation possible. First and foremost, I would like to thank my major professor Dr. Fatemeh Akhlaghi for giving me the opportunity to work in her laboratory and having the confidence in me. I am extremely indebted to her for the help, advice, encouragement and continuous support throughout my Ph.D. journey. Without her guidance and persistent support this dissertation would not have been possible. For everything you have done for me, Dr. Akhlaghi, I sincerely thank you.

I thank our collaborator, Dr. Suzanne M. De La Monte from Brown University (Providence, RI) for her advice through alcoholic treatment, transmission electron microscopy images, and providing alcoholic-treated rat gastrointestinal samples.

I would like to thank Dr. Ali Keshavarzian, from Rush University Medical Center (Chicago, IL) for generously providing human sigmoidoscopic samples.

In addition, I would like to thank Dr. Lorenzo Leggio that for being involved in grant number 1UH3TR000963 (PIs: Akhlaghi and Leggio) from the National Center for Advancing Translational Sciences (NCATS) and National Institutes of Health (NIH).

I would like to extend sincere thanks to each of my doctoral committee members, Dr. Ingrid Lofgren Dr. Jie Shen, and Dr. Noah Daniels.

I thank my parents Nahid and Mohammad Ali for their support, motivation and prayers and patience all through this time. Also, I cannot thank enough, my older brother, Shahin, and his wife Naghme who have been a continuous source of motivation and support throughout my life.

I thank all my present and past lab members for all the team work and support (Mwlod, Sravani, and Enoch). I would like to especially thank, Anitha Sravankumar, Rohitash Jamwal, and Benjamin Barlock for their valuable comment during my research, especially in proteomics section.

I would like to thank Kathy Hayes, Geralyn Perry, Kim Andrews and Dr. Al Bach for their help throughout these years. In addition, I would like to extend my sincere thanks to College of Pharmacy at URI for giving me the opportunity to pursue my graduate studies here.

## PREFACE

This dissertation was prepared according to the University of Rhode Island Thesis/Dissertation Process: From Proposal to Defense standards for Manuscript format. This dissertation consists of four manuscripts that have been combined to satisfy the requirements of the Department of Biomedical and Pharmaceutical Sciences, College of Pharmacy, University of Rhode Island. Moreover, two other manuscripts that were not part of Thesis/Dissertation are also included.

**MANUSCRIPT-I: Development of a Physiologically Based Pharmacokinetic Model for Prediction of Ethanol Concentration-Time Profile in Different Organs**

This manuscript has been prepared for submission as a research article to the *European Journal of Pharmaceutics and Biopharmaceutics.*

**MANUSCRIPT-II: The Effect of Alcohol on Expression and Functionality of P-Glycoprotein in Caco-2 cell Monolayer**

This manuscript has been prepared for submission as a research article to the Journal of *Molecular Pharmaceutics.*

**MANUSCRIPT-III: The Effect of Alcohol on Paracellular Barrier and Tight Junction Proteins in Caco-2 cell Monolayer**

This manuscript has been prepared for submission as a research article to the Journal of *Biochimica et Biophysica Acta – Biomembrane.*

**MANUSCRIPT-IV: SWATH-MS Proteomic Analysis of Gastrointestinal Tract in Alcoholic Rat Model and Human Subjects**

This manuscript has been prepared for submission as a research article to the Journal of *Proteomics - Clinical Applications.*

**TABLE OF CONTENTS**

**LIST OF TABLES**

**LIST OF FIGURES**

**MANUSCRIPT I**

This manuscript has been prepared for submission to the *"European Journal of Pharmaceutics and Biopharmaceutics"*

# Development of a Physiologically Based Pharmacokinetic Model for Prediction of Ethanol Concentration-Time Profile in Different Organs

Armin Sadighi[a], Lorenzo Leggio[b, c], Fatemeh Akhlaghi[a*]

[a]Clinical Pharmacokinetics Research Laboratory, Department of Biomedical and Pharmaceutical Sciences, College of Pharmacy, University of Rhode Island, Kingston, RI, USA

[b]Section on Clinical Psychoneuroendocrinology and Neuropsychopharmacology, Laboratory of Clinical and Translational Studies, National Institute on Alcohol Abuse and Alcoholism, Bethesda, MD, USA

[c]Center for Alcohol and Addiction Studies, Department of Behavioral and Social Sciences,
Brown University, Providence, RI 02903, USA

---

[*]**Corresponding author:** Fatemeh Akhlaghi; Clinical Pharmacokinetics Research Laboratory; University of Rhode Island; Office 495 A; 7 Greenhouse Road; Kingston; RI 02881, USA. **Tel:** (401) 874 9205; **Fax:** (401) 874 5787; **Email:** fatemeh@uri.edu

**Abstract**

A full physiologically based pharmacokinetic (PBPK) model was developed for ethanol (EtOH) using advanced dissolution, absorption, and metabolism (ADAM) model fully integrated into the Simcyp Simulator® 15 (Simcyp Ltd., Sheffield, UK). Three alcoholic beverages including beer (325 mg/kg body weight), wine (300 mg/kg body weight), and whisky (400 mg/kg body weight) were chosen to predict the concentration-time profile of EtOH in stomach and duodenum as well as plasma and peripheral tissues. Simcyp modeling overestimated the stomach EtOH concentrations compared to the observed values. However, increased intragastric fluid in fed-state resulted in predicting closer values to the observed data. The observed duodenal EtOH concentrations were overestimated. Higher entered EtOH from the stomach and the activity of EtOH metabolizing enzymes in stomach are reasons for EtOH overestimation in duodenum. Furthermore, the observed EtOH plasma concentration in both fasted and fed conditions were underestimated by the predicted values. Overestimation of oxidative metabolism of alcohol in our model as well as the ADH polymorphisms in the studied populations could be responsible for this variation. Finally, EtOH concentration-time profile in well- and poorly-perfused tissues was estimated. Providing the tissue-specific bioavailability parameters for EtOH is advantageous to estimate the drug-EtOH interactions in their site of action. Results present that liver and muscle showed the highest and lowest rate of EtOH absorption, respectively.

**Keywords:** Ethanol (EtOH), PBPK modeling, Simcyp® simulator, ADAM model, intragastric EtOH concentration, EtOH plasma concentration.

## Introduction

The effect of drinking alcohol on drug absorption and bioavailability has received considerable attention during recent years.[1-3] Ethanol (EtOH) alters the body exposure to the extended-release drug formulations through induction of dose dumping.[4-6] While, the increased release of the dosage incorporated in prolonged-release formulations has serious safety concerns, FDA has recommended to characterize the effect of alcohol on the release profile of drugs.[5] Apart from the effect of alcohol on drug release and solubility behaviors, many EtOH-drug interactions have been reported. [7, 8] For instance, analgesics [9], antidepressants [10], antibiotics [11], anticoagulants [12], and antidiabetics [13] have been proven to show adverse reactions in acute and chronic alcohol drinkers. Hence, the alcohol destination in human body could reveal its profound role in various metabolic pathways that affects the metabolism and disposition of drug substances.

When alcohol is absorbed, it undergoes two main oxidative and non-oxidative metabolic pathways. Those include **(i)** reversible oxidative conversion to acetaldehyde catalyzed by alcohol dehydrogenases (ADH1A, ADH1B*1, ADH1C*2, and ADH4) [14-16] and cytochrome P450 2E1 (CYP2E1) [17] in liver and intestine followed by irreversible oxidation to acetate and acetyl Co-A by aldehyde dehydrogenase 2 (ALDH2) [18], and acyl-coenzyme A synthetase short-chain family member 2 (ACSS2) [19]; **(ii)** EtOH involvement in sugars, amino and fatty acids through acetyl Co-A; **(iii)** oxidation via the tricarboxylic acid (TCA) cycle to $CO_2$; and **(iv)** non-oxidative conversion to fatty acid ethyl esters (FAEE) and phosphatidylethanols [20]. **Fig. 1** shows a schematic illustration of EtOH role in different metabolic pathways

occurring in human GI tract and liver (hepatocytes). In this scheme, EtOH oxidation to acetaldehyde and acetate (**Fig. 1a**), conversion of acetate to acetyl CoA (**Fig. 1b**), and acetyl CoA transformation to citrate and fatty acyl CoA (**Figs 1c** and **d**) have been shown.

The actual site and magnitude of EtOH first-pass metabolism in human remained controversial over the years. Some researches confirmed that a significant fraction of administered EtOH is cleared by first-pass metabolism primarily in gastric mucosa. Julkunen *et al*., [21], has shown that significant EtOH first-pass metabolism in rat is taking place in GI tract, mainly due to the presence of ADH4 in stomach. Meanwhile, other works suggested that approximately entire EtOH first-pass metabolism occurs in liver and gastric metabolism accounts for a small fraction of total EtOH clearance.[22]

While determination of EtOH concentration in different organs is not easy to be experimentally measured, development of an *in silico* model to predict the concentration-time profile of EtOH in human tissues seems to be beneficial. One of the most helpful theoretical approaches that widely used in drug discovery and development is physiologically based pharmacokinetic (PBPK) modeling and simulation methodology.[23] The concept of PBPK modeling was first introduced by Teorell [24] in 1937 and developed rapidly during recent years due to emerging commercially available softwares (Simcyp®, GastroPlus™, and PK-Sim®) [25] and ease of access to preclinical data.[26] Nowadays, a number of drug labels affirm that PBPK modeling was used to conduct clinical studies. Therefore, PBPK modeling is considered as a powerful tool in prediction of clinical data via evaluation of intrinsic (population properties, and genetics) and extrinsic (drug-drug interaction) factors. It

combines the physicochemical data for a compound with the predefined physiological and biological properties of a specific population to obtain a mechanistic approach for that compound in the biological system.[27]

In the current study, a full PBPK model was built in Simcyp Simulator® 15 (Simcyp Ltd., Sheffield, UK) to predict the concentration-time profile of EtOH in human stomach and duodenum. Subsequently, the predicted values for EtOH concentrations in gastrointestinal (GI) tract and plasma in fasted- and fed-state were validated according to the corresponded observed values reported in literature. Moreover, the concentration-time profile of EtOH was predicted in liver, gut, brain, kidney, pancreas, spleen, skin, heart, muscle, and lung after ingestion of three common alcoholic beverages (beer, wine, and whisky). Finally, the bioavailability parameters of EtOH including area under the plasma concentration-time curve (AUC), maximum concentration observed ($C_{max}$), and time to achieve $C_{max}$ ($T_{max}$) were predicted and discussed in various tissues in fasted- and fed-states.

## 2. Methods and modeling approaches

### *2.1. EtOH PBPK model*

A whole-body PBPK model was constructed according to the advanced dissolution, absorption, and metabolism (ADAM) model integrated in Simcyp® (**Fig. 2)**. In this model, GI tract is divided into nine parts including stomach, duodenum, jejunum, ileum, and colon comprising of 1, 1, 2, 4, and 1 segments, respectively. This model shows the body as composed of 13 tissue compartments and 2 blood compartments (arterial and venous pools). The methodology and structure of the

Simcyp® population-based PBPK modeling was described in detail, previously [28-30]. Anatomical and physiological parameters were modified according to the published literatures when it was essential (**Table 1**).

The simulation of fasted-and fed-state gastrointestinal concentration of EtOH after ingestion of three common alcoholic beverages was implemented onto a PBPK modeling platform (Simcyp® Simulator) and was validated based on the *in vivo* data obtained from literature. Physicochemical properties, physiological/population details, and trial design used for EtOH modeling have been summarized in **Table 1**. In all trial designs standard adult body weight was set as 70 kg.[31] Three common alcoholic beverages, including beer (325 mg EtOH/kg body weight, 500 mL), wine (300 mg EtOH/kg body weight, 200 mL), and whisky (400 mg EtOH/kg body weight, 80 mL) were modeled in fasted- and fed-state using healthy human adult population. In the modeling of fed-state, a volume of 250 mL of liquid meal was applied and initial volume of stomach fluid was modified accordingly in population details. Furthermore, other model input parameters such as, mean gastric emptying time, initial volume of stomach fluid, volume of intake alcohol, and dosage were retrieved from the literature and used for model development (**Table 1**).

*2.2. EtOH absorption, distribution, and elimination*

After ingestion of alcoholic beverages orally, EtOH is absorbed rapidly from GI tract via passive diffusion.[32] The EtOH absorption starts from mouth and continues along the GI tract. About 15% of the initial EtOH dose is absorbed into stomach in fasted state, while only 30% of alcohol is passed to the GI tract once EtOH is

administered with food. [22] According to the ADAM model EtOH oral absorption from luminal fluid to enterocytes was incorporated into unstirred boundary layer (UBL) (Simcyp® manual). A permeability-limited membrane (basolateral side of enterocytes), which separates the enterocytes from intestinal interstitial fluid (ISF), is considered as the second step. Finally, a lymphatic route of absorption facilitates the EtOH entering systemic circulation.

Although the predominant site of EtOH metabolism is liver, the presence of ADH isozymes in mucosa of stomach, duodenum and jejunum begins the alcohol metabolism before liver.[33] The presence of ADH4 in stomach and upper sides of GI tract are proposed to be responsible for first pass metabolism of EtOH before reaching to liver.[32] Less than 2% of the ingested dose is metabolizing by gastric ADH4.[22] While, almost the whole EtOH elimination is taking place in liver, less than 10% of alcohol is excreted from lung, kidney, and skin. The breath alcohol clearance is 0.16 L/h, renal clearance is 0.06 L/h, and sweat clearance is 0.02 L/h.[34] Additional sites of EtOH clearance that were reported in the previously published literatures were applied in this modeling to simulate more realistic pharmacokinetic behavior.

*2.3. The genetics of alcohol metabolism by ADHs*

The list of the involved ADHs in EtOH metabolism and their corresponding Michaelis-Menten kinetic parameters has been shown in **Table 2**. According to the table, there are several forms of ADHs named from ADH1 to ADH7. Gene polymorphism exists for some of these enzymes, while the well-known of which identified for ADH1. Three types of ADH1 that occurred in human populations are

ADH1A, ADH1B, and ADH1C.[14] Among them, the most important polymorphisms have been identified for gene ADH1B, including ADH1B*1, ADH1B*2, and ADH1B*3.[14, 35] ADH1B*2 is very common in East Asian populations, relatively common in Middle East people, and very rare in European and African populations. Researches show that people who carry ADH1B*2, and ADH1B*3 alleles are less prone to be alcoholic. It means that these alleles have protective function against the alcoholism in Caucasian and Asian populations who carry those alleles. ADH1B*3 polymorphism is less in overall populations but it is prevalent in African and African-American populations, meanwhile this allele is rare elsewhere.[36-38] While, EtOH concentration in Caucasian human healthy volunteers was simulated in this study, the kinetic parameters for ADH1A, ADH1B*1, ADH1C*2, and ADH4 were used. In addition, hepatic CYP2E1 was also considered for the model development.

*2.4. Simulation of Ethanol concentration in stomach, duodenum, plasma, and other tissues*

The EtOH concentration in stomach and duodenum after ingestion of three common alcoholic beverages was predicted and compared to the observed available data. Rubbens *et al.*, have reported the EtOH concentration in stomach and duodenum of human healthy volunteers using head space gas chromatography in fasted- [39]and fed-state [40], previously. To extract the numerical data from the published literature, plot digitizer software (http://arohatgi.info/WebPlotDigitizer) was used. Moreover, the plasma alcohol concentration-time profile was predicted and compared to the observed data reported by Levitt *et al.*[22] Moreover, the concentration-time profile of

EtOH in GI tract, liver, brain, kidney, pancreas, spleen, skin, heart, muscle, and lung after ingestion of three common alcoholic beverages (beer, wine, and whisky) were simulated.

## 3. Results

### *3.1. EtOH concentration-time profile in stomach and duodenum*

**Fig. 3** and **4** show the EtOH concentration-time profiles in stomach and duodenum of healthy human volunteers after drinking alcoholic beverages in fasted- and fed-state. In these plots, Simcyp® predictions versus observed data reported by Rubbens and co-workers[39, 40] are illustrated together. **Fig. 3a)** shows the observed and predicted EtOH concentration-time profiles in stomach after beer (500 mL) intake. Based on the results, no significant difference was observed in experimental and theoretical values for stomach EtOH concentration neither in fasted- nor in fed-state (**Fig. 3a and b**). **Fig. 3c** shows approximately two times overestimation of $C_{max}$ after ingestion of wine (200 mL) in predicted EtOH concentration compare to the observed values in fasted-state stomach. After 50 min, predicted and observed EtOH concentrations were aligned with each other. According to the **Fig. 3d**, predicted and observed EtOH concentration-time profiles in fed-state found to be in good agreement with each other. **Fig. 3e** illustrates EtOH profile after ingestion of whisky (80 mL) in fasted-state. The initial predicted EtOH concentration was two times higher than that in the observed experiments; however, after 30 min they became aligned. **Fig. 3f** indicates EtOH profile after consumption of the same amount of whisky in fed-state.

Results show that there is no significant difference in the predicted versus observed profiles of EtOH in stomach.

The EtOH concentration-time profile in duodenum of healthy human volunteers in fasted- (**Fig. 4a**) and fed-state (**Fig. 4b**) after beer intake are shown. According to **Fig. 4a**, the predicted EtOH concentration values were overestimated compared to the observed values. However, the observed and predicted concentrations show similar trends after 40 min of drink. Based on the illustrated graphs for the predicted and observed EtOH concentrations in **Fig. 4b**, the predicted EtOH concentration at the maximum value was ~ 26% overestimated compare to the observed value. **Fig. 4c** and **d** show the EtOH concentration-time profile in duodenum after wine intake in fasted- and fed-state, respectively. The predicted $C_{max}$ of EtOH in fasted- and fed-state is approximately two times higher than that in the observed graphs. **Fig. 4e** shows the overestimation of EtOH concentration in fasted-state after ingestion of whisky. According to the graphs, the predicted and observed results were the same after 30 min of drink. **Fig. 4f** illustrates that predicted EtOH concentration at $C_{max}$ is two times greater than that in the observed plot, while the difference between predicted and observed values for EtOH concentration decreased by the time.

*3.2. Key bioavailability parameters of EtOH in stomach and duodenum*

**Table 3** shows key bioavailability parameters of EtOH in fasted-and fed-state after intake of alcoholic beverages. It summarizes $C_{max}$, $T_{max}$, and AUC of EtOH after drinking alcoholic beverages.

Results for beer show that $C_{max}$ of EtOH in fasted-state stomach is higher than that in fed-state. Similar trend was observed in duodenal EtOH $C_{max}$ in fasted- versus fed-state. While, duodenal $C_{max}$ of EtOH was decreased from 29.76 g/L in fasted-state to 16.67 g/L in fed-state, $T_{max}$ was roughly doubled (**Table 3**). According to the obtained data for $AUC_{0\text{-}180}$, there is a significant increase in $AUC_{0\text{-}180}$ of EtOH in fed-state stomach compare to fasted-state. However, the increased $AUC_{0\text{-}180}$ in fed-state duodenum was not as much. In the case of wine, $C_{max}$ of EtOH in fed-state stomach was lower than that in fasted-state. Likewise, duodenal EtOH $C_{max}$ in fed-state was less than that in fasted-state. Duodenal EtOH $T_{max}$ in fed-state was more than two times greater than that in fasted-state (**Table 3**). $AUC_{0\text{-}180}$ results for wine show increased values in fed-state of stomach and duodenum compare to the same $AUC_{0\text{-}180}$ values in fasted-state. According to **Table 3**, $C_{max}$ of EtOH in fasted-state stomach after ingestion of whisky was 232.62 g/L, which is three times greater than that in fed-state stomach. Similarly, higher duodenal $C_{max}$ was observed in fasted-state than that in fed-state. $T_{max}$ of EtOH after whisky ingestion was comparable with the $T_{max}$ obtained for wine in duodenal fasted- and fed-state. Interestingly, $AUC_{0\text{-}180}$ of EtOH did not show any significant alteration in stomach and duodenum from fasted- to fed-state.

*3.3. EtOH fraction dose absorbed and metabolized in GI tract*

**Fig. 5** shows the EtOH fraction dose absorbed ($F_{abs}$) and fraction dose metabolized ($F_{met}$) after ingestion of different alcoholic beverages. **Fig. 5a** and **b** illustrate $F_{abs}$ and $F_{met}$ of EtOH after beer intake. No significant difference in EtOH

$F_{abs}$ and $F_{met}$ in different parts of GI tract was detected between fasted- and fed-state. Similar pattern was observed in EtOH $F_{abs}$ and $F_{met}$ following wine (**Fig. 5c** and **d**) and whisky (**Fig. 5e** and **f**) administration. In all depicted graphs, the highest $F_{abs}$ and $F_{met}$ were corresponded to the upper GI tract sides which decreased by moving toward the lower GI tract areas.

*3.4. EtOH plasma concentration-time profile*

**Fig. 6** shows Simcyp® predicted plasma EtOH concentration-time profile after intake of beer, wine and whisky in fasted- **(a)** and fed-state **(b)**. In order to validate the predicted EtOH concentration-time profiles, the experimentally reported values for EtOH concentration, which was administered orally (150 mg/kg body weight) in fasted- and fed-state [22], were also illustrated. **Fig. 6a** shows the predicted EtOH profile in plasma after ingestion of three different alcoholic beverages as long as the observed values reported by Levitt *et al* [22] for plasma EtOH plasma concentration in fasted-state. **Fig. 6a** shows that the observed EtOH $C_{max}$ in plasma was 290.3 mg/L, while the predicted EtOH plasma $C_{max}$ was 191.0, 117.0, and 97.5 mg/L after administration of whisky, beer, and wine in fasted-state, respectively.

According to the **Fig. 6a**, the predicted EtOH $C_{max}$ after ingestion of whisky was 34% underestimated the observed EtOH plasma concentration in fasted-state. After 50 min of alcohol administration, the predicted and observed EtOH concentration values more aligned with each other. (**Fig. 6b**) shows that the highest predicted EtOH concentration after ingestion of whisky was ~ 60% underestimated the observed plasma EtOH $C_{max}$.

**Table 4** summarizes the pharmacokinetic parameters of EtOH in plasma obtained from Simcyp® simulation in fasted- and fed-state. According to **Table 4**, $T_{max}$ for EtOH was between 23.56 min for wine in fasted-state to 37.82 min for whisky in fed-state. For all the alcoholic drinks, the obtained $AUC_{0-\infty}$ in fed-states was lower than that in fasted-state. The lowest $AUC_{0-\infty}$ was 37.46 mg·h/L for fed-state wine and the highest was 201.83 mg·h/L acquired for the fasted-state whisky.

*3.5. EtOH bioavailability parameters in well-and poor- perfused organs*

**Table 5** shows the $C_{max}$, $t_{max}$, and AUC achieved for EtOH in different organs of healthy human Caucasian population after ingestion of alcoholic beverages. In this table, the EtOH bioavailability parameters were obtained using the Simcyp® model for well-perfused organs (e.g., gut, liver, lung, heart, and kidney) and poor-perfused tissues (e.g., skin, muscle, and brain). Based on the results, the highest and lowest EtOH $C_{max}$ were acquired for liver and muscle tissues, respectively.

**Fig. 7** shows the concentration-time profile of EtOH in liver-gut-brain axis after ingestion of three alcoholic beverages. **Fig. 7a** and **b)** show EtOH concentration-time profile in liver for fast- and fed-state, respectively. Higher $C_{max}$ for EtOH in fasted-state was mentioned compare to that in fed-state. Fed-state EtOH $T_{max}$ was later than that in fasted-state. However, AUC drastically decreased in the case of fed-state. EtOH concentration-time profile in gut for fast- (**Fig. 7c**) and fed-state (**Fig. 7d**) conditions are illustrated. Higher $C_{max}$ for EtOH in fasted-state was observed compare to that in fed-state. According to the graphs, the elimination phase of EtOH in fed-state was slower than that in fasted-state. AUC of EtOH in gut tissue decreased in fed-

state compare to the fasted-state. $C_{max}$, $T_{max}$, and AUC of EtOH in brain were depicted in fasted-(**Fig. 7e**) and fed-state (**Fig. 7f**). EtOH concentration-time profile in brain found to be close to the profile presented for gut tissue. As indicated in **Fig. 7e** and **f**, brains EtOH $C_{max}$, $T_{max}$, and AUC in fasted-state were higher than that in fed-state.

**4. Discussion**

Physiologic properties of human GI tract greatly affect the intragastric EtOH concentration. The observed mean EtOH concentrations were approximately two times overestimated by the predicted gastric EtOH concentration. However, the difference between predicted and observed concentration values became smaller in fed-state compared to the fasted condition. The underestimation of residual gastric volume could be responsible for overestimation of EtOH concentration immediately after drinking in fasted-state. Meanwhile, according to the fed-state results, the difference between predicted and observed profiles decreased. The residual gastric fluid, the volume of liquid meal (fed-state), the gastric emptying time, and gastric transit time are considered as effective parameters in determining the gastric EtOH concentration-time profile. In the presence of meal in fed-state, the gastric fluid volume will be increased, which results in more EtOH dilution and low gastric concentration. Lower EtOH concentrations in fed-state compare to the fasted-state profiles was illustrated in predicted EtOH values. Moreover, it has been found that gastric emptying time in fed-state is longer than that in fasted-state. That could be the reason for why higher EtOH concentration in stomach (fed-state) was observed compare to that in fasted-state. Similarly, the delayed gastric emptying time results in

delayed duodenal EtOH concentration drop in fed-state compare to that in fasted-state. The delayed gastric emptying time, elongated EtOH residency in GI tract, and higher AUC for gastric EtOH in fed-state were explored experimentally by Rubbens *et al.*, [39, 40] using head space gas chromatography. The $C_{max}$ for duodenal EtOH concentration was overestimated compared to the observed concentrations. Higher gastric EtOH concentration enters to the duodenum seems to be responsible for the corresponding higher EtOH in intestine. Moreover, the catalytic activity of gastric CYP2E1 and ADH4 could be a reason for why observed EtOH concentration was lower than predicted values.

The range of EtOH plasma $C_{max}$ previously reported in literatures varies from 108.41 mg/L after oral administration of EtOH (150 mg/kg body weight) [22] in fed-state to 774 mg/L followed by vodka/tonic ingestion (500 mg/kg body weight) [41] in fasted-state. In addition, various $T_{max}$ values were reported in the published articles. The lowest $T_{max}$ was achieved by Levitt et al., [22], which was 8.72 min, while the highest $T_{max}$ (62 ± 23 min) was observed by Mitchell *et al.*, [41] after beer intake. The extensive gene polymorphism found in ADHs and different experimental designs are considered as main reasons for the variation in observed plasma EtOH profiles. In our study, the observed plasma $C_{max}$ was underestimated by the predicted value in fasted- and fed-state. One probable reason could be the overestimation of oxidative metabolism of alcohol in our model. Particularly, the abundance of ADH polymorphisms with higher $K_m$ values in Causation population might be a reason for higher observed EtOH concentration in experimental studies.

The present model provided the possibility to prediction EtOH concentration-time profile in organ and tissues. Among all organ and tissues, liver showed the highest $C_{max}$ and the lowest $T_{max}$ and AUC. That means higher rate and lower extent of EtOH absorption into the liver compare to the other organs. A probable justification for these results could be this fact that liver is one of the well-perfused organs and it is the main organ for EtOH metabolism. Conversely, muscle showed the lowest $C_{max}$ and highest $T_{max}$. The reason is that muscle is one of the poor-perfused organs. The predicted EtOH concentration profile in the liver-gut-brain axis illustrated the significant decrease in EtOH concentrations in fed-state compare to the fasted condition. The lower concentration of EtOH in fed-state tissues concordant with the reduced plasma concentration of EtOH after food intake.

**5. Conclusion**

In the present study, a full PBPK model was developed for EtOH using ADAM oral absorption model integrated in Simcyp Simulator®. Three alcoholic beverages including beer (325 mg/kg body weight), wine (300 mg/kg body weight), and whisky (400 mg/kg body weight) were selected to simulate gastric, duodenal, plasma, and tissue EtOH concentration-time profiles in fasted- and fed-state. Simcyp modeling overestimated stomach EtOH $C_{max}$ compared to the observed values in fasted-state. However, increased intragastric fluid in fed-state resulted in predicting closer values to the observed data. The observed duodenal EtOH concentrations were overestimated in both fasted- and fed-state. Higher entered EtOH from stomach and the activity of EtOH metabolizing enzymes in stomach are reasons for EtOH overestimation in

duodenum. Furthermore, the observed EtOH plasma concentration in both fasted and fed conditions were underestimated by the predicted values. Overestimation of oxidative metabolism of alcohol in our model as well as the ADH polymorphisms in the studied populations could be responsible for this variation. Finally, EtOH concentration-time profile in well- and poorly-perfused tissues was estimated. Liver and muscle showed the higher and lower rate of EtOH absorption, respectively.

**Acknowledgement**

This work was supported by grant number 1UH3TR000963 (PIs: Akhlaghi and Leggio) from the National Center for Advancing Translational Sciences (NCATS), National Institutes of Health (NIH).

**Table I- 1.** Physicochemical properties, physiological/population details, and trial design for simulating the fasted and fed EtOH PBPK modeling in Simcyp®

| Input data to Simcyp® simulator | Fed | Fasted | Reference |
|---|---|---|---|
| **Physicochemical properties** | | | |
| Molecular weight (g/mol) | 46.68 | | |
| Log $P_{O:W}$ | -0.35 | | |
| Compound type | Neutral | | |
| Blood/plasma binding ratio | 0.89 | | |
| $K_D$ for HSA (µM) | 1000 | | |
| Absorption model | ADAM[a] | | |
| $P_{app}$ rat intestinal tissue ( $\times 10^{-6}$ cm/S) | 56.7 ± 14.8 | | [40] |
| Polar surface area (Å$^2$) | 20.23 | | |
| Vss (L/Kg) | 0.53 | | [34] |
| Elimination | Enzyme kinetic (Table I-2) | | |
| **physiological/population details** | | | |
| Mean gastric emptying time (h) | 1.2 | 0.21 | [42, 43] |
| Initial volume of stomach fluid (mL) | 250 | 35 | [40, 43] |
| Weibull distribution of transit time | 2.92 (α) and 4.04 (β) | | Simcyp |
| Mean small intestinal transit time (h) | 3.33 | | Simcyp |
| Mean colon transit time (h) | 12 | | Simcyp |
| **Trial design and dosing regimen** | | | |
| Population | Human healthy volunteer | | |
| No. of trials | 5 | | |
| No. of subjects in trial | 5 | | |
| Minimum age (years) | 20 | | |
| Maximum age (years) | 50 | | |
| Proportion of females | 0.5 | | |
| Standard adult body weight (kg) | 70 | | [31] |
| Fluid intake with dose (mL) | 500 (beer), 200 (wine), 80 (whisky) | | [39, 40] |
| Single dose (mg/kg body weight) | 325 (beer), 300 (wine), 400 (whisky) | | [39, 40] |
| Proportion of dose inhaled (%) | 15 | | [22] |

[a]ADAM: advanced dissolution absorption and metabolism, Log$P_{O:W}$ (octanol:water partition coefficient), α and β are scale and shape parameters in Weibull distribution, respectively. $P_{app}$: apparent permeability, $K_D$: dissociation constant of the EtOH-protein complex, HAS: human serum albumin.

**Table I- 2.** Michaelis-Menten kinetic parameters for the involved enzymes in EtOH oxidation

| Enzyme | $K_m$ (mM) | $V_{max}$ ($min^{-1}$) | Tissue distribution | Reference |
|---|---|---|---|---|
| ADH1A | 4 | 30 | L | 14-16 |
| ADH1B*1 | 0.05 | 4 | L | 14-16, 44 |
| ADH1B*2 | 0.9 | 350 | L | 14, 16 |
| ADH1B*3 | 40 | 300 | L | 14, 16 |
| ADH1C*1 | 1 | 90 | L, S, D, J | 14, 16 |
| ADH1C*2 | 0.6, 0.05 | 40 | L, S, D, J | 14, 16 |
| ADH4 | 30 | 20 | L, S | 14, 16 |
| ADH5 | 1000 | 100 | K | |
| ADH6 | | – | L, S | |
| ADH7 | 30 | 1800 | S, E | 14, 16 |
| CYP2E1[a] | 10 | 23 | L | 14, 16 |

**Abbreviations:** $K_m$ **(**Michaelis-Menten constant), $V_{max}$ (maximum rate of enzymatic reaction at saturating EtOH concentration), ADH (alcohol dehydrogenase), L (Liver), S (stomach), D (duodenum), J (jejunum), K (kidney), E (esophagus), and CYP2E1 (cytochrome P450 2E1).

[a] CYP2E1 is upregulated in upper GI tract in chronic alcohol users. [17, 45, 46]

**Table I- 3.** Key bioavailability parameters ($C_{max}$, $T_{max}$, and AUC) of EtOH in stomach and duodenum simulated by Simcyp®

| **Alcoholic beverage** | **EtOH dose (mg/kg body weight)** | **Fasted-state** | | **Fed-state** | |
|---|---|---|---|---|---|
| **Beer** | | **Stomach** | **Duodenum** | **Stomach** | **Duodenum** |
| $C_{max}$ (g/L) | 325 | 41.99 | 29.76 | 27.69 | 16.67 |
| $T_{max}$ (min) | | 0 | 5.42 | 0 | 10.90 |
| AUC $_{0\text{-}180}$(g·min/L) | | 1764.15 | 1067.86 | 3250.34 | 1711.30 |
| **Wine** | | | | | |
| $C_{max}$ (g/L) | 300 | 87.02 | 51.32 | 41.51 | 21.86 |
| $T_{max}$ (min) | | 0 | 5.44 | 0 | 12.70 |
| AUC $_{0\text{-}180}$ (g·min/L) | | 2873.35 | 1648.41 | 4270.11 | 2087.01 |
| **Whisky** | | | | | |
| $C_{max}$ (g/L) | 400 | 232.62 | 108.22 | 74.80 | 35.47 |
| $T_{max}$ (min) | | 0 | 7.21 | 0 | 12.71 |
| AUC $_{0\text{-}180}$ (g·min/L) | | 6053.86 | 3051.01 | 6985.33 | 3230.38 |

**Abbreviation:** $C_{max}$ (the highest concentration), $T_{max}$ (time needed to reach $C_{max}$), and AUC (area under the concentration-time curve. AUC was calculated according to trapezoidal rule using Excel® software.

**Table I- 4.** Key bioavailability parameters ($C_{max}$, $T_{max}$, and AUC) of EtOH in plasma simulated by Simcyp®

| Alcoholic beverage | EtOH dose (mg/kg body weight) | Fasted-state | Fed-state |
|---|---|---|---|
| **Beer** | | | |
| $C_{max}$ (mg/L) | 325 | 123.24 | 27.05 |
| $T_{max}$ (min) | | 25.24 | 34.37 |
| AUC $_{0-\infty}$(mg·h/L) | | 123.31 | 43.83 |
| **Wine** | | | |
| $C_{max}$ (mg/L) | 300 | 101.88 | 22.64 |
| $T_{max}$ (min) | | 23.56 | 34.25 |
| AUC $_{0-\infty}$ (mg·h/L) | | 102.06 | 37.46 |
| **Whisky** | | | |
| $C_{max}$ (mg/L) | 400 | 197.60 | 43.86 |
| $T_{max}$ (min) | | 25.28 | 37.82 |
| AUC $_{0-\infty}$ (mg·h/L) | | 201.83 | 68.48 |

**Abbreviation:** $C_{max}$ (the highest concentration), $T_{max}$ (time needed to reach $C_{max}$), and AUC (area under the concentration-time curve. AUC was calculated according to trapezoidal rule using Excel® software.

**Table I- 5.** The kinetic parameters ($C_{max}$, $t_{max}$, and AUC) of EtOH simulated in different organs using Simcyp®.

| Alcoholic beverage | EtOH dose (mg/kg body weight) | Fasted-/fed-state | Mean pharmacokinetic parameters | Tissues | | | | | | | | | |
|---|---|---|---|---|---|---|---|---|---|---|---|---|---|
| | | | | Liver | Gut | Brain | Kidney | Pancreas | Spleen | Skin | Heart | Muscle | Lung |
| Beer | 325 | Fasted | $C_{max}$ | 149.74 | 97.75 | 108.05 | 104.97 | 104.59 | 105.41 | 84.02 | 100.68 | 62.01 | 106.61 |
| | | | $t_{max}$ | 0.33 | 0.42 | 0.45 | 0.42 | 0.45 | 0.42 | 0.54 | 0.42 | 0.75 | 0.42 |
| | | | AUC | 73.95 | 100.95 | 112.55 | 107.95 | 108.55 | 108.87 | 99.07 | 104.11 | 103.75 | 109.71 |
| | | Fed | $C_{max}$ | 19.09 | 24.09 | 26.74 | 25.78 | 25.84 | 26.98 | 22.45 | 24.82 | 18.61 | 26.23 |
| | | | $t_{max}$ | 0.51 | 0.57 | 0.6 | 0.54 | 0.57 | 0.57 | 0.69 | 0.57 | 0.96 | 0.54 |
| | | | AUC | 17.47 | 40.19 | 44.85 | 43.01 | 43.26 | 43.38 | 39.45 | 41.49 | 41.19 | 43.67 |
| Wine | 300 | Fasted | $C_{max}$ | 123.28 | 81.47 | 89.77 | 87.33 | 86.97 | 87.81 | 70.48 | 83.89 | 51.28 | 88.79 |
| | | | $t_{max}$ | 0.3 | 0.42 | 0.45 | 0.42 | 0.42 | 0.42 | 0.54 | 0.42 | 0.75 | 0.39 |
| | | | AUC | 59.04 | 84.33 | 94.02 | 90.17 | 90.68 | 90.95 | 82.74 | 86.97 | 86.61 | 91.63 |
| | | Fed | $C_{max}$ | 15.24 | 20.57 | 22.83 | 22.01 | 22.06 | 22.17 | 19.15 | 21.18 | 15.84 | 22.37 |
| | | | $t_{max}$ | 0.51 | 0.54 | 0.57 | 0.54 | 0.57 | 0.54 | 0.69 | 0.54 | 0.96 | 0.54 |
| | | | AUC | 13.95 | 34.84 | 38.88 | 37.28 | 37.51 | 37.61 | 34.21 | 35.97 | 35.71 | 37.86 |
| Whisky | 400 | Fasted | $C_{max}$ | 241.86 | 154.84 | 171.22 | 165.97 | 165.61 | 166.91 | 136.27 | 159.48 | 100.86 | 168.75 |
| | | | $t_{max}$ | 0.33 | 0.45 | 0.48 | 0.45 | 0.48 | 0.45 | 0.57 | 0.45 | 0.81 | 0.42 |
| | | | AUC | 130.33 | 161.97 | 180.58 | 173.19 | 174.17 | 174.68 | 158.99 | 167.05 | 166.56 | 176.04 |
| | | Fed | $C_{max}$ | 33.95 | 37.33 | 41.45 | 39.93 | 40.04 | 40.24 | 34.88 | 38.45 | 29.16 | 40.61 |
| | | | $t_{max}$ | 0.57 | 0.63 | 0.66 | 0.63 | 0.63 | 0.63 | 0.75 | 0.63 | 1.02 | 0.6 |
| | | | AUC | 32.16 | 60.45 | 67.41 | 64.64 | 65.01 | 65.21 | 59.31 | 62.36 | 61.96 | 65.65 |

Maximum concentration of EtOH ($C_{max}$, mg/L), time to reach $C_{max}$ ($t_{max}$, h), and area under the concentration-time curve (AUC, mg·h/L) after ingestion of three common alcoholic beverages (beer 500 mL, wine 200 mL, and whisky 80 mL) during 6 h. *$C_{max}$ of EtOH in liver after intake of alcoholic beverages in fasted-state was higher than the other organs. However, it was not statistically significant compared to all other organs (data were not shown).

**Figure. I-1**

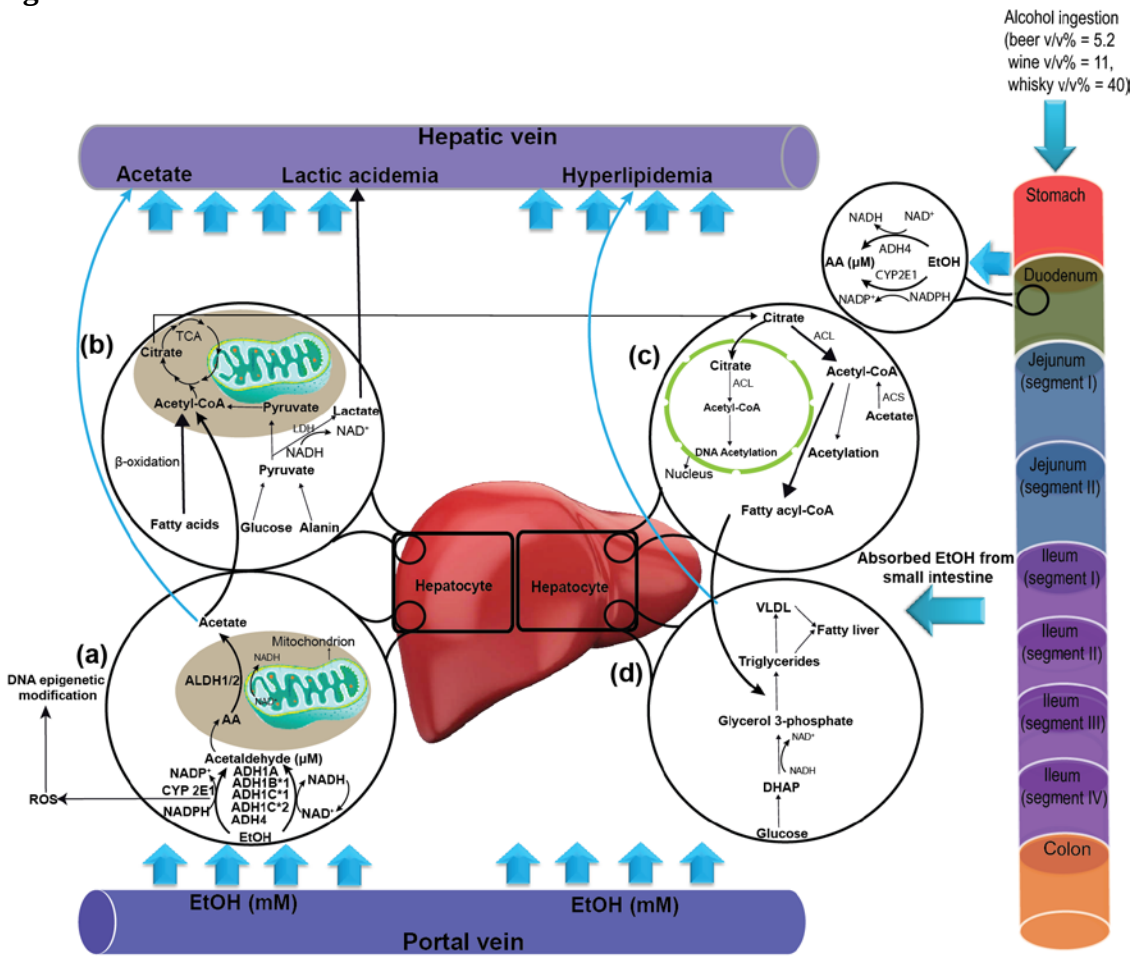


**Figure I- 1.** Schematic illustration of ethanol (EtOH) destination in human body after ingestion of alcoholic beverages.

**a)** EtOH is oxidized to acetaldehyde in hepatocytes through alcohol dehydrogenases (ADH1A, ADH1B*1, ADH1C*1, ADH1C*2, and ADH4) and cytochrome P450 2E1 (CYP2E1). Reactive oxygen species (ROS) are generated due to the interference of EtOH with electron transport complexes in mitochondrial membrane. Acetaldehyde is converted to acetate by aldehyde dehydrogenases (ALDH1/2). **b)** Acetate is metabolized to acetyl CoA, which considered as an important metabolic intermediate of tricarboxylic acid (TCA) and β-oxidation of fatty acids. **c)** Citrate could be converted to acetyl CoA by ATP citrate lyase (ACL). The generated acetyl CoA may result in DNA acetylating or involve in fatty acyl CoA production. **d)** Fatty acyl CoA is associated with lipogenesis reactions, which results in triglycerides, very low-density lipoproteins (VLDL) and finally alcoholic fatty liver in chronic alcoholic patients. The excess amount of EtOH in chronic alcoholic patients may result in elevated acetate in blood, lactic acidemia, and hyperlipidemia.

**Figure I-2**

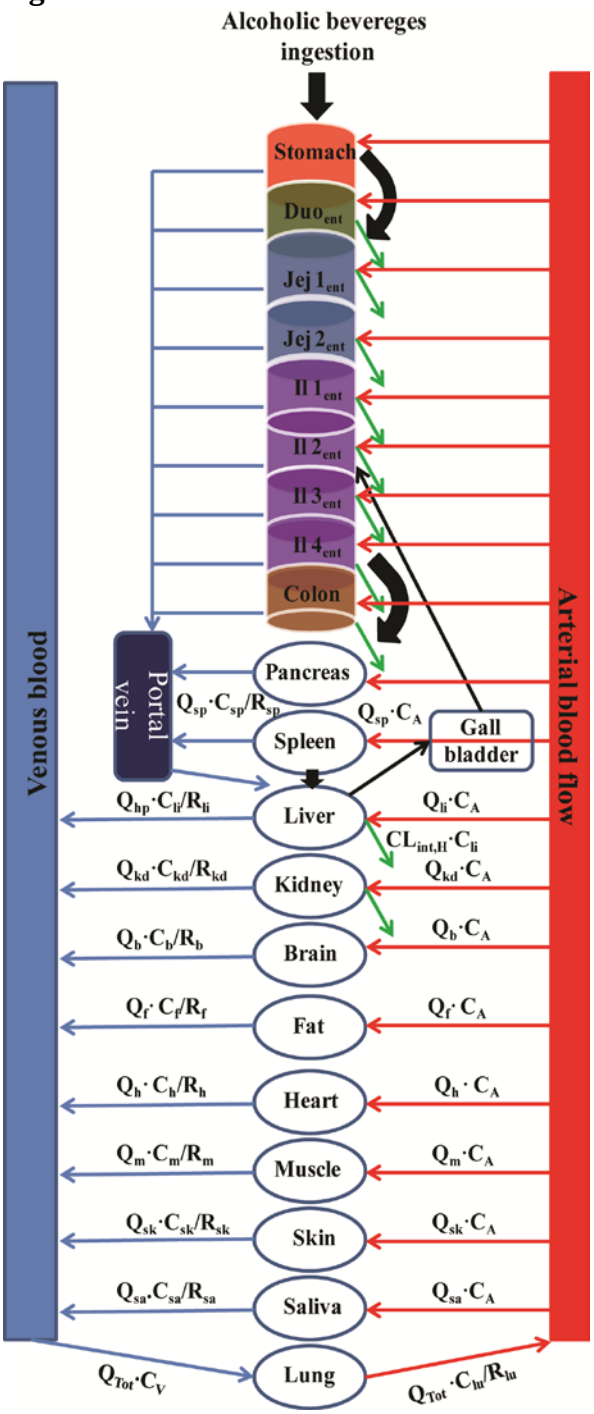


**Figure I- 2.** A whole-body physiologically based pharmacokinetic model (PBPK) suggested for EtOH consumption.

**Abbreviation:** $Duo_{ent}$ (duodenum), $Jej_{ent}$ (jejunum), $Il_{ent}$ (ileum), $C_A$ (arterial blood concentration), $C_V$ (venous blood concentration), $Q_{Tot}$ (total cardiac output), $Q_{hp}$ (blood flow perfusing the hepatic portal vein), R (tissue-to-blood partition coefficient), $C_{lint,\ H}$ **(hepatic** intrinsic clearance), b (brain), h (heart), li (liver), sp (spleen), lu (lungs), kd (kidney) f (fat), sk (skin), sa (saliva), and m (muscle).

**Figure I-3**

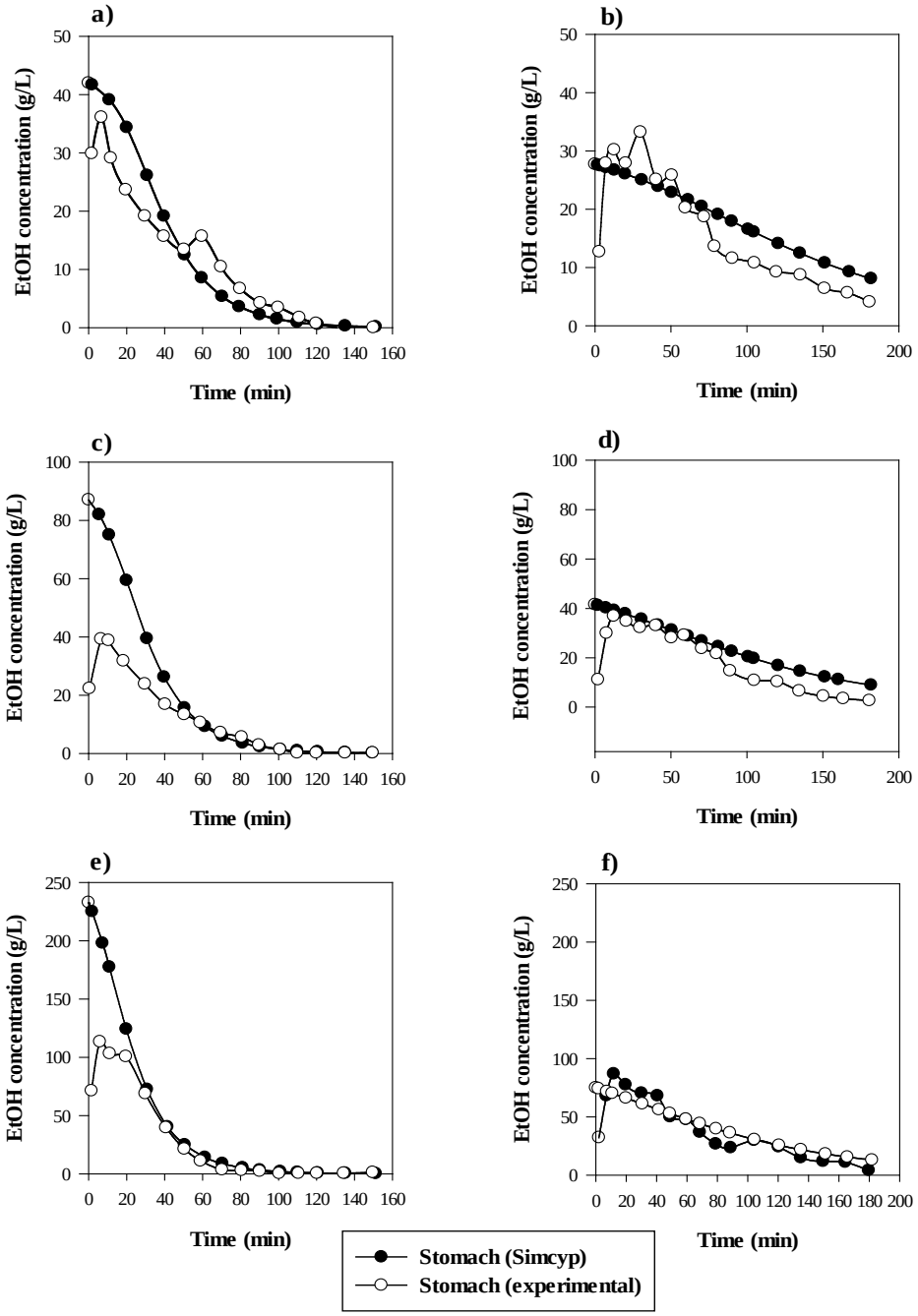


**Figure I-3**. EtOH concentration-time profile in stomach after ingestion of different alcoholic beverages.
**a**) beer-fast, **b**) beer-fed, **c)** wine-fast, **d)** wine-fed, **e)** whisky-fast, and **f)** whisky-fed states. The EtOH doses for beer, wine, and whisky were 325, 300, and 400 mg/kg body weight. The standard human body weight was considered as 70 kg. The Simcyp® data were compared with the experimental data reported by Rubbens *et al* [38, 39], while the numerical data points were visualized using Plot Digitizer (http://plotdigitizer.sourceforge.net).

**Figure I- 4**

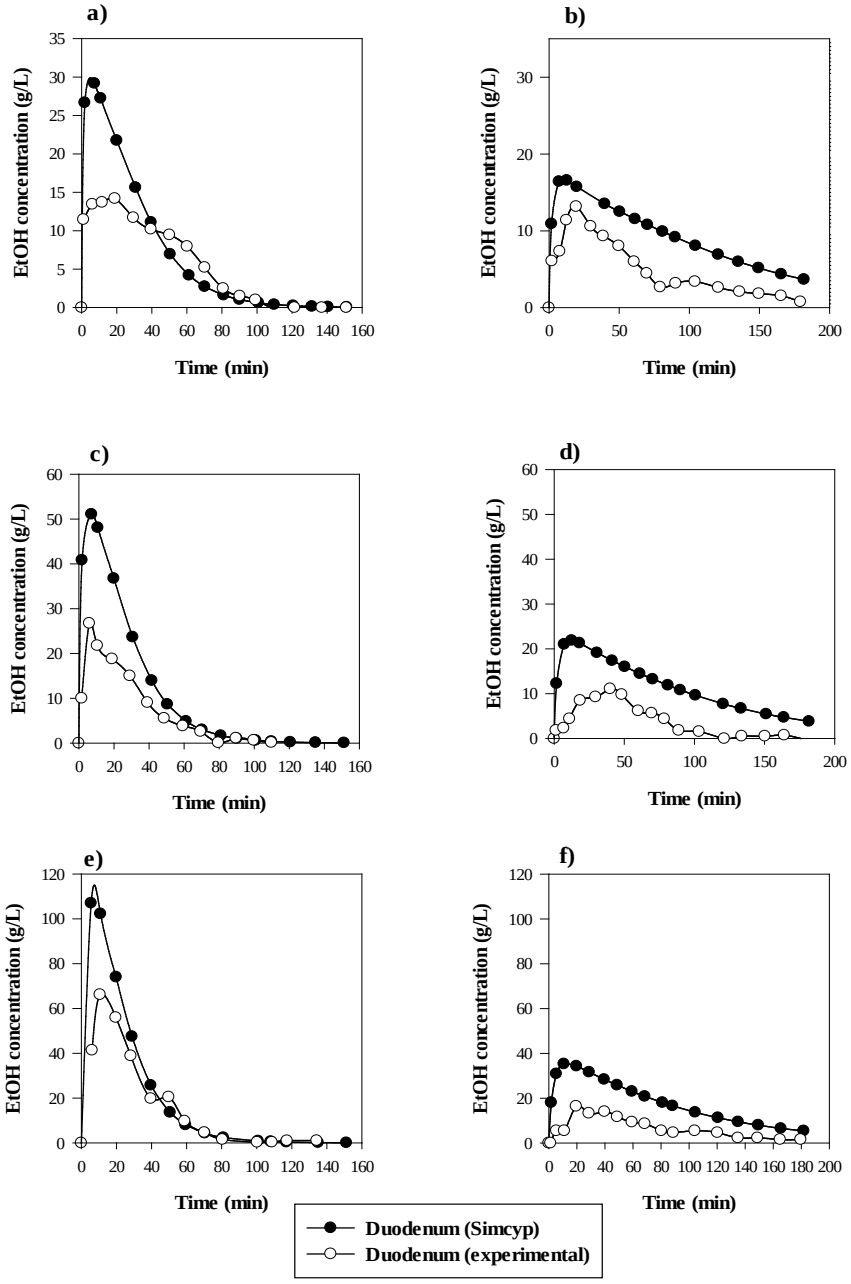


**Figure I- 4**. Duodenal EtOH concentration-time profile after ingestion of different alcoholic beverages.
**a**) beer-fast, **b**) beer-fed, **c)** wine-fast, **d)** wine-fed, **e)** whisky-fast, and **f)** whisky-fed states. The EtOH doses for beer, wine, and whisky were 325, 300, and 400 mg/kg body weight. The average body weight for healthy human was considered as 70 kg. The Simcyp® data were compared with the experimental data reported by Rubbens *et al*, while the numerical data points were visualized using Plot Digitizer (http://plotdigitizer.sourceforge.net).

**Figure I- 5**

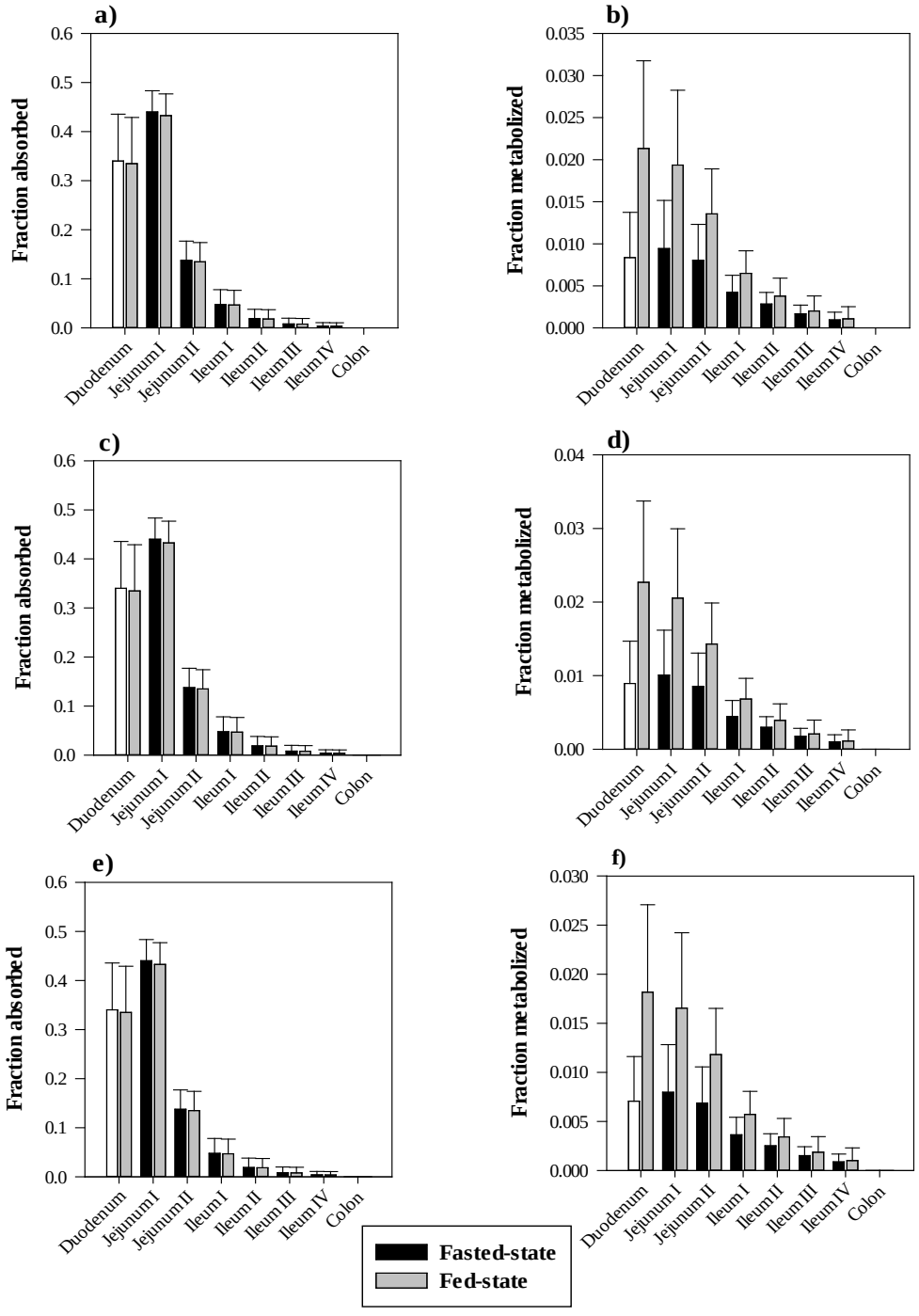


**Figure I- 5**. The Simcyp® simulation results for regional distribution of EtOH fraction dose absorbed ($F_{abs}$) and metabolized ($F_{met}$).
**(a** beer-$F_{abs}$, **b)** beer-$F_{met}$, **c)** wine-$F_{abs}$, **d)** wine-$F_{met}$, **e)** whisky-$F_{abs}$, and **f)** whisky-$F_{met}$. Data are shown as Mean ± Standard Error of Mean (Mean ± SEM).

**Figure I- 6**

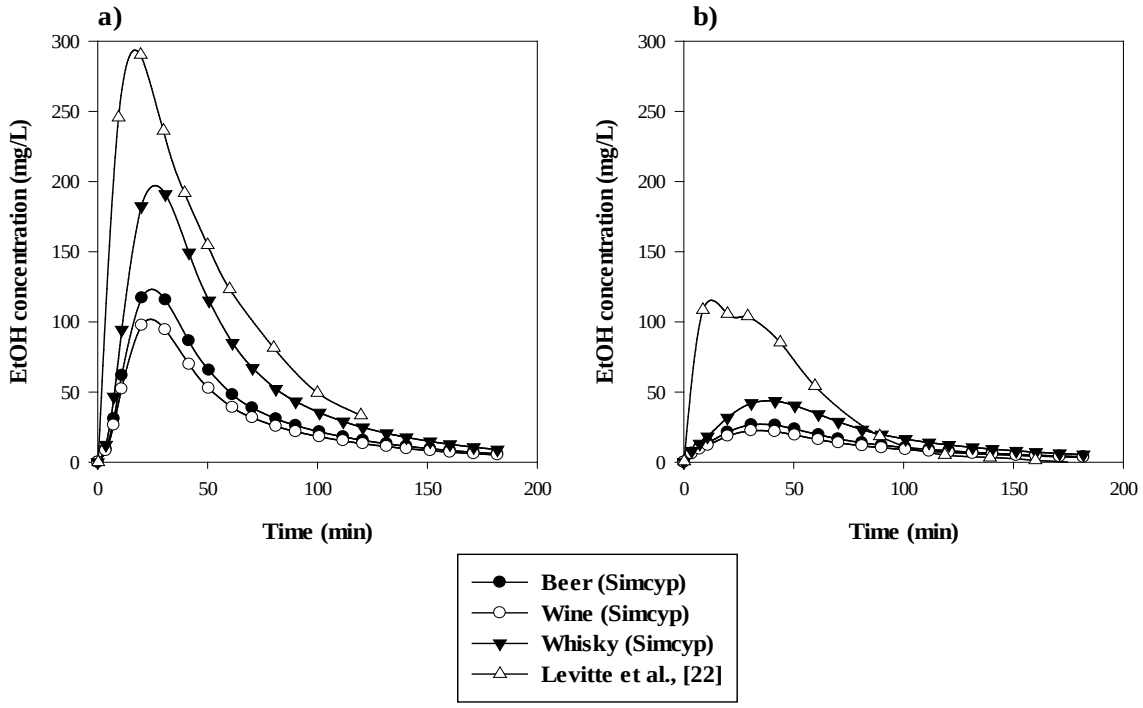


**Figure I- 6**. The Simcyp® simulation results for EtOH plasma concentration-time profiles.
**a)** fasted- and **b)** fed-state. The EtOH doses for beer, wine, and whisky were 325, 300, and 400 mg/kg body weight. The average human body weight was considered as 70 kg. The experimental values for systemic plasma concentration of EtOH were adopted from Levitt *et al.*, [22] and visualized using Plot Digitizer (http://plotdigitizer.sourceforge.net). The amount of EtOH in their study, which was administered orally, was 150 mg/kg body weight.

**Figure I- 7**

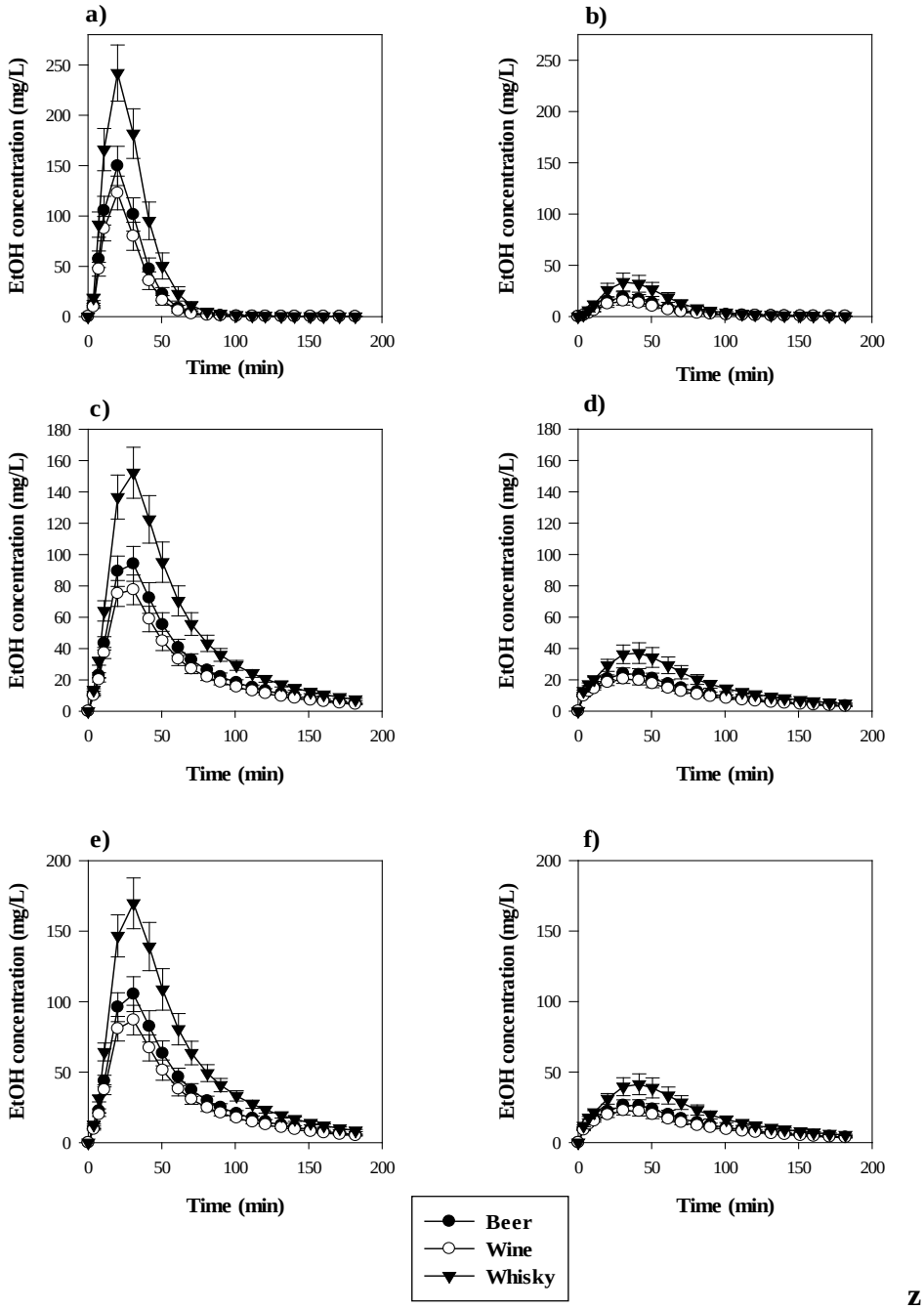


**Figure I- 7.** The Simcyp® simulation results for EtOH concentration-time profile in tissues.
**a)** liver-fast, **b)** liver-fed, **c)** gut-fast, **d)** gut-fed, **e)** brain-fast, and **f)** brain-fed states. The EtOH doses for beer, wine, and whisky were 325, 300, and 400 mg/kg body weight. The average human body weight was considered as 70 kg. Data are shown as mean ± standard error of mean (Mean ± SEM).

**References**


1. Bushra, R.; Aslam, N.; Khan, A. Y. Food-drug interactions. *Oman. Med. J.* **2011,** *26*, (2), 77-83.
2. Fagerberg, J. H.; Sjögren, E.; Bergström, C. A. Concomitant intake of alcohol may increase the absorption of poorly soluble drugs. *Eur. J. Pharm. Sci.* **2015,** *67*, 12-20.
3. Lennernas, H. Ethanol-drug absorption interaction: potential for a significant effect on the plasma pharmacokinetics of ethanol vulnerable formulations. *Mol. Pharmaceutics.* **2009,** *6*, (5), 1429-40.
4. Darwish, M.; Bond, M.; Yang, R.; Tracewell, W.; Robertson, P. Assessment of Alcohol-Induced Dose Dumping with a Hydrocodone Bitartrate Extended-Release Tablet Formulated with CIMA® Abuse Deterrence Technology. *Clinic. drug. investig.* **2015,** *35*, (10), 645-652.
5. Meyer, R. J.; Hussain, A. S. Awareness topic: mitigating the risks of ethanol induced dose dumping from oral sustained/controlled release dosage forms. *Food and Drug Administration* **2015**.
6. Newcorn, J. H.; Stark, J. G.; Adcock, S.; McMahen, R.; Sikes, C. A Randomized Phase I Study to Assess the Effect of Alcohol on the Pharmacokinetics of an Extended-release Orally Disintegrating Tablet Formulation of Amphetamine in Healthy Adults. *Clin. Ther.* **2017,** *39*, (8), 1695-1705.
7. Johnson, B. A.; Seneviratne, C., Alcohol–medical drug interactions. In *Handbook of clinical neurology*, Elsevier: 2014; Vol. 125, pp 543-559.
8. Weathermon, R.; Crabb, D. W. Alcohol and medication interactions. *Alcohol research & health : the journal of the National Institute on Alcohol Abuse and Alcoholism* **1999,** *23*, (1), 40-54.
9. Neutel, C. I.; Appel, W. C. The effect of alcohol abuse on the risk of NSAID-related gastrointestinal events. *Annals of epidemiology* **2000,** *10*, (4), 246-50.
10. Immonen, S.; Valvanne, J.; Pitkälä, K. H. The prevalence of potential alcohol–drug interactions in older adults. *Scandinavian journal of primary health care* **2013,** *31*, (2), 73-78.
11. Larson, J. M.; Tavakkoli, A.; Drane, W. E.; Toskes, P. P.; Moshiree, B. Advantages of azithromycin over erythromycin in improving the gastric emptying half-time in adult patients with gastroparesis. *Journal of neurogastroenterology and motility* **2010,** *16*, (4), 407-13.
12. Baker, R. I.; Coughlin, P. B.; Gallus, A. S.; Harper, P. L.; Salem, H. H.; Wood, E. M.; Warfarin Reversal Consensus, G. Warfarin reversal: consensus guidelines, on behalf of the Australasian Society of Thrombosis and Haemostasis. *Med. J. Aust.* **2004,** *181*, (9), 492-7.
13. Vasiliou, V.; Malamas, M.; Marselos, M. The mechanism of alcohol intolerance produced by various therapeutic agents. *Basic Clin. Pharmacol. Toxicol.* **1986,** *58*, (5), 305-310.
14. Edenberg, H. J. The genetics of alcohol metabolism: role of alcohol dehydrogenase and aldehyde dehydrogenase variants. *Alcohol. Res. Health.* **2007,** *30*, (1), 5-13.

15. Lee, S. L.; Chau, G. Y.; Yao, C. T.; Wu, C. W.; Yin, S. J. Functional assessment of human alcohol dehydrogenase family in ethanol metabolism: significance of first-pass metabolism. *Alcohol. Clin. Exp. Res.* **2006,** *30*, (7), 1132-42.
16. Zakhari, S. Overview: how is alcohol metabolized by the body? *Alcohol. Res. Health.* **2006,** *29*, (4), 245-255.
17. Forsyth, C. B.; Voigt, R. M.; Shaikh, M.; Tang, Y.; Cederbaum, A. I.; Turek, F. W.; Keshavarzian, A. Role for intestinal CYP2E1 in alcohol-induced circadian gene-mediated intestinal hyperpermeability. *Am. J. Physiol. Gastrointest. Liver Physiol.* **2013,** *305*, (2), G185-95.
18. Crabb, D. W.; Edenberg, H. J.; Bosron, W. F.; Li, T.-K. Genotypes for aldehyde dehydrogenase deficiency and alcohol sensitivity. The inactive ALDH2 (2) allele is dominant. *J. Clin. Invest.* **1989,** *83*, (1), 314-316.
19. Schug, Z. T.; Peck, B.; Jones, D. T.; Zhang, Q.; Grosskurth, S.; Alam, I. S.; Goodwin, L. M.; Smethurst, E.; Mason, S.; Blyth, K.; McGarry, L.; James, D.; Shanks, E.; Kalna, G.; Saunders, R. E.; Jiang, M.; Howell, M.; Lassailly, F.; Thin, M. Z.; Spencer-Dene, B.; Stamp, G.; van den Broek, N. J.; Mackay, G.; Bulusu, V.; Kamphorst, J. J.; Tardito, S.; Strachan, D.; Harris, A. L.; Aboagye, E. O.; Critchlow, S. E.; Wakelam, M. J.; Schulze, A.; Gottlieb, E. Acetyl-CoA synthetase 2 promotes acetate utilization and maintains cancer cell growth under metabolic stress. *Cancer Cell* **2015,** *27*, (1), 57-71.
20. Best, C. A.; Laposata, M. Fatty acid ethyl esters: toxic non-oxidative metabolites of ethanol and markers of ethanol intake. *Front Biosci* **2003,** *8*, e202-17.
21. Julkunen, R. J.; Tannenbaum, L.; Baraona, E.; Lieber, C. S. First pass metabolism of ethanol: an important determinant of blood levels after alcohol consumption. *Alcohol* **1985,** *2*, (3), 437-41.
22. Levitt, M. D.; Li, R.; Demaster, E. G.; Elson, M.; Furne, J.; Levitt, D. G. Use of measurements of ethanol absorption from stomach and intestine to assess human ethanol metabolism. *Am. J. Physiol. Gastrointest. Liver Physiol.* **1997,** *273*, (4), G951-G957.
23. Jones, H. M.; Chen, Y.; Gibson, C.; Heimbach, T.; Parrott, N.; Peters, S. A.; Snoeys, J.; Upreti, V. V.; Zheng, M.; Hall, S. D. Physiologically based pharmacokinetic modeling in drug discovery and development: a pharmaceutical industry perspective. *Clin. Pharmacol. Ther.* **2015,** *97*, (3), 247-62.
24. Teorell, T. Kinetics of distribution of substances administered to the body, I: the extravascular modes of administration. *Arch. Int. Pharmacodyn. Ther.* **1937,** *57*, 205-225.

25. Sjögren, E.; Thorn, H.; Tannergren, C. In silico modeling of gastrointestinal drug absorption: predictive performance of three physiologically based absorption models. *Mol. Pharmaceutics.* **2016,** *13*, (6), 1763-1778.
26. Zhuang, X.; Lu, C. PBPK modeling and simulation in drug research and development. *Acta. Pharm. Sin B.* **2016,** *6*, (5), 430-440.
27. Kuepfer, L.; Niederalt, C.; Wendl, T.; Schlender, J. F.; Willmann, S.; Lippert, J.; Block, M.; Eissing, T.; Teutonico, D. Applied concepts in PBPK modeling: how to build a PBPK/PD model. *CPT Pharmacometrics. Syst. Pharmacol.* **2016,** *5*, (10), 516-531.

28. Jamei, M.; Marciniak, S.; Feng, K.; Barnett, A.; Tucker, G.; Rostami-Hodjegan, A. The Simcyp® population-based ADME simulator. *Expert. Opin. Drug. Metab, Toxicol.* **2009,** *5*, (2), 211-223.
29. Jamei, M.; Turner, D.; Yang, J.; Neuhoff, S.; Polak, S.; Rostami-Hodjegan, A.; Tucker, G. Population-based mechanistic prediction of oral drug absorption. *AAPS J* **2009,** *11*, (2), 225-37.
30. Jamei, M.; Marciniak, S.; Edwards, D.; Wragg, K.; Feng, K.; Barnett, A.; Rostami-Hodjegan, A. The simcyp population based simulator: architecture, implementation, and quality assurance. *In Silico. Pharmacol.* **2013,** *1*, (1), 9.
31. Emoto, C.; Fukuda, T.; Johnson, T. N.; Adams, D. M.; Vinks, A. A. Development of a Pediatric Physiologically Based Pharmacokinetic Model for Sirolimus: Applying Principles of Growth and Maturation in Neonates and Infants. *CPT: Pharmacometrics & Systems Pharmacology* **2015,** *4*, (2), e17.
32. Cederbaum, A. I. Alcohol metabolism. *Clin. Liver. Dis.* **2012,** *16*, (4), 667-85.
33. Chi, Y. C.; Lee, S. L.; Lai, C. L.; Lee, Y. P.; Lee, S. P.; Chiang, C. P.; Yin, S. J. Ethanol oxidation and the inhibition by drugs in human liver, stomach and small intestine: Quantitative assessment with numerical organ modeling of alcohol dehydrogenase isozymes. *Chem. Biol. Interact.* **2016,** *258*, 134-41.
34. Holford, N. H. Clinical pharmacokinetics of ethanol. *Clin. Pharmacokinet.* **1987,** *13*, (5), 273-92.
35. Dasgupta, A., *Alcohol and Its Biomarkers: Clinical Aspects and Laboratory Determination*. Elsevier: 2015; Vol. 1.
36. Ehlers, C. L. Variations in ADH and ALDH in Southwest California Indians. *Alcohol. Res. Health.* **2007,** *30*, (1), 14-7.
37. Eng, M. Y.; Luczak, S. E.; Wall, T. L. ALDH2, ADH1B, and ADH1C genotypes in Asians: a literature review. *Alcohol. Res. Health.* **2007,** *30*, (1), 22-7.
38. Ramchandani, V. A., Genetics of alcohol metabolism. In *Alcohol, nutrition, and health consequences*, Springer: 2013; pp 15-25.
39. Rubbens, J.; Brouwers, J.; Wolfs, K.; Adams, E.; Tack, J.; Augustijns, P. Ethanol concentrations in the human gastrointestinal tract after intake of alcoholic beverages. *Eur. J. Pharm. Sci.* **2016,** *86*, 91-5.
40. Rubbens, J.; Riethorst, D.; Brouwers, J.; Wolfs, K.; Adams, E.; Tack, J.; Augustijns, P. Gastric and Duodenal Ethanol Concentrations after Intake of Alcoholic Beverages in Postprandial Conditions. *Mol. Pharmaceutics.* **2017,** *14*, (12), 4202-4208.
41. Mitchell, M. C., Jr.; Teigen, E. L.; Ramchandani, V. A. Absorption and peak blood alcohol concentration after drinking beer, wine, or spirits. *Alcohol. Clin. Exp. Res.* **2014,** *38*, (5), 1200-4.
42. Franke, A.; Teyssen, S.; Harder, H.; Singer, M. Effect of ethanol and some alcoholic beverages on gastric emptying in humans. *Scand. J. Gastroenterol.* **2004,** *39*, (7), 638-644.
43. Mudie, D. M.; Murray, K.; Hoad, C. L.; Pritchard, S. E.; Garnett, M. C.; Amidon, G. L.; Gowland, P. A.; Spiller, R. C.; Amidon, G. E.; Marciani, L. Quantification of gastrointestinal liquid volumes and distribution following a 240 mL dose of water in the fasted state. *Mol. Pharmaceutics.* **2014,** *11*, (9), 3039-3047.

44. Yin, S. J. Alcohol dehydrogenase: enzymology and metabolism. *Alcohol. Alcohol. Suppl.* **1994,** *2*, 113-9.
45. Jin, M.; Ande, A.; Kumar, A.; Kumar, S. Regulation of cytochrome P450 2e1 expression by ethanol: role of oxidative stress-mediated pkc/jnk/sp1 pathway. *Cell. Death. Dis.* **2013,** *4*, (3), e554.
46. Forsyth, C. B.; Voigt, R. M.; Keshavarzian, A. Intestinal CYP2E1: A mediator of alcohol-induced gut leakiness. *Redox Biol* **2014,** *3*, 40-6.

## MANUSCRIPT II

This manuscript has been prepared for submission to the Journal of "*Molecular Pharmaceutics*"

# The Effect of Alcohol on Expression and Functionality of P-Glycoprotein in Caco-2 cell Monolayer

Armin Sadighi[a], Lorenzo Leggio[b, c], Fatemeh Akhlaghi[a*]

[a]Clinical Pharmacokinetics Research Laboratory, Department of Biomedical and Pharmaceutical Sciences, College of Pharmacy, University of Rhode Island, Kingston, RI, USA

[b]Section on Clinical Psychoneuroendocrinology and Neuropsychopharmacology, Laboratory of Clinical and Translational Studies, National Institute on Alcohol Abuse and Alcoholism, Bethesda, MD, USA

[c]Center for Alcohol and Addiction Studies, Department of Behavioral and Social Sciences,

Brown University, Providence, RI 02903, USA

---

[*]**Corresponding author:** Fatemeh Akhlaghi; Clinical Pharmacokinetics Research Laboratory; University of Rhode Island; Office 495 A; 7 Greenhouse Road; Kingston; RI 02881, USA. **Tel:** (401) 874 9205; **Fax:** (401) 874 5787; **Email:** fatemeh@uri.edu

**ABSTRACT**

In this study, the effect of clinically relevant ethanol (EtOH) concentrations on the expression and functionality of P-glycoprotein (P-gp) was explored in Caco-2 cell monolayer. EtOH did not show significant alteration in cell viability at concentrations found in GI tract. To investigate the EtOH effect on P-gp, expression of P-gp was induced by treating normal cells with vinblastine (10 nM). Immunofluorescent (IF) images of normal and P-gp induced Caco-2 showed that the abundance of P-gp decreased by increasing EtOH concentration and treatment time. Moreover, the effect of EtOH on abundance of xenobiotic transporters in normal and P-gp induced Caco-2 cells was analyzed. Sequential Windowed data independent Acquisition of the Total High-resolution Mass Spectra (SWATH-MS) proteomics approach showed that the abundance of P-gp polypeptides was diminished after treatment of normal and P-gp induced Caco-2 cells with EtOH for 4 and 24 h. Moreover, Calcein-AM assay showed that by increasing the time and concentration of EtOH, the efflux activity of P-gp was reduced in P-gp induced Caco-2 cells. Furthermore, EtOH effect on transport parameters of talinolol (Tal, a P-gp substrate) and PF-5190457 (PF-57), an alcohol craving treatment currently undergoing clinical trials) were investigated in the presence and absence of verapamil (P-gp inhibitor). According to the results, EtOH showed significant decrease in efflux ratio (ER) of Tal in Caco-2-treated cells with 50 mM EtOH for 24 h in the presence of verapamil. However, EtOH did not show significant effect on ER of PF-57 in the presence or absence of verapamil.

**KEYWORDS:** Ethanol, Caco-2 cell monolayer, P-glycoprotein, SWATH-MS proteomics, Talinolol transport, Calcein-AM assay

## INTRODUCTION

The effect of drinking alcohol on drug absorption and bioavailability has received considerable attention during recent years.[1, 2] Ethanol (EtOH) alters the body exposure to the extended-release drug formulations through induction of dose dumping.[3-5] Hence, US Food and Drug Administration (FDA) has recommended to characterize the effect of alcohol on drug release profile.[6] Furthermore, EtOH affects the pharmacokinetic and pharmacodynamic of medication such as, ezogabine,[7] elvitegravir,[8] and opioids[9] in alcoholic patients. Acute EtOH consumption primarily affects the rate and extent of drug absorption[10] and to a lesser extend drug clearance.[11] Hence, estimation of EtOH interaction with the involved absorption mechanisms in gastrointestinal (GI) tract is beneficial to understand how EtOH alters the disposition of oral drugs.

The human colorectal adenocarcinoma cell line Caco-2 is widely used as a standard model for human intestinal epithelium to assess drug permeation and transport mechanisms.[12, 13] Caco-2 monolayer has been broadly used to study all four possible drug transport pathways across epithelial cells including passive transcellular, paracellular, carrier mediated routes, and transcytosis.[14, 15] One of the most abundant transporters in Caco-2 cell line and human GI tract that plays an important role in drugs absorption and disposition, is permeability-glycoprotein (P-gp).

P-gp, also known as multi drug resistant protein-1 (MDR-1), is a 170 kDa transmembrane efflux transporter encoded by ATP-binding cassette (ABC) superfamily.[16-18] P-gp (ABCB1) is the most extensively studied transporter in mammalian that was first discovered in colchicine-resistant Chinese hamster ovary

cells.[19] In human, P-gp is expressed on the apical side of GI epithelial cells, the apical side of epithelial cells in proximal tubules of kidney, the apical surface of epithelium in placenta, the biliary canalicular membrane of hepatocytes in liver, and endothelial cells in blood brain barrier (BBB).[20] Intestinal P-gp plays a significant role in absorption and disposition of a wide variety of drugs by limiting their cellular uptake from intestinal lumen into the enterocytes. Consequently, the functionality of P-gp and its expression level greatly influence the pharmacokinetic, safety, and efficacy profiles of drugs.

The expression of P-gp has been extensively investigated at mRNA and protein levels.[21, 22] While, the mRNA level of P-gp does not necessarily translate into the amount of expressed protein,[23] the quantification of protein seems to be more reliable approach for P-gp expression assessment.[24, 25] Enzyme-linked Immunosorbent Assay (ELISA),[26] flow cytometry,[27] and immunoblotting (Western blotting)[28] methods are the most well-known methods for identification and quantification of P-gp and other transporters. However, those methods suffer from some limitations such as, low throughput performance, intensive laboring, applying expensive antibodies, and low specificity. Mass spectrometry (MS), which avoids a vast majority of those flaws, has gained a great demand in protein studies.[29-31] Among all MS-based proteomics methods, the Sequential Windowed data independent Acquisition of the Total High-resolution Mass Spectra (SWATH-MS) offers superior advantages, like high accuracy and reproducibility over the other MS approaches.[32]

Transport behavior of P-gp substrates across Caco-2 cell monolayer is broadly used by pharmaceutical industries to measure human intestinal P-gp activity.[33, 34]

Caco-2 cell monolayer transport assay is considered as a well-established method to determine if a compound is substrate, inhibitor or both for P-gp. While, P-gp is expressed in various organs (e.g., GI tract, BBB, liver, and kidney), inhibition of P-gp greatly affect the pharmacokinetic and efficacy of P-gp substrates. Consequently, inhibition of P-gp in GI tract increases the oral absorption of drugs that are P-gp substrate. Elevated plasma concentration of drugs with narrow therapeutic index can cause severe toxicity. Therefore, dose adjustment is needed for P-gp substrates once they are co-administered with a P-gp inhibitor.

In addition to Caco-2 monolayer transport assay, fluorescent probe efflux assay can also be used to evaluate P-gp functionality. Calcein-acetoxymethylester (calcein-AM) is a non-fluorescent P-gp substrate that cleaves by intracellular esterases to form fluorescent impermeable calcein.[35, 36] This method is widely used as a high-throughput, facile, and real-time P-gp inhibition assay.[37]

In the present study, the effect of EtOH on expression and functionality of P-gp in normal and P-gp induced Caco-2 cell monolayer was analyzed. EtOH cytotoxicity in Caco-2 cells was examined and immunohistochemistry staining was used to visualize the expressed P-gp on the Caco-2 cell membrane. Moreover, SWATH-MS proteomics approach was used to find out if EtOH can alter the expression level of P-gp in Caco-2 cell monolayer. Furthermore, the transport behavior of talinolol (Tal, $\beta_1$-antaginist) and PF-5190457 (PF-57, a ghrelin reverse agonist), as two model drugs, was investigated to find out the effect of EtOH P-gp activity. Finally, the Calcein-AM fluorescent assay was conducted to prove the effect of EtOH on P-gp efflux functionality.

## EXPERIMENTAL SECTION

**Chemical and Reagents.** Molecular biology grade EtOH >99.5%, iodoacetamide (IAA), dithiothreitol (DTT), ammonium bicarbonate, and sodium deoxycholate were purchased from Sigma Aldrich (St. Louis, MO). Racemic talinolol (Tal), the internal standard (IS) Tal-d5 and vinblastine sulfate were purchased from Toronto Research Chemicals (TRC, Toronto, Ontario, Canada). RPMI 1640, Dulbecco's modified Eagle medium (DMEM), fetal bovine serum (FBS), Pierce™ BCA protein assay kit, and Vybrant™ cell adhesion assay kit was obtained from Thermo Fisher Scientific Inc (Waltham, MA, USA). ProteoExtract™ Native Membrane Protein Extraction Kit was obtained from EMD Millipore (Billerica, MA). WST-1 (2-(4-iodophenyl)-3-(4-nitrophenyl)-5-(2,4-disulfophenyl)-2H-tetrazolium, monosodium salt) was purchased from Roche (Mannheim, Germany). Hank's balanced salt solution (HBSS), penicillin/streptomycin, and trypsin-EDTA (0.25%) were acquired from the American Type Culture Collection (ATCC, VA, USA). Optima™ LC-MS/MS grade of acetonitrile, methanol, and formic acid were purchased from Fisher Scientific (Fair Lawn, NJ, USA). Deionized water was obtained using a Milli-Q® Synthesis A10 system fitted with a Q-Gard 2 Purification Pack (Millipore, Bedford, MA, USA). Proteomics grade trypsin and trypsin-predigested β-galactosidase (originated from *Escherichia coli*) were purchased from SCIEX (Framingham, MA). All other reagents used in this study were of analytical grade.

**Cell Culture and EtOH Treatment.** Caco-2 cells (ATCC® HTB-37™, passage number 50–65) were maintained at 37 °C and grown in 25-ml flasks in an incubator

with a controlled, humidified atmosphere consisting of 5% $CO_2$ and 95% air. Cells were cultured in an enriched medium consists of RPMI-1640, DMEM, FBS and penicillin/streptomycin in a ratio of 50:35:15:1 [38]. In order to enhance the expression of P-gp in Caco-2 cell line, normal Caco-2 cells were treated with 10 nM vinblastine for 4–5 passages to induce the expression of P-gp and form P-gp-induced Caco-2 cell line.[16, 39] The culture medium was changed every second days and cells were trypsinized by trypsin–EDTA (1%) after reaching 70–80% confluence. Normal and P-gp-induced Caco-2 cells were seeded onto semi-permeable PET filter inserts (Corning Costar Corporation, Corning, NY) with 6.4 mm diameter, 0.33 $cm^2$ growth area, and 0.4 μm pore size. Each membrane of the 24-transwell permeable insert received 0.2 mL of a $3.2 \times 10^5$ cells/mL suspension and 0.6 mL culture medium into the wells. Caco-2 cells were then grown and differentiated for 21 days. Medium changed every two days for the first two weeks and then every day until day 21 when a fully differentiated monolayer had achieved.

To assess the effect of EtOH on Tal transport in mature normal and P-gp-induced Caco-2 monolayer, the plates containing transwell inserts were put into chambers filled with 95% air, 5% $CO_2$ and kept in humid incubator at 37 °C. Various EtOH concentrations (25, 50, and 100 mM) diluted in culture medium were added to the both apical and basolateral sides of cells. In each treatment, the atmosphere of chambers was saturated by the same concentration of EtOH.

**Cytotoxicity Assay.** The cytotoxicity of EtOH treatment on the Caco-2 cells was evaluated according to the colorimetric method using a water-soluble tetrazolium salt (WST-1). In this method, the cleavage of the tetrazolium salt to formazan by active

cellular mitochondrial dehydrogenases indicates the viable cells. For this purpose, Caco-2 cells were seeded at a concentration of $2 \times 10^4$ cells/well in a 96-well plate for 2–3 days to achieve 70% confluence. The culture medium was removed and replaced by different EtOH (0–1000 mM) and placed in the corresponding chambers saturated with EtOH and AA vapor contained 95% air and 5% $CO_2$ and placed in incubator. Clotrimazol was used as a positive control at different concentrations (20, 40, 60, 80, and 100 µM). Cells were incubated for 24, 48, and 72 h at 37 °C in an incubator with a controlled atmosphere. At the end of treatment, 10 µl of WST-1 was added to each well and incubated for 4 h at 37 °C. The absorbance of each well against background control was measured at 450 nm, while reference wavelength set at 650 nm.

**Transepithelial Electrical Resistance (TEER).** TEER assay was used as a real-time, non-destructive, and label free method to characterize the quality of the cell monolayer integrity. TEER of the normal and P-gp-induced Caco-2 cell monolayers were evaluated by an EVOM$^2$ (World Precision Instruments, Sarasota, FL) equipped with STX2 "chopstick" silver/silver chloride (Ag/AgCl) electrodes.

TEER assay was performed 21-days post seeding of normal and P-gp induced Caco-2 cells on filter inserts. TEER measurements were done before starting of EtOH treatment as well as 4 and 24 h after alcohol exposure to the Caco-2 monolayers. The relative changes in TEER values before and after EtOH treatments were compared to that for buffer treatment, as the control group. TEER values were calculated according to the following equation:

$$\text{TEER} = (R_{\text{monolayer}} - R_{\text{blank}}) \times A \ (\Omega\text{cm}^2), \quad (2)$$

where, $R_{monolayer}$ is the measured resistance of cell monolayer, $R_{blank}$ represents the resistance of filter inserts without cell monolayer, and $A$ is the available filter inserts surface area.

**Immunohistochemistry.** Normal and P-gp induced Caco-2 cells were grown on 24-transwell permeable insert for 21-days and the culture media were changed every two days in the first week and every day in the following 14 days. Then, the cells were incubated with EtOH to assess the effects of different EtOH concentrations (0, 25, and 50 mM) on the expression of P-gp after 24 h of incubation. Culture medium containing 25 and 50 mM of EtOH were added to the apical (AP, 200 µL) and basolateral (BL, 600 µL) sides, respectively. Culture medium containing phosphate buffered saline (PBS, 50 mM) was applied as negative control. Then, the 24-well plates containing filter grown Caco-2 cells were placed in the chambers saturated with the corresponding EtOH concentration and PBS (control). Chambers were kept at 37 °C for 24 h in incubator. At the end of treatments, the culture media were removed from AP and BL sides and washed three times using PBS. The cells were fixed with 4% formaldehyde for 10 min. Then, the cells were rinsed with PBS and permeabilized with 0.1% TX-100/PBS for 15–20 min and washed. The monolayer was block with 1% Bovine serum albumin (BSA)/PBS for 45 min followed by incubation with mouse IgG1 anti-human P-gp primary antibodies (1:10 dilution, Thermo Fisher Scientific, Waltham, MA, USA) for 60 min at room temperature. The filters were rinsed 3 times in PBS and then incubated with Cy5-conjugated goat anti-rabbit IgG secondary antibody (Thermo Fisher Scientific, Waltham, MA, USA) for 60 min at room temperature in the dark. Then, the secondary antibody was aspirated, and the PET

bottom of the filter inserts were cut and fixed on glass slides, while the BL side of the cells facing up the slide. The filters were incubated with VECTASHIELD® antifade mounting medium with DAPI (Vector Laboratories, catalog number: H-1200, CA, USA) for 10 min to preserve fluorescence. Finally, slides were imaged on an EVOS FL Auto fluorescent microscope (Life Technologies; Thermo Fisher Scientific) using Cy®5 light cube (excitation 628/40 nm; emission 685/40 nm) and DAPI light cube (excitation 357/44 nm; emission 447/60 nm).

**Membrane Protein Extraction and Sample Preparation.** Membrane associated proteins were extracted from normal and P-gp induced Caco-2 cells using the ProteoExtract™ Native Membrane Protein Extraction Kit (M-PEK, EMD Millipore, Billerica, MA). For this purpose, normal and P-gp induced Caco-2 cells (passage number 55–65) were seeded at the density of $6.5 \times 10^4$ cells per each 24-well PET filter inserts for 15–21 days. By the end of time needed for cell differentiation, cells were treated with EtOH (25, 50, and 100 mM) and placed in saturated chambers filled with 95% air, 5% $CO_2$ for 4 and 24 h and kept in humid incubator at 37 °C. To obtain membrane associated proteins from filter-grown Caco-2 cells, the attached cells were scratched by cell scraper from the filter inserts. Then, the cells were incubated in 100 µl of extraction buffer I containing 0.5 µl of protease inhibitor cocktail according to the protocol supplied by the vendor. The cell suspension was gently shaken for 10 min at 4 °C and the homogenate was centrifuged at 3000 × g for 5 min to separate soluble proteins from cell pellet. To extract the membrane proteins, 100 µl of extraction buffer II containing 0.5 µl of protease inhibitor cocktail was added to the

cells and shacked at 4 °C for 30 min. Finally, the enriched homogenate with membrane bounded proteins was collected from supernatant.

To digest proteins, 100 µL of 1 mg/mL of soluble and membrane bounded proteins were incubated with 15 µL of dithiothreitol (100 mM) and 50 ml of ammonium bicarbonate buffer (50 mM, pH 7.4) at 95 °C for 10 min. Afterward, 15 µL of iodoacetamide (150 mM) was added to the mixture and incubated at room temperature for 30 min in the dark. Ice-cold chloroform extraction solution (0.5 mL) which contains (MeOH 50%, $CHCl_3$ 25%, and water 25%) was added to each sample and centrifuged at 4 °C for 5 min at 16000 × g. The protein pellet was washed with ice-cold methanol (250 µL) and resuspended in 46.5 µL of sodium deoxycholate (3% w/v) solution prepared in ammonium bicarbonate buffer (50 mM, pH 7.4). Then, 3.5 µL of trypsin (1 mg/mL) was added to the latter solution and put in the Barocycler® 2320 EXT (Pressure Biosciences; West Bridgewater, MA) to digest the proteins. Protein to trypsin ratio was 20:1 (w/w). Barocycler repeated cycles of hydrostatic pressure at 35000 psi for 90 cycles (90 min) to improve the protein digestion. Afterwards, 10 µL of 2.5% formic Acid in 1:1 (v/v) mixture of water/acetonitrile was added to the digest and centrifuged at 10,000 ×*g* for 5 minutes at 4°C. Finally, 2.5 µL of β-galactosidase (31.25 pmol), as an external control, was added to the digested protein solution before injection to LC-MS/MS.

**SWATH-MS Analysis.** The SWATH-MS proteomics analysis and data processing were accomplished based on the previously published method.[40, 41] Briefly, A SCIEX 5600 TripleTOF mass spectrometer equipped with a DuoSpray ion source (SCIEX, Concord, Canada) coupled to Acquity UHPLC HClass system

(Waters Corp., Milford, MA, USA) was used. The mass spectrometer was operated in positive electrospray ionization (ESI) mode for all the experiments. Compound and source/gas parameters used in SWATH-MS method were as follows: DP = 120 V, CE = 10 V, collision energy spread (CES = 5V), TEM = 400 °C, ISVF = 5500 V, GS1 = 55 psi, and GS2 = 60 psi. TOF masses were collected from *m/z* 300 to 1500. SWATH data was acquired in the range of *m/z* 400 to 1100 over 70 SWATH windows per cycles with a window size of *m/z* 10. The total cycle time for SWATH acquisition was 3.95 sec.

The digested P-gp peptides were separated on an Acquity UHPLC Peptide BEH C18 (2.1 × 150 $mm^2$, 300 Å, 1.7 µm) equipped with Acquity VanGuard precolumn (2.1 × 5 $mm^2$ , 300 Å, 1.7 µm). Autosampler temperature was kept at 10 °C and the column temperature was maintained at 40 °C during all injections. The chromatographic separation was performed with a runtime of 120 min at 100 µL/min with a gradient method using mobile phase A (98% water, 2% acetonitrile, 0.1% formic acid) and mobile phase B (98% acetonitrile, 2% water, 0.1% formic acid). A gradient chromatographic elusion method was performed as follows: 98% A from 0 to 3 min, 60% to 90% A from 3 to 48 min, 20% A held from 49 to 52 min to flush the column, 98% A at 53 min. The column was equilibrated at 98% A from 53 to 60 min before the start of next run. The amount of protein per injection on the column was 10 µg. In each batch, trypsin-digested β- galactosidase that is a quality control standard (1.65 pmol/injection) was injected to each sample to monitor mass calibration of the TOF detector and normalization of peptides intensity in SWATH label free

quantification (LFQ) approach. The LFQ was performed using Skyline, which is an open source application for targeted proteomics quantitative data analysis.

**Protein Quantification.** Membrane Proteins and digested peptides concentrations were analyzed using Pierce™ BCA protein assay kit (Thermo Fisher Scientific, Rockford, IL, USA) and NanoDrop™ 2000 (Thermo Fisher Scientific, Wilmington, USA) by measuring UV-vis absorbance at wavelengths of 562 and 280 nm, respectively. Protease-free bovine serum albumin (BSA) solutions (125–2000 µg/mL) were used as the standard calibration line for the BCA protein quantification method.

**Calcein-AM Functional Assay.** Vybrant™ multi-drug resistance kit (Thermo Fisher Scientific, MA, USA) was used to measure the effect of different EtOH concentrations on the efflux properties of ABCB1 in P-gp induced Caco-2 cells. In this assay, the fluorogenic dye calcein-AM was used as a substrate for efflux activity of ABCB1 transporter in P-gp induced Caco-2 cells after 4 and 24 h of treatments with EtOH. Calcein-AM is a lipophilic ester that easily enters cells through passive diffusion. Inside the cells, cytoplasmic hydrolases can convert non-fluorescent calcein-AM to fluorescent calcein. Both compounds are well retained in cytosol, however, P-gp induced Caco-2 cells can rapidly extrude calcein-AM out of the cells and decrease the accumulation of fluorescent calcein in the cytosol. The higher fluorescent yield of cells reflects the lower activity of P-gp to efflux calcein-AM out of the cells. In this method, P-gp induced Caco-2 cells ($5.0 \times 10^4$ cells/each well, passage number 55–65) were seeded on CELLSTAR black, clear-bottom 96-well plate (Grenier, #M0562) for 2–3 days prior to EtOH treatment. Then, cells were incubated

with different EtOH concentrations (25, 50, and 100 mM) in culture medium as well as negative control group (100 mM PBS, pH 7.4) for 4 and 24 h. On the day of experiment, medium containing EtOH and PBS were aspirated from the cells and then 100 µL of calcein-AM solution in culture medium (1 µM) was added to each well and incubated at 37 °C for 30 min. Afterwards, the cells in plate were washed and centrifuged (400 × g) twice with 200 µl cold RPMI1640 culture medium. Finally, a Molecular Device SpectraMax® M 5 plate reader (Molecular Devices, Sunnyvale, CA) was used to measure the fluorescence intensity

**Chromatographic Conditions and Triple Quadruple Tandem Mass Spectrometry.** Chromatographic detection of Tal and PF-57 were performed using an Acquity UPLC BEH C18 (2.1 mm × 50 mm) with 5 µm particle size and 130 Å pore size analytical column (Waters Corp, Milford, MA). The column was maintained at 45 °C and auto-sampler temperature was kept at 10 °C. A gradient elution method was applied with a mobile phase consisting of water containing 0.1 % formic acid (solvent A) and 100 % acetonitrile containing 0.1 % formic acid (solvent B). The flow rate was set at 0.4 mL/min. Each chromatographic cycle for Tal initiated at 90 % solvent (A), which gradually decreased to 70 and 20% over 0.5 and 1 min, respectively. The solvent proportion maintained at this condition until 1.25 min. To re-equilibrate the column for the next run, the proportion of solvent (A) was increased gradually to 70 and 90% at 1.5 and 2 min and maintained constant until the end of the run at 2.5 min. The retention time for Tal was 1.07 min.

Mass spectral detection of positive ions in MRM mode was performed using an API 3200 LC-MS/MS quadrupole tandem mass spectrometer (Applied Biosystems/

MDS Sciex Inc., Ontario, Canada). The 268.2 → 116.1 m/z MRM transition (precursor → product ions) was chosen for Tal. Compound and source/gas parameters used for ESI-positive modes of Tal were as follow; declustering potential (DP = 50 V), entrance potential (EP = 10 V), collision cell entrance potential (CEP = 12 V), collision energy (CE = 34 V), cell exit potential (CXP = 3 V), curtain gas (CUR = 10 psi), collision gas (CAD = 5 psi), ion spray voltage floating (ISVF = 5500 V), temperature (TEM = 500 °C), nebulizer gas (GS1 = 10 psi), and turbo gas (GS2 = 10 psi). The chromatographic and mass spectral conditions for PF-57 were optimized according to our published literature, previously[42].

**Drug Transport Studies.** Normal and P-gp-induced Caco-2 monolayers were used for transport experiments 21-days post seeding on Transwell inserts. All experiments were conducted at 37 °C under laminar airflow. To assess the effect of EtOH on Tal transport in normal and P-gp-induced Caco-2 monolayer, the plates containing transwell inserts were put into chambers filled with 95% air, 5% $CO_2$ and kept in humid incubator at 37 °C. Various EtOH concentrations (25, 50, and 100 mM) diluted in culture medium were added to the both AP and BL sides of cells. Culture medium containing PBS was applied as negative control (0 mM EtOH). In each treatment, the atmosphere of chambers was saturated by the same concentration of EtOH or buffer (for negative control).

Prior to the transport experiments, cells were washed twice with PBS and preincubated with HBSS supplemented with 25 mM HEPES (pH 7.4 and 6.5) for 30 min. Tal was added to the AP and BL compartments of the monolayer at a final concentration of 5 µM in HBSS-HEPES buffer. The AP and BL sides of the

monolayer contained 0.2 and 0.6 ml of the transition buffer, respectively. All transport analyses were conducted in the AP to BL (AP-BL) and BL to AP (BL-AP) direction of the monolayer. After 4 h of transport, 100 µl of samples were withdrawn from the AP and BL sides of the monolayer and replaced with an equal amount of fresh transition buffer. The collected samples were analyzed using the previously described LC-MS/MS methods for Tal.

Apparent permeability coefficient ($P_{app}$) of Tal was calculated according to the following equation:

$$P_{app} = \frac{dM_r}{dt} \times \frac{1}{A \times C_D(0)}, \quad (3)$$

where, $A$ stands for surface area of the cell monolayer (0.33 $cm^2$), $C_D(0)$ is the initial concentration of the drug added to the donor compartment, t is the time of transport, $M_r$ represents the mass of compound in the receiver side, and $dM_r/dt$ accounts for the flux of the drug across the cell monolayer. Uptake ratio (UR) and efflux ratio (ER) were obtained as below;

$$\text{UR} = \frac{P_{app\ (AP\text{-}BL)}}{P_{app\ (BL\text{-}AP)}} \quad (4)$$

$$\text{ER} = \frac{P_{app\ (BL\text{-}AP)}}{P_{app\ (AP\text{-}BL)}} \quad (5)$$

where, $P_{app\ (AP\text{-}BL)}$ and $P_{app\ (BL\text{-}AP)}$ stand for apparent permeability from AP to BL and BL to AP sides, respectively.

**2.8. Statistical Analysis.** Results are reported as Mean ± Standard Error of Mean (SEM) from three independent experiments unless otherwise mentioned. The normality of data sets in each experiment was checked with Shapiro-Wilks test. One-

way analysis of variance (ANOVA) with Dunnett's T3 post hoc test (SPSS 23, SPSS, Inc.) was used for normally distributed observations. Kruskal-Wallis one-way ANOVA (non-parametric ANOVA) with Dunn's multiple comparison post hoc test was used for non-normally distributed data. In all analyses, probability values <0.05 was considered significant.

## RESULTS

**WST-1 Cytotoxicity.** Normal Caco-2 cells were examined by WST-1 assay to determine the EtOH-induced cytotoxicity. EtOH and buffer exposure experiments showed that alcohol cytotoxicity was increased in a time- and EtOH concentration-dependent manner (**Figure 1**). According to **Figure 1**, the viability% of Caco-2 cells was reduced by increasing EtOH treatment time from 24 to 72 h. Moreover, by increasing EtOH concentration from 0 to 1000 mM, the cell viability was decreased, accordingly. **Figure 1** shows that after 72 h of treatment, the viability of Caco-2 cells was decreased to 85, 78, and 47% at EtOH concentrations of 250, 500, and 1000 mM, respectively. In the case of buffer treatment, cell viability was 85% in 1000 mM buffer-treated group after 72 h treatment (**Figure. 1**). Treatment of Caco-2 cells with the positive control (clotrimazole, 100 µM) reduced the viability to 80.4 ± 9.0, 75.4 ± 2.3, and 17.9 ± 3.4 % after 24, 48, and 72 h of treatment, respectively. Results showed that at EtOH concentration < 500 mM, which is more clinically relevant, no significant cytotoxicity is induced by EtOH compared to the control group (buffer-treated cells).

**TEER Assay.** The TEER was evaluated for the normal and P-gp induced Caco-2 cell monolayers after EtOH treatments to show the effect of EtOH on the integrity of junctional proteins. **Figure 2** illustrates the comparison of TEER values measured for normal and P-gp induced Caco-2 cells after 4 and 24 h of treatment with 50 mM EtOH. According to the results, P-gp induced cells showed significantly higher TEER values compared to the normal cells (**Figure 2**). In addition, a significant decrease in TEER values was observed for the EtOH-treated normal and P-gp induced Caco-2 cells compared to the buffer-treated cells. **Figure 2** shows that the TEER values of normal Caco-2 cells was decreased after 4 h of treatment with EtOH compared to the buffer-treated (P-value = 0.001) cells. Similarly, a reduction in TEER value was observed for the P-gp induced cells compare to the buffer-treated cells after 4 h of treatment (P-value = 0.05). Furthermore, the TEER values of normal and P-gp induced Caco-2 cells was drastically decreased (P-value = <0.001) after 24 h of treatment with EtOH (50 mM) compared to the control group. The reduction in TEER values in the presence of EtOH evident the effect of EtOH on the integrity of Caco-2 cells. This may arise from the effect of EtOH on the organization of paracellular proteins.

**Immunohistochemistry.** **Figure 3** shows the immunofluorescent (IF) microscope images of P-gp protein in normal (**Figure 3a**, **c**, and **e**) and P-gp induced (**Figure 3b**, **d**, and **f**) Caco-2 cells after buffer (**Figure 3a** and **b**) and EtOH (**Figure 3c-f**) treatments for 24 h. The higher expression level of P-gp proteins in the P-gp induced Caco-2 cells are clearly mentioned in IF images. In the absence of EtOH, no clear sign of P-gp was observed in normal Caco-2 cells (**Figure 3a**), while the

localization of P-gp is clearly mentioned in P-gp-induced cells by monoclonal P-gp antibody (**Figure 3b**). **Figure 3c** and **d** show the normal and P-gp-induced cells after 24 h of treatment with EtOH (25 mM). There is no change in the appearance of normal and P-gp-induced cells after treatment with 25 mM EtOH. However, by increasing EtOH concentration to 50 mM, a clear decrease in the number of cells with distinct P-gp localization was observed (**Figure 3f**).

**SWATH-MS.** Two P-gp digested peptides including K.LVTMQTAGNEVELENAADESK.S and K.GTQLSGGQK.Q were recognized and normalized according to the trypsin digested β-galactosidase intensity and total protein content. The cellular position of each peptide has been shown in **Figure 4**. **Table 2** shows the abundance of six efflux transporters in 25, 50, and 100 mM EtOH-treated cells to the control group. According to the results, no significant difference was observed in the abundance of P-gp in control versus EtOH treated normal Caco-2 cells after 4 and 24 h of treatment (**Table 2**). Similarly, MRP-2, MRP-3, and MRP-4 showed signs of reduced expression in EtOH-treated groups versus control (**Table 2**).

**Calcein-AM Functional Assay.** To investigate the effect of EtOH on the functionality of P-gp, Calcein-AM assay was conducted to ensure the remained fluorescent yield of calcein inside the cells. **Figure 5** shows the relative fluorescent yield of calcein remained inside the P-gp induced Caco-2 cells after 4 and 24 h treatment with different EtOH concentrations (0–100 mM). Results indicated that the functionality of P-gp was decreased after treatment of cells with EtOH for 4 and 24 h. According to **Figure 5**, after (4 h) treatment of P-gp induced cells with 25 mM EtOH, the fluorescent yield of calcein was 29.3 ± 14.05% higher than that in control group.

Meanwhile, the calcein fluorescent yield was 49.5 ± 10.3% higher than that in buffer-treated cells after 24 h of incubation with EtOH (**Figure 5**). The fluorescent yield of calcein at higher EtOH concentrations (50 and 100 mM) was not dramatically changed compare to the 25 mM. It suggests that at 25 mM concentration, the inhibitory effect of EtOH on P-gp was nearly saturated and increased EtOH concentration did not further affect the P-gp functionality.

**Tal and PF-57 Transport.** To evaluate the functionality of P-gp in normal and P-gp induced Caco-2 cells, Tal and PF-57 transport assays were conducted in the presence and absence of P-gp inhibitor (verapamil, 200 µM). $P_{app\ (AP-BL)}$ and $P_{app\ (BL-AP)}$ as well as UR and ER were measured for Tal and results are shown in **Table 1**. No significant difference was observed in Tal $P_{app\ (AP-BL)}$, $P_{app\ (BL-AP)}$, UR, and ER in normal Caco-2 cells in the presence and absence of verapamil. However, in the presence of verapamil, Tal $P_{app\ (BL-AP)}$ and ER in P-gp induced Caco-2 cells were lower than that in absence of verapamil. Similarly, there was no difference in ER of PF-57 in the presence and absence of verapamil (ER <2). According to the **Table 1**, the ER of PF-57 in P-gp induced Caco-2 cells was 7.1 ± 0.6 (ER>2) that proves PF-57 is a P-gp substrate. The ER of PF-57 was dropped to 1.7 ± 0.1 in the presence of verapamil.

**Figure 6a and b** show the ER of Tal and PF-57 in the presence and absence of verapamil (200 µg/mL), respectively. In these experiments, the P-gp induce Caco-2 cells were treated with different EtOH concentrations (0–100 mM) for 24 h. Results show that ER of Tal and PF-57 was significantly (P = 0.002) decreased in the presence of verapamil (**Figure 6a** and **b**). Moreover, P-gp induced Caco-2 cells treated with 50 mM EtOH showed significant decrease in ER of Tal in the presence of P-gp inhibitor

(P = 0.04) compare to the control group. Further, the ER of PF-57 did not show any significant changes by increasing EtOH concentration (**Figure 6b**).

## DISCUSSION

The mitochondrial toxicity of alcohol was examined after 24, 48, and 72 h treatment of Caco-2 cells with different EtOH concentrations. Results showed that no significant cell toxicity was induced by EtOH at clinically relevant concentrations in GI tract. Rubbens *et al* has reported the EtOH concentrations in human GI tract after ingestion of common alcoholic beverages.[43, 44] They have shown that the maximum duodenal concentration of EtOH after beer (500 mL, 866 mM), wine (200 mL, 1832 mM), and whisky (80 mL, 6662 mM) intake was 233, 233, and 300 mM, respectively.[44] According to our results and the experimentally measured EtOH concentrations, no significant cell toxicity is expected to be arisen from drinking alcohol in human GI tract.

To investigate the effect of drinking alcohol on the expression and functionality of P-gp, vinblastine was used to induce the expression of P-gp in Caco-2 cells.[45] Shirsaka and co-workers had previously explored that the mRNA level of P-gp in P-gp induced Caco-2 cells (vinblastine-induced cells) is approximately five times higher than that in normal Caco-2 cells.[46] Moreover, the increased expression level of P-gp was reported in other works at mRNA and protein levels.[39, 47, 48] In our study, the effect of vinblastine on paracellular integrity of P-gp induced Caco-2 cells was compared to the normal cells before and after EtOH treatment. Comparison of TEER values in normal and P-gp induced Caco-2 cells clearly showed that the integrity of

vinblastine-induced Caco-2 cell was enhanced compared to the normal cells. The higher TEER for vinblastine-induced Caco-2 cell versus normal cells was comparable to the previously reported data.[49] Furthermore, in both normal and P-gp induced Caco-2 cells, EtOH treatments resulted in decreased paracellular integrity and lowering TEER values compared to the control. The reduction in TEER values by EtOH and its major metabolite acetaldehyde in Caco-2 cells was extensively reported, previously.[50-53]

To visualize the expression of P-gp in normal and P-gp induced Caco-2 cells, the IF images of normal and P-gp induced Caco-2 cells were compared before and after EtOH treatment. Immunohistochemistry studies of normal and P-gp induced Caco-2 cells illustrated the higher expression of P-gp in P-gp induced Caco-2 cells compare to the normal cells. Moreover, EtOH treatment studied showed that increasing EtOH concentration from 25 to 50 mM resulted in decreased expression of P-gp. The disappearance of red color (indicated for P-gp) around the DAPI stained nuclei mentioned the reduction of P-gp expression.

SWATH-MS proteomics was used to verify any probable changes induced by EtOH (50 mM) in the expression of P-gp peptides. According to the obtained results, the expression level of the most efflux transporters including MDR-1, MRP-2, MRP-3, and MRP-4 were decreased in EtOH-treated P-gp induced Caco-2 cells but not significantly. The role of EtOH in molecular induction or inhibition of transporters might be helpful to describe the EtOH effects on transporters expression. Geick and co-workers has investigated for the first time that nuclear receptor PXR (pregnane X receptor) is involved in xenobiotic induction of MDR-1.[54] More recently, Choi and

coworkers has shown that chronic EtOH ingestion significantly upregulated hepatic *Pxr* and constitutive androstane activated receptor (*car*) mRNA expression in binge mice models[55]. According to the current study and the previous findings about EtOH effects on the induction of P-gp, it could be hypothesized that induction of nuclear receptors does not necessarily translate to protein expression.

The functionality of P-gp in transport of Tal was investigated in P-gp induced Caco-2 cells. The ER of Tal was significantly decreased at 50 mM EtOH after 24 h treatment in the presence verapamil. However, the decrease in ER of Tal was not observed in the absence of verapamil. The effect of EtOH on P-gp activity in *in vivo* bioavailability of paclitaxel (P-gp substrate) was investigated previously by Fisher and co-workers.[52] They concluded that the increased bioavailability of paclitaxel in the presence of EtOH did not arise from EtOH and/or acetaldehyde effect on P-gp; however, EtOH-induced perturbation in TJs could be the reason. In our study, EtOH significantly decreased the ER of Tal in the presence of P-gp inhibitor. Meanwhile, in the absence of verapamil, the ER was insignificantly increased. According to the transport results, it could be hypothesized that EtOH decreased the AP-BL transport of Tal, which was resulted in increased ER. However, neither the ER, nor the AP-BL transports of PF-57 were affected by EtOH treatment. Probably, the different drugs binding sites on the P-gp describe this discrimination in EtOH-induced difference in transport.

## CONCLUSION

In this study, the effect of clinically relevant EtOH concentrations on the expression and functionality of P-gp was explored in Caco-2 cell monolayer. IF images showed that the abundance of P-gp decreased by increasing EtOH concentration and treatment time. Moreover, SWATH-MS proteomics approach showed that the abundance of P-gp polypeptides was diminished after treatment of normal and P-gp induced Caco-2 cells with EtOH for 4 and 24 h. Moreover, Calcein-AM assay showed that by increasing the time and concentration of EtOH, the efflux activity of P-gp was reduced in P-gp induced Caco-2 cells. Furthermore, to evaluate the effect of EtOH on P-gp efflux functionality, ER of Tal was measured to show if EtOH treatment at different concentrations affects the Tal efflux. According to the results, EtOH decreased the P-gp efflux activity in the presence of verapamil.

**Acknowledgement**

This work was supported by grant number 1UH3TR000963 (PIs: Akhlaghi and Leggio) from the National Center for Advancing Translational Sciences (NCATS), National Institutes of Health (NIH).

**Table II- 1.** Transport parameters of talinolol (Tal) and PF-57 conducted in normal and P-gp induced Caco-2 monolayers

| Probe Drug | Inhibitor (verapamil, 200 µM) | Normal Caco-2 | | | | P-gp induced Caco-2 | | | |
|---|---|---|---|---|---|---|---|---|---|
| | | $P_{app\ (AP-BL)}$ ($\times 10^{-6}$ cm/s) | $P_{app\ (BL-AP)}$ ($\times 10^{-6}$ cm/s) | UR | ER | $P_{app\ (AP-BL)}$ ($\times 10^{-6}$ cm/s) | $P_{app\ (BL-AP)}$ ($\times 10^{-6}$ cm/s) | UR | ER |
| Tal | + | 5.5 ± 3.3 | 16.1 ± 1.8 | 0.3 ± 0.01 | 2.8 ± 1.2 | 2.1 ± 0.8 | 6.8 ± 2.9 | 0.1 ± 0.01 | 3.2 ± 0.7 |
| | – | 5.4 ± 0.3 | 15.1 ± 6.6 | 0.3 ± 0.2 | 2.7 ± 0.6 | 0.86 ± 0.02 | 11.7 ± 1.1 | 0.07 ± 0.05 | 13.5 ± 1.1 |
| PF-57 | + | 14.3 ± 1.1 | 27.1 ±3.6 | 0.5 ± 0.1 | 1.9 ± 0.2 | 12.6 ± 0.4 | 22.4 ± 2.8 | 0.6 ±.04 | 1.7 ± 0.1 |
| | – | 6.6 ± 0.3 | 11.4 ± 0.4 | 0.5 ±0.01 | 1.7 ± 0.03 | 3.1 ± 0.3 | 21.8 ± 0.5 | 0.1 ± 0.01 | 7.1 ± 0.6 |

Apical to basolateral apparent permeability ($P_{app\ (AP-BL)}$) and basolateral to apical apparent permeability ($P_{app\ (BL-AP)}$) as well as uptake ratio (UR) and efflux ratio (ER) across normal and P-gp induced Caco-2 cell lines are shown for Tal. Based on the reported data, ER of Tal was increased in P-gp induced Caco-2 cells, in which P-gp is overexpressed. All experiments were done in triplicate and data were shown as Mean ± Standard Error of Mean (Mea ± SEM, $n = 3$).

**Table II- 2**. Expression level of efflux transporters at the apical side of normal and P-gp induced Caco-2 cells analyzed by SWATH-MS proteomics.

| Proteins | EtOH Treatments | Normalized protein abundance (Intensity/µg total protein) | | | |
|---|---|---|---|---|---|
| | | 4 h treatment | | 24 h treatment | |
| | | Normal Caco-2 | P-gp Induced Caco-2 | Normal Caco-2 | P-gp Induced Caco-2 |
| MDRI | 0 (Control) | 0.19 | 0.41 | 0.17 | 0.21 |
| | | 0.31 | – | 0.22 | – |
| | 25 | 0.22 | 0.25 | 0.14 | 0.22 |
| | | 0.19 | 0.05 | 0.11 | 0.11 |
| | 50 | 0.19 | – | 0.20 | 0.17 |
| | | 0.19 | 0.08 | 0.16 | 0.10 |
| | 100 | 0.14 | 0.10 | 0.12 | – |
| | | – | 0.11 | 0.10 | – |
| BCRP | 0 (Control) | 0.25 | 0.24 | 0.26 | 0.11 |
| | | 0.44 | | 0.35 | |
| | 25 | 0.36 | 0.23 | 0.32 | 0.15 |
| | | 0.26 | 0.05 | 0.22 | 0.09 |
| | 50 | 0.12 | | 0.38 | 0.30 |
| | | 0.33 | 0.12 | 0.26 | 0.15 |
| | 100 | 0.24 | 0.16 | 0.25 | – |
| | | | 0.14 | 0.14 | – |
| MRP1 | 0 (Control) | 0.04 | 0.13 | 0.05 | 0.05 |
| | | 0.09 | – | 0.08 | – |
| | 25 | 0.10 | 0.16 | 0.10 | 0.12 |
| | | 0.06 | 0.03 | 0.05 | 0.04 |
| | 50 | 0.09 | – | 0.12 | 0.10 |
| | | 0.07 | 0.05 | 0.06 | 0.07 |
| | 100 | 0.08 | 0.13 | 0.10 | – |
| | | 0.04 | 0.05 | 0.05 | – |
| MRP2 | 0 (Control) | 0.04 | 0.13 | 0.05 | 0.10 |
| | | 0.09 | – | 0.05 | – |
| | 25 | 0.05 | 0.09 | 0.04 | 0.13 |
| | | 0.03 | 0.04 | 0.03 | – |
| | 50 | 0.09 | – | 0.06 | 0.06 |
| | | 0.03 | 0.03 | 0.03 | 0.03 |
| | 100 | 0.04 | 0.06 | 0.06 | – |
| | | – | 0.02 | 0.04 | – |
| MRP3 | 0 (Control) | 0.12 | 0.33 | 0.18 | 0.20 |
| | | 0.16 | – | 0.23 | – |
| | 25 | 0.19 | 0.32 | 0.15 | 0.24 |
| | | 0.09 | – | 0.15 | – |
| | 50 | 0.17 | – | 0.17 | 0.15 |
| | | 0.11 | 0.07 | 0.09 | 0.15 |

**Table II– 2**. Expression level of efflux transporters at the apical side of normal and P–gp induced Caco-2 cells analyzed by SWATH-MS proteomics.

| Proteins | EtOH Treatments (mM) | Normalized protein abundance (intensity/µg total protein) | | | |
|---|---|---|---|---|---|
| | | 4 h treatment | | 24 h treatment | |
| | | Normal Caco-2 | P-gp Induced Caco-2 | Normal Caco-2 | P-gp Induced Caco-2 |
| MRP3 | 100 | 0.11 | 0.17 | 0.10 | – |
| | | – | 0.08 | 0.07 | – |
| MRP4 | 0 (Control) | 0.04 | 0.18 | 0.08 | 0.13 |
| | | 0.10 | – | 0.05 | – |
| | 25 | 0.09 | 0.16 | 0.06 | 0.17 |
| | | 0.07 | 0.03 | – | 0.03 |
| | 50 | 0.09 | – | 0.07 | 0.05 |
| | | 0.07 | 0.04 | 0.05 | 0.04 |
| | 100 | 0.04 | 0.06 | 0.05 | – |
| | | – | 0.05 | 0.05 | – |

**MDR1:** Multidrug resistance protein 1, **BCRP:** Breast cancer resistance protein, **MRP1:** Multidrug resistance-associated protein 1, **MRP2:** Multidrug resistance-associated protein 2, **MRP3:** Multidrug resistance-associated protein 3, **MRP4:** Multidrug resistance-associated protein 4.

**Figure II-1**

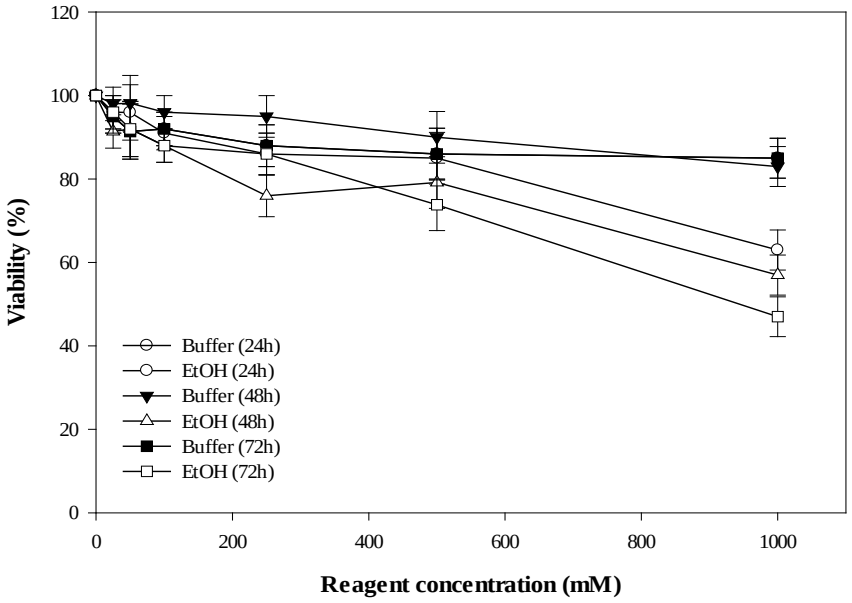


**Figure II- 1**. The water-soluble tetrazolium salt (WST-1) cytotoxicity assay
WST-1 was conducted for Caco-2 cells treated with different EtOH concentrations (0–1000 mM) for 24, 48, and 72 h. Data are shown as Mean ± Standard Error of Mean (Mean ± SEM). No significant cytotoxicity was observed for clinically relevant EtOH concentrations (<400 mM) for 24 h.

**Figure II- 2**

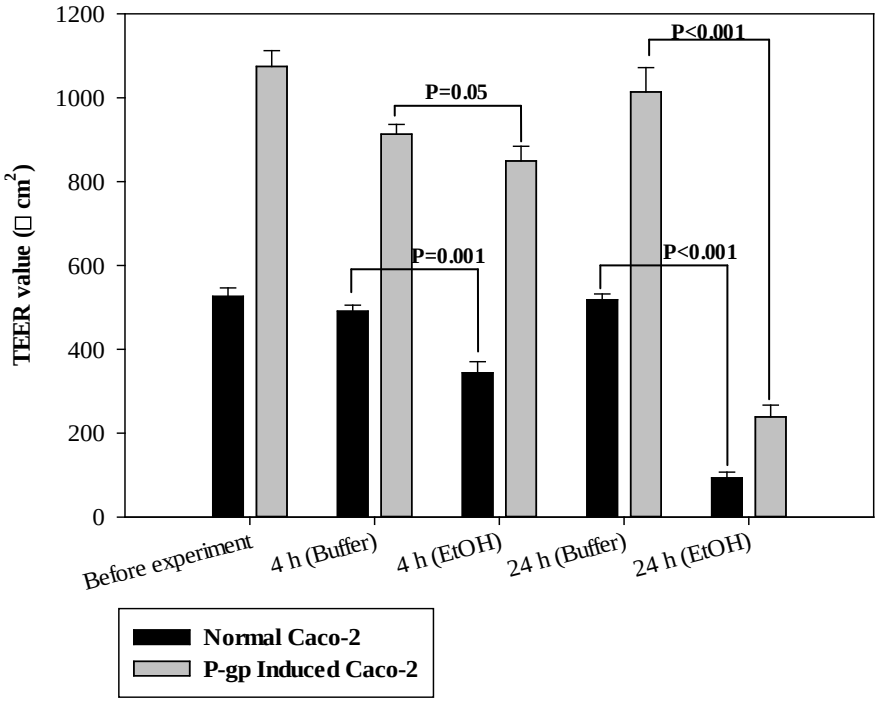


**Figure II- 2**. The Transepithelial Electrical Resistance (TEER) values for normal and P-gp induced Caco-2 cells.
TEER values were compared after 4 and 24 h of EtOH treatments. The TEER value of normal Caco-2 cells was significantly decreased after 4 h of treatment with 50 mM EtOH compared to the control group. The TEER values of normal and P-gp induced Caco-2 cells were significantly decreased after 24 h of treatment with the same EtOH concentration compared to the control group. Experiments were done in triplicate and data are shown as Mean ± Standard Error of Mean (Mean ± SEM).

**Figure II- 3**

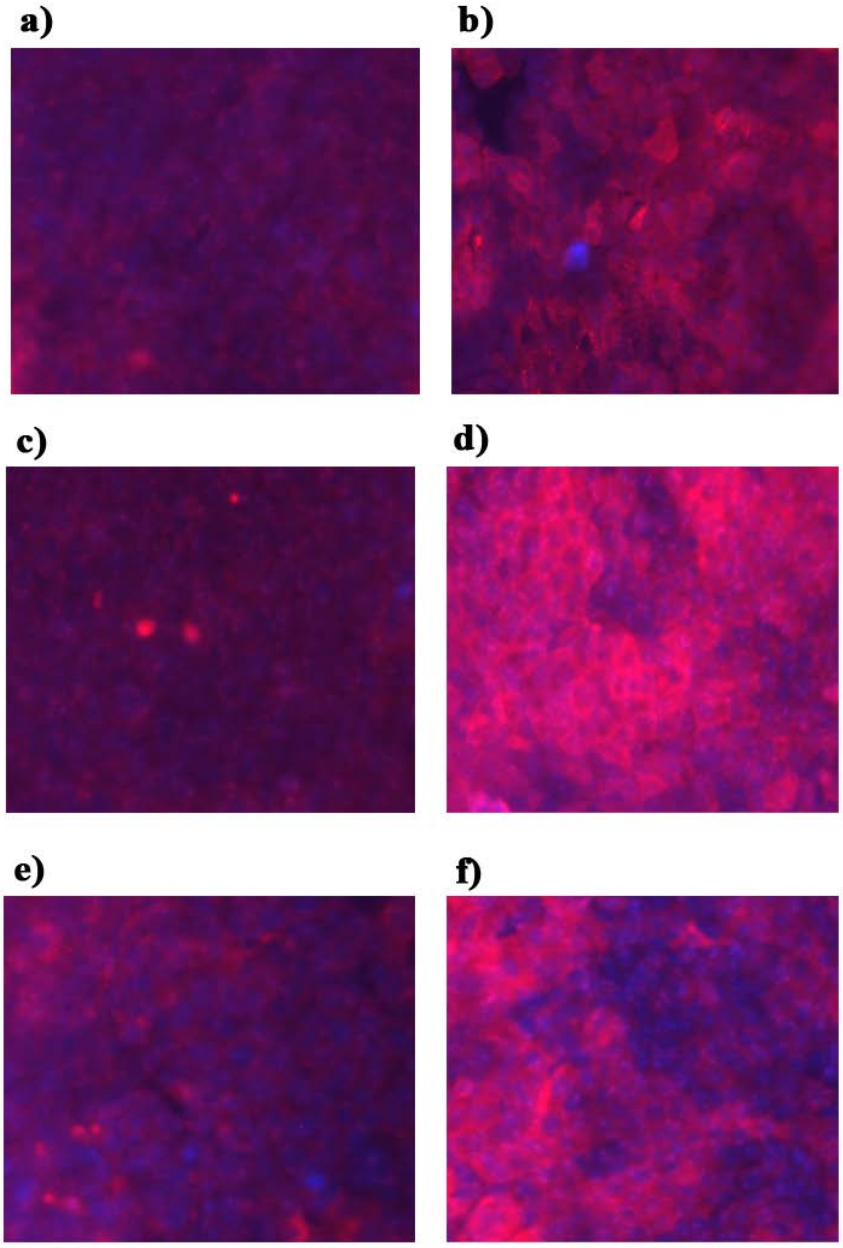


**Figure II- 3**. Immunofluorescent (IF) images of normal and P-gp induced Caco-2 cells treated with ethanol (EtOH) for 24 h.
Panels **a)** and **b)** show the immunofluorescent (IF) images of normal and P-gp-induced Caco-2 monolayer in the absence of EtOH, respectively. **c)** Shows the normal cells treated with 25 mM EtOH and **d)** illustrates the P-gp-induced cells treated with EtOH (25 mM) for 24 h. Panels **e)** and **f)** indicate the normal and P-gp-induced cells, respectively, 24 h after treatment with 50 mM EtOH.

**Figure II- 4**

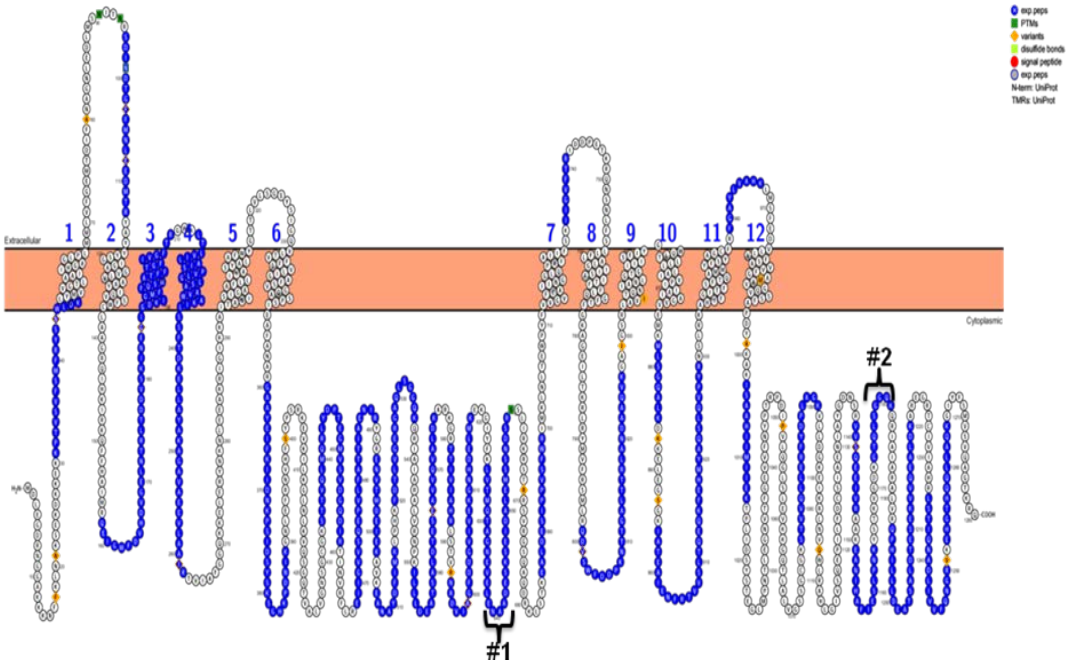


**Figure II- 4**. The cellular localization of P-glycoprotein (P-gp) and the quantified peptides.
Two peptides including K.LVTMQTAGNEVELENAADESK.S (#1) and K.GTQLSGGQK.Q (#2) are illustrated.

**Figure II- 5**

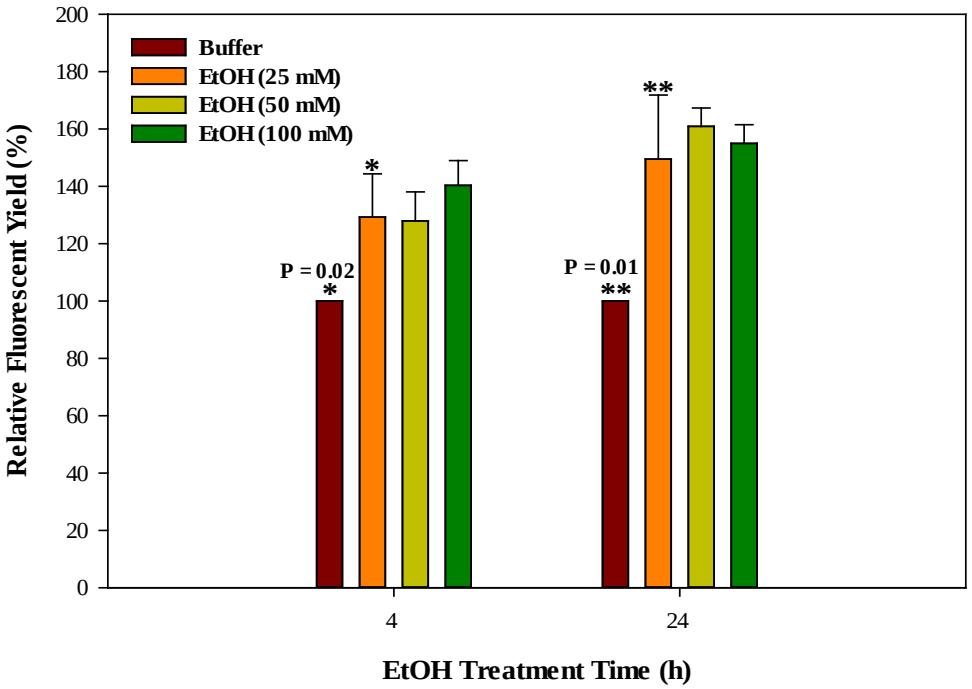


**Figure II- 5**. Fluorescent yield of Calcein in P-gp induced Caco-2 cells after treatment with ethanol (EtOH).
Fluorescent yield of Calcein in P-gp induced Caco-2 cells were measured after treatment with different EtOH concentrations (0–100 mM) for 4 and 24 h. The concentration dependent increase in calcein fluorescent yield proved to 25 mM EtOH and no significant increase observed in higher EtOH concentrations. Date are shown as Mean ± Standard Error of Mean (Mean ± SEM, $n$ = 3) and P-value <0.05 considered significant.

**Figure II- 6**

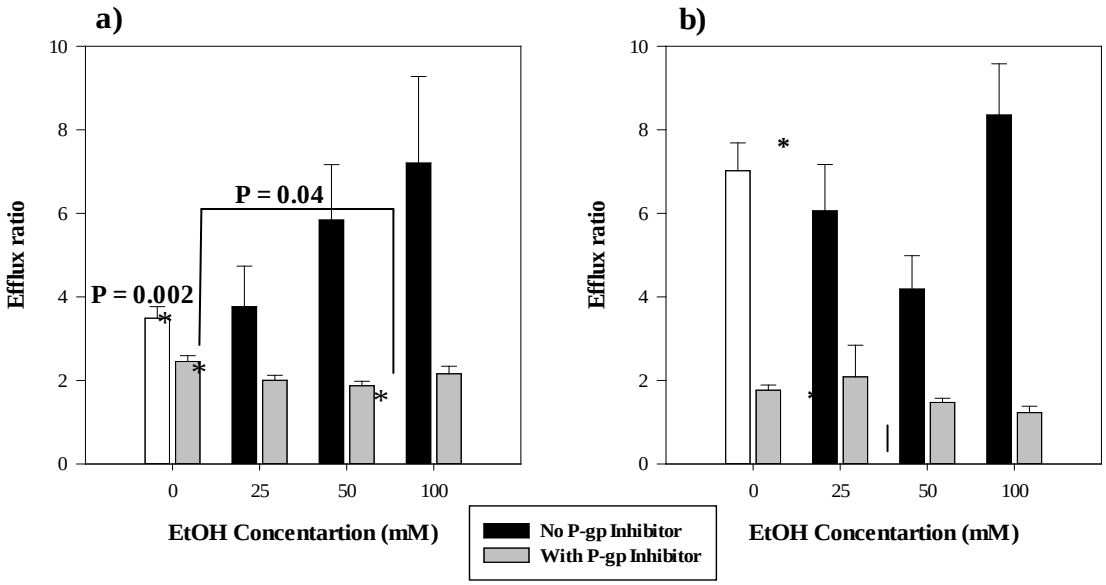


**Figure II- 6**. The effect of ethanol (EtOH) on the efflux ratio of talinolol (Tal) and PF-5190457 (PF-57) in the presence and absence of P-gp inhibitor.
**a)** ER of Tal and **b)** PF-57 in the presence and absence of verapamil (200 µg/mL) after treatment of P-gp induce Caco-2 cells with different EtOH concentrations (0–100 mM) for 24 h. Results show that ER of Tal and PF-57 was significantly (P = 0.002) decreased in the presence of verapamil (P-gp inhibitor). Moreover, P-gp induced Caco-2 cells treated with 50 mM EtOH showed significant decrease in ER of Tal in the presence of P-gp inhibitor (P = 0.04) compare to the control group. Data are shown as Mean ± Standard Error of Mean (SEM, *n* = 3) and P-values <0.05 considered significant.

**References**


1. Jedinger, N.; Khinast, J.; Roblegg, E. The design of controlled-release formulations resistant to alcohol-induced dose dumping–a review. *Eur. J. Pharm. Biopharm*. **2014,** *87*, (2), 217-226.
2. Lennernas, H. Ethanol-drug absorption interaction: potential for a significant effect on the plasma pharmacokinetics of ethanol vulnerable formulations. *Mol Pharm* **2009,** *6*, (5), 1429-40.
3. D'Souza, S.; Mayock, S.; Salt, A. A review of in vivo and in vitro aspects of alcohol-induced dose dumping. *AAPS Open* **2017,** *3*, (1), 5.
4. Cvijić, S.; Aleksić, I.; Ibrić, S.; Parojčić, J. Assessing the risk of alcohol-induced dose dumping from sustained-release oral dosage forms: in vitro–in silico approach. *Pharmaceutical development and technology* **2017**, 1-12.
5. Murray, S.; Wooltorton, E. Alcohol-associated rapid release of a long-acting opioid. *CMAJ* **2005,** *173*, (7), 756.
6. Guidance, D. Guidance for Industry. *Center for Biologics Evaluation and Research (CBER)* **1996**.
7. Crean, C. S.; Tompson, D. J. The effects of ethanol on the pharmacokinetics, pharmacodynamics, safety, and tolerability of ezogabine (retigabine). *Clin Ther* **2013,** *35*, (1), 87-93.
8. Midde, N. M.; Sinha, N.; Lukka, P. B.; Meibohm, B.; Kumar, S. Alterations in cellular pharmacokinetics and pharmacodynamics of elvitegravir in response to ethanol exposure in HIV-1 infected monocytic (U1) cells. *PLOS ONE* **2017,** *12*, (2), e0172628.
9. Johnson, B. A.; Seneviratne, C., Chapter 31 - Alcohol–medical drug interactions. In *Handbook of Clinical Neurology*, Sullivan, E. V.; Pfefferbaum, A., Eds. Elsevier: 2014; Vol. 125, pp 543-559.
10. Fagerberg, J. H.; Sjögren, E.; Bergström, C. A. S. Concomitant intake of alcohol may increase the absorption of poorly soluble drugs. *European Journal of Pharmaceutical Sciences* **2015,** *67*, 12-20.
11. Chan, L.-N.; Anderson, G. D. Pharmacokinetic and pharmacodynamic drug interactions with ethanol (alcohol). *Clinical pharmacokinetics* **2014,** *53*, (12), 1115-1136.
12. Artursson, P.; Palm, K.; Luthman, K. Caco-2 monolayers in experimental and theoretical predictions of drug transport1PII of original article: S0169-409X(96)00415-2. The article was originally published in Advanced Drug Delivery Reviews 22 (1996) 67–84.1. *Advanced Drug Delivery Reviews* **2001,** *46*, (1), 27-43.
13. Hidalgo, I. J.; Raub, T. J.; Borchardt, R. T. Characterization of the human colon carcinoma cell line (Caco-2) as a model system for intestinal epithelial permeability. *Gastroenterology* **1989,** *96*, (3), 736-749.
14. Artursson, P.; Palm, K.; Luthman, K. Caco-2 monolayers in experimental and theoretical predictions of drug transport. *Advanced drug delivery reviews* **2001,** *46*, (1-3), 27-43.
15. Ghaffarian, R.; Muro, S. Models and Methods to Evaluate Transport of Drug Delivery Systems Across Cellular Barriers. *Journal of visualized experiments : JoVE* **2013**, (80), e50638-e50638.

16. Anderle, P.; Niederer, E.; Rubas, W.; Hilgendorf, C.; Spahn-Langguth, H.; Wunderli-Allenspach, H.; Merkle, H. P.; Langguth, P. P-Glycoprotein (P-gp) Mediated Efflux in Caco-2 Cell Monolayers: The Influence of Culturing Conditions and Drug Exposure on P-gp Expression Levels. *Journal of Pharmaceutical Sciences* **1998,** *87*, (6), 757-762.
17. Leonard, G. D.; Fojo, T.; Bates, S. E. The role of ABC transporters in clinical practice. *The oncologist* **2003,** *8*, (5), 411-424.
18. Robey, R. W.; Pluchino, K. M.; Hall, M. D.; Fojo, A. T.; Bates, S. E.; Gottesman, M. M. Revisiting the role of ABC transporters in multidrug-resistant cancer. *Nature Reviews Cancer* **2018**.
19. Juliano, R. L.; Ling, V. A surface glycoprotein modulating drug permeability in Chinese hamster ovary cell mutants. *Biochim Biophys Acta* **1976,** *455*, (1), 152-62.
20. Thiebaut, F.; Tsuruo, T.; Hamada, H.; Gottesman, M. M.; Pastan, I.; Willingham, M. C. Cellular localization of the multidrug-resistance gene product P-glycoprotein in normal human tissues. *Proceedings of the National Academy of Sciences* **1987,** *84*, (21), 7735-7738.
21. Krawczenko, A.; Bielawska-Pohl, A.; Wojtowicz, K.; Jura, R.; Paprocka, M.; Wojdat, E.; Kozłowska, U.; Klimczak, A.; Grillon, C.; Kieda, C.; Duś, D. Expression and activity of multidrug resistance proteins in mature endothelial cells and their precursors: A challenging correlation. *PLOS ONE* **2017,** *12*, (2), e0172371.
22. Roy, S.; Kenny, E.; Kennedy, S.; Larkin, A.; Ballot, J.; De Villarreal, M. P.; Crown, J.; O'DRISCOLL, L. MDR1/P-glycoprotein and MRP-1 mRNA and protein expression in non-small cell lung cancer. *Anticancer research* **2007,** *27*, (3A), 1325-1330.
23. Blokzijl, H.; Vander Borght, S.; Bok, L. I.; Libbrecht, L.; Geuken, M.; van den Heuvel, F. A.; Dijkstra, G.; Roskams, T. A.; Moshage, H.; Jansen, P. L.; Faber, K. N. Decreased P-glycoprotein (P-gp/MDR1) expression in inflamed human intestinal epithelium is independent of PXR protein levels. *Inflamm Bowel Dis* **2007,** *13*, (6), 710-20.
24. McInerney, M. P.; Pan, Y.; Short, J. L.; Nicolazzo, J. A. Development and Validation of an In-Cell Western for Quantifying P-Glycoprotein Expression in Human Brain Microvascular Endothelial (hCMEC/D3) Cells. *Journal of pharmaceutical sciences* **2017,** *106*, (9), 2614-2624.
25. Prasad, B.; Unadkat, J. D. Optimized approaches for quantification of drug transporters in tissues and cells by MRM proteomics. *The AAPS journal* **2014,** *16*, (4), 634-648.
26. Zhang, J.-C.; Xie, F.; Yu, X.-H.; Deng, Z.-Y.; Wang, Y.; Liang, P.; Sun, L.; Zhang, F.-X. Expression levels of P-glycoprotein in peripheral blood CD8+ T lymphocytes from HIV-1-infected patients on antiretroviral therapy. *International journal of molecular medicine* **2014,** *33*, (2), 431-440.
27. Hogg, K.; Thomas, J.; Ashford, D.; Cartwright, J.; Coldwell, R.; Weston, D. J.; Pillmoor, J.; Surry, D.; O'Toole, P. Quantification of proteins by flow cytometry: quantification of human hepatic transporter P-gp and OATP1B1 using flow cytometry and mass spectrometry. *Methods* **2015,** *82*, 38-46.

28. Greiner, B.; Eichelbaum, M.; Fritz, P.; Kreichgauer, H.-P.; von Richter, O.; Zundler, J.; Kroemer, H. K. The role of intestinal P-glycoprotein in the interaction of digoxin and rifampin. *The Journal of Clinical Investigation* **1999,** *104*, (2), 147-153.
29. Ong, S.-E.; Mann, M. Mass spectrometry–based proteomics turns quantitative. *Nature chemical biology* **2005,** *1*, (5), 252.
30. Bantscheff, M.; Schirle, M.; Sweetman, G.; Rick, J.; Kuster, B. Quantitative mass spectrometry in proteomics: a critical review. *Analytical and bioanalytical chemistry* **2007,** *389*, (4), 1017-1031.
31. Han, X.; Aslanian, A.; Yates, J. R. Mass Spectrometry for Proteomics. *Current opinion in chemical biology* **2008,** *12*, (5), 483-490.
32. Zhu, F.-Y.; Chen, M.-X.; Su, Y.-W.; Xu, X.; Ye, N.-H.; Cao, Y.-Y.; Lin, S.; Liu, T.-Y.; Li, H.-X.; Wang, G.-Q.; Jin, Y.; Gu, Y.-H.; Chan, W.-L.; Lo, C.; Peng, X.; Zhu, G.; Zhang, J. SWATH-MS Quantitative Analysis of Proteins in the Rice Inferior and Superior Spikelets during Grain Filling. *Frontiers in Plant Science* **2016,** *7*, 1926.
33. Tan, H.-Y.; Trier, S.; Rahbek, U. L.; Dufva, M.; Kutter, J. P.; Andresen, T. L. A multi-chamber microfluidic intestinal barrier model using Caco-2 cells for drug transport studies. *PLOS ONE* **2018,** *13*, (5), e0197101.
34. Hubatsch, I.; Ragnarsson, E. G.; Artursson, P. Determination of drug permeability and prediction of drug absorption in Caco-2 monolayers. *Nature protocols* **2007,** *2*, (9), 2111-9.
35. Glavinas, H.; von Richter, O.; Vojnits, K.; Mehn, D.; Wilhelm, I.; Nagy, T.; Janossy, J.; Krizbai, I.; Couraud, P.; Krajcsi, P. Calcein assay: a high-throughput method to assess P-gp inhibition. *Xenobiotica* **2011,** *41*, (8), 712-719.
36. Holló, Z.; Homolya, L.; Davis, C. W.; Sarkadi, B. Calcein accumulation as a fluorometric functional assay of the multidrug transporter. *Biochimica et Biophysica Acta (BBA)-Biomembranes* **1994,** *1191*, (2), 384-388.
37. Miles, F. L.; Lynch, J. E.; Sikes, R. A. Cell-based assays using calcein acetoxymethyl ester show variation in fluorescence with treatment conditions. *Journal of biological methods* **2015,** *2*, (3).
38. Sadighi, A.; Ostad, S.; Rezayat, S.; Foroutan, M.; Faramarzi, M.; Dorkoosh, F. Mathematical modelling of the transport of hydroxypropyl-β-cyclodextrin inclusion complexes of ranitidine hydrochloride and furosemide loaded chitosan nanoparticles across a Caco-2 cell monolayer. *International journal of pharmaceutics* **2012,** *422*, (1-2), 479-488.
39. Chen, Q.; Bian, Y.; Zeng, S. Involvement of AP-1 and NF-kappaB in the up-regulation of P-gp in vinblastine resistant Caco-2 cells. *Drug metabolism and pharmacokinetics* **2014,** *29*, (2), 223-6.
40. Jamwal, R.; de la Monte, S. M.; Ogasawara, K.; Adusumalli, S.; Barlock, B. B.; Akhlaghi, F. Nonalcoholic fatty liver disease and diabetes is associated with decreased CYP3A4 protein expression and activity in human liver. *Molecular pharmaceutics* **2018**.
41. Jamwal, R.; Barlock, B. J.; Adusumalli, S.; Ogasawara, K.; Simons, B. L.; Akhlaghi, F. Multiplex and Label-Free Relative Quantification Approach for Studying Protein Abundance of Drug Metabolizing Enzymes in Human Liver Microsomes Using SWATH-MS. *Journal of proteome research* **2017,** *16*, (11), 4134-4143.

42. Ghareeb, M.; Leggio, L.; El-Kattan, A.; Akhlaghi, F. Development and validation of an UPLC-MS/MS assay for quantitative analysis of the ghrelin receptor inverse agonist PF-5190457 in human or rat plasma and rat brain. *Analytical and bioanalytical chemistry* **2015,** *407*, (19), 5603-5613.
43. Rubbens, J.; Brouwers, J.; Wolfs, K.; Adams, E.; Tack, J.; Augustijns, P. Ethanol concentrations in the human gastrointestinal tract after intake of alcoholic beverages. *European journal of pharmaceutical sciences* **2016,** *86*, 91-95.
44. Rubbens, J.; Riethorst, D.; Brouwers, J.; Wolfs, K.; Adams, E.; Tack, J.; Augustijns, P. Gastric and duodenal ethanol concentrations after intake of alcoholic beverages in postprandial conditions. *Molecular pharmaceutics* **2017,** *14*, (12), 4202-4208.
45. Shirasaka, Y.; Konishi, R.; Funami, N.; Kadowaki, Y.; Nagai, Y.; Sakaeda, T.; Yamashita, S. Expression levels of human P-glycoprotein in In Vitro cell lines: correlation between mRNA and protein levels for P-glycoprotein expressed in cells. *Biopharmaceutics & drug disposition* **2009,** *30*, (3), 149-152.
46. Shirasaka, Y.; Kawasaki, M.; Sakane, T.; Omatsu, H.; Moriya, Y.; Nakamura, T.; Sakaeda, T.; Okumura, K.; Langguth, P.; Yamashita, S. Induction of human P-glycoprotein in Caco-2 cells: development of a highly sensitive assay system for P-glycoprotein-mediated drug transport. *Drug metabolism and pharmacokinetics* **2006,** *21*, (5), 414-423.
47. Doppenschmitt, S.; Spahn-Langguth, H.; Regårdh, C. G.; Langguth, P. Role of P-glycoprotein-mediated secretion in absorptive drug permeabiity: An approach using passive membrane permeability and affinity to P-glycoprotein. *Journal of Pharmaceutical Sciences* **1999,** *88*, (10), 1067-1072.
48. Vine, K. L.; Belfiore, L.; Jones, L.; Locke, J. M.; Wade, S.; Minaei, E.; Ranson, M. N-alkylated isatins evade P-gp mediated efflux and retain potency in MDR cancer cell lines. *Heliyon* **2016,** *2*, (1), e00060.
49. Hellinger, É.; Bakk, M. L.; Pócza, P.; Tihanyi, K.; Vastag, M. Drug penetration model of vinblastine-treated Caco-2 cultures. *European Journal of Pharmaceutical Sciences* **2010,** *41*, (1), 96-106.
50. Dunagan, M.; Chaudhry, K.; Samak, G.; Rao, R. K. Acetaldehyde disrupts tight junctions in Caco-2 cell monolayers by a protein phosphatase 2A-dependent mechanism. *American Journal of Physiology-Gastrointestinal and Liver Physiology* **2012,** *303*, (12), G1356-G1364.
51. Elamin, E.; Jonkers, D.; Juuti-Uusitalo, K.; van Ijzendoorn, S.; Troost, F.; Duimel, H.; Broers, J.; Verheyen, F.; Dekker, J.; Masclee, A. Effects of Ethanol and Acetaldehyde on Tight Junction Integrity: In Vitro Study in a Three Dimensional Intestinal Epithelial Cell Culture Model. *PLoS ONE* **2012,** *7*, (4), e35008.
52. Fisher, S. J.; Swaan, P. W.; Eddington, N. D. The ethanol metabolite acetaldehyde increases paracellular drug permeability in vitro and oral bioavailability in vivo. *Journal of Pharmacology and Experimental Therapeutics* **2010,** *332*, (1), 326-333.
53. Ma, T. Y.; Nguyen, D.; Bui, V.; Nguyen, H.; Hoa, N. Ethanol modulation of intestinal epithelial tight junction barrier. *The American journal of physiology* **1999,** *276*, (4 Pt 1), G965-74.

54. Geick, A.; Eichelbaum, M.; Burk, O. Nuclear receptor response elements mediate induction of intestinal MDR1 by rifampin. *Journal of Biological Chemistry* **2001,** *276*, (18), 14581-14587.
55. Choi, S.; Gyamfi, A. A.; Neequaye, P.; Addo, S.; Gonzalez, F. J.; Gyamfi, M. A. Role of the Pregnane X Receptor in Binge Ethanol-Induced Steatosis and Hepatotoxicity. *Journal of Pharmacology and Experimental Therapeutics* **2018,** *365*, (1), 165-178.

## MANUSCRIPT III

This manuscript has been prepared for submission to the Journal of "*Biochimica et Biophysica Acta (BBA)-Biomembranes*"

# The Effect of Alcohol on Paracellular Barrier and Tight Junction Proteins in Caco-2 cell Monolayer

Armin Sadighi[a], Lorenzo Leggio[b, c], Fatemeh Akhlaghi[a*]

[a]Clinical Pharmacokinetics Research Laboratory, Department of Biomedical and Pharmaceutical Sciences, College of Pharmacy, University of Rhode Island, Kingston, RI, USA

[b]Section on Clinical Psychoneuroendocrinology and Neuropsychopharmacology, Laboratory of Clinical and Translational Studies, National Institute on Alcohol Abuse and Alcoholism, Bethesda, MD, USA

[c]Center for Alcohol and Addiction Studies, Department of Behavioral and Social Sciences,

Brown University, Providence, RI 02903, USA

---

[*]**Corresponding author:** Fatemeh Akhlaghi; Clinical Pharmacokinetics Research Laboratory; University of Rhode Island; Office 495 A; 7 Greenhouse Road; Kingston; RI 02881, USA. **Tel:** (401) 874 9205; **Fax:** (401) 874 5787; **Email:** fatemeh@uri.edu

**ABSTRACT**

In this study, the effect of clinically relevant ethanol (EtOH) concentrations on the organization of paracellular membrane proteins in Caco-2 cell monolayer was explored. Neither EtOH, nor its metabolite, acetaldehyde (AA), showed significant alteration in cell viability at concentrations found in GI tract. Transepithelial electrical resistance (TEER) assay showed that the paracellular hyper permeability of Caco-2 cells induced by EtOH and AA was reversible. Fluorescent Lucifer yellow (LY) permeation showed that paracellular transport of LY was enhanced after treatment of Caco-2 cells with EtOH. Transmission electron microscopy (TEM) images of EtOH-treated Caco-2 cells showed the disintegration of membrane proteins including tight junctions (TJs), adherent junctions (AJs), and desmosomes (DS). Moreover, the Sequential Windowed data independent Acquisition of the Total High-resolution Mass Spectra (SWATH-MS) proteomics was used to analyze the EtOH effects on paracellular proteins. SWATH-MS showed that the abundance of TJs, AJs, and DS were diminished after treatment of Caco-2 cells with EtOH for 4 and 24 h.

**KEYWORDS:** Ethanol (EtOH), acetaldehyde (AA), Caco-2 cell monolayer, tight junctions, adherence junction, TEER, SWATH-MS proteomics

**Abbreviation:**

**AA:** Acetaldehyde

**AD:** Adherense junction

**CDH17:** Cadherin-17

**CDH23:** Cadherin-23

**CTNA2:** Catenin alpha-2

**CTNB1:** Catenin beta-1

**DSC-1:** Desmocollin-1

**DSG 3:** Desmoglein-3

**DESP:** Desmoplakin

**DS:** Desmosomes

**EtOH:** Ethanol

**JAM:** Junctional adhesion molecule A

**OCLN:** Occludin

**SWATH-MS:** Sequential Windowed data independent Acquisition of the Total High-resolution Mass Spectra

**TEER:** Transepithelial electrical resistance

**TJ:** Tight junction proteins

**ZO-3:** Zonula occludens-3

## 1. Introduction

Alcohol affects the gastrointestinal (GI) epithelium by altering the integrity of epithelial cells [1]. GI tract is considered as the first line of body in contact with the highest concentration of ingested ethanol (EtOH). Furthermore, conversion of EtOH to its metabolite acetaldehyde (AA), which begins in upper parts of GI tract, enhances the harmful effects of EtOH [2]. Research show that chronic EtOH exposure results in intestinal hyper permeability (leaky gut) which has been implicated in inflammatory bowel disorders (IBDs) [3, 4]. The role of metabolites produced by gut microbiota has been investigated in alcohol-mediated liver diseases [5-7]. It has been evident that existence of a gut-liver-brain axis is important in EtOH-induced organ damage [8, 9]. Therefore, understanding the effect of alcohol on GI epithelium that plays a pivotal role in permeation of pro-inflammatory substances is crucial to avoid further damages in other organs. The effect of EtOH on intestinal paracellular barriers has been investigated *in vitro* and *in vivo* [10-12]. However, the relative quantification of paracellular proteins affected by EtOH exposure has not been elucidated.

The human colorectal adenocarcinoma cell line Caco-2 is widely used as a standard model for human intestinal epithelium [13, 14]. Intestinal epithelium consists of a single layer of epithelial cells lining the gut lumen with two main roles; First, avoiding the passage of unwanted and harmful substances and second, the absorption of essential nutrients. The intestinal epithelium mediates permeability through two different routes: transepithelial and paracellular [15]. Solute transporters at the apical side of epithelial cells are mainly responsible for transcellular permeation. The paracellular pathway consists of the intercellular protein complexes between the cells.

**Figure 1a** shows a schematic illustration of paracellular and transcellular pathways of absorption. **Figure 1b** demonstrates the localization of uptake and efflux transporters on apical (AP) and basolateral (BL) sides of epithelial cells. Moreover, paracellular proteins including tight junctions (TJs), adherens junctions (AJs), and desmosomes (DS) are depicted.

TJs form the intercellular barrier between epithelial cells that separate the tissue space from gut lumen and regulate the solutes permeation. TJs consists of more than 40 proteins such as claudins, junctional adhesion molecule A (JAM-A) and occludin. These transmembrane proteins are linked to the actin cytoskeleton by zonula occludens (ZO-1, ZO-2, and ZO-3). TJs are mainly located at the apical side of lateral membrane and are essential to form cells polarity an d mucosal barrier [16]. Like TJs, AJs provide extracellular cell contacts through initiation and stabilization of the cell-cell adhesion. AJs regulate the actin cytoskeleton and incorporate in intracellular signaling and regulation of transcription. E-cadherin, α-catenin, and β-catenin are the most well-known protein classes in AJs [17]. DS are intercellular junctional proteins contributing in strong adhesion between epithelial cells. Further, DS provide high mechanical strength in tissue because of their linkage to intermediate filament cytoskeleton [18]. Desmoplakin, desmogleins, and desmocollins are the most well-known DS that have been extensively identified in epidermal and epithelial cells [19, 20].

Enzyme-linked Immunosorbent Assay (ELISA) [21], flow cytometry [22], and immunoblotting (Western blotting) [23] methods are the most well-known methods for identification and quantification of proteins. However, those methods suffer from some limitations such as, low throughput performance, intensive laboring, applying

expensive antibodies, and low specificity. In contrast to those methods, mass spectrometry (MS) has gained a great demand in protein studies [24-26]. Among all MS-based proteomics methods, the Sequential Windowed data independent Acquisition of the Total High-resolution Mass Spectra (SWATH-MS) offers superior advantages, like high accuracy and reproducibility over the other MS approaches [27].

In the present study, the effect of EtOH on paracellular permeability of Caco-2 cell monolayer was analyzed. The cytotoxicity of EtOH and its major metabolite AA in Caco-2 cells was examined. Transepithelial electrical resistance (TEER) assay was used to determine the effect of EtOH and AA on opening of tight junctions. Transmission electron microscopy (TEM) was used to visualize the EtOH effect on paracellular proteins. The effect of EtOH and AA on paracellular transport of Lucifer yellow (LY) was investigated. Finally, SWATH-MS proteomics approach was used to find out if EtOH treatment can alter the expression level of TJs, AJs, and Ds in Caco-2 cells.

## 2. Material and methods

### *2.1. Chemical and Reagents*

Molecular biology grade EtOH and AA >99.5%, iodoacetamide (IAA), dithiothreitol (DTT), ammonium bicarbonate, and sodium deoxycholate were purchased from Sigma Aldrich (St. Louis, MO). RPMI 1640, Dulbecco's modified Eagle medium (DMEM), fetal bovine serum (FBS), and Pierce™ BCA protein assay kit were obtained from Thermo Fisher Scientific Inc (Waltham, MA, USA). ProteoExtract™ Native Membrane Protein Extraction Kit was obtained from EMD

Millipore (Billerica, MA). WST-1 (2-(4-iodophenyl)-3-(4-nitrophenyl)-5-(2,4-disulfophenyl)-2H-tetrazolium, monosodium salt) was purchased from Roche (Mannheim, Germany). Hank's balanced salt solution (HBSS), penicillin/streptomycin, and trypsin-EDTA (0.25%) were acquired from the American Type Culture Collection (ATCC, VA, USA). Optima™ LC-MS/MS grade of acetonitrile, methanol, and formic acid were purchased from Fisher Scientific (Fair Lawn, NJ, USA). Deionized water was obtained using a Milli-Q® Synthesis A10 system fitted with a Q-Gard 2 Purification Pack (Millipore, Bedford, MA, USA). Proteomics grade trypsin and trypsin-predigested β-galactosidase (originated from *Escherichia coli*) were purchased from SCIEX (Framingham, MA). All other reagents used in this study were of analytical grade.

*2.2. Cell Culture and EtOH Treatment*

Caco-2 cells (ATCC® HTB-37™, passage number 55–65) were kept at 37 °C and grown in 25-ml flasks in an incubator with a controlled, humidified atmosphere consisting of 5% $CO_2$ and 95% air. Cells were cultured in an enriched medium consists of RPMI-1640, DMEM, FBS and penicillin/streptomycin in a ratio of 50:35:15:1. The culture medium was changed every second days and cells were trypsinized by trypsin–EDTA (1%) after reaching 70–80% confluence. Caco-2 cells were seeded onto semi-permeable PET filter inserts (Corning Costar Corporation, Corning, NY) with 6.4 mm diameter, 0.33 $cm^2$ growth area, and 0.4 μm pore size. Each membrane of the 24-transwell permeable insert received 0.2 mL of a $3.2 \times 10^5$ cells/mL suspension and 0.6 mL culture medium into the wells. Caco-2 cells were

then grown and differentiated for 21 days. Medium changed every two days for the first two weeks and then every day until day 21 when a fully differentiated monolayer had achieved.

The effect of EtOH and AA on paracellular membrane proteins in normal and P-gp-induced (10 nM vinblastine-induced) Caco-2 monolayer was assessed. Briefly, the plates containing transwell inserts were put into chambers filled with 95% air, 5% $CO_2$ and kept in humid incubator at 37 °C. Various EtOH (25, 50, and 100 mM) and AA (100 µM) diluted in culture medium were added to the both apical and basolateral sides of cells. In each treatment, the atmosphere of chambers was saturated by the same concentration of EtOH and AA.

*2.3. Cytotoxicity Assay*

The cytotoxicity of EtOH and AA treatment on the Caco-2 cells was evaluated according to the colorimetric method using a water-soluble tetrazolium salt (WST-1). In this method, the cleavage of the tetrazolium salt to formazan by active cellular mitochondrial dehydrogenases indicates the viable cells. For this purpose, Caco-2 cells were seeded at a concentration of $2 \times 10^4$ cells/well in a 96-well plate for 2–3 days to achieve 70% confluence. The culture medium was removed and replaced by different EtOH (0–1000 mM) and AA (0–1000 µM) concentrations and placed in the corresponding chambers saturated with EtOH and AA vapor contained 95% air and 5% $CO_2$ and placed in incubator. Clotrimazol was used as a positive control at different concentrations (20, 40, 60, 80, and 100 µM). Cells were incubated for 24, 48, and 72 h at 37 °C in an incubator with a controlled atmosphere. At the end of

treatment, 10 µl of WST-1 was added to each well and incubated for 4 h at 37 °C. The absorbance of each well against background control was measured at 450 nm, while reference wavelength set at 650 nm.

*2.4. Transepithelial Electrical Resistance (TEER)*

TEER is widely used as a real-time, non-destructive, and label free method to characterize the quality of the epithelial or endothelial barrier function in cell monolayer. TEER assay was used as a real-time, non-destructive, and label free method to characterize the quality of the cell monolayer integrity. The TEER of the normal and P-gp-induced Caco-2 cell monolayers were evaluated by an EVOM$^2$ (World Precision Instruments, Sarasota, FL) equipped with STX2 "chopstick" silver/silver chloride (Ag/AgCl) electrodes. TEER comprises from four different resistance on cell membrane that has been mentioned in **Eq. 1.**

$$TEER = \frac{(R_a + R_b).(R_{tj} + R_{ic})}{(R_a + R_b) + (R_{tj} + R_{ic})} \quad (1)$$

Where, $R_a$ stands for apical cell membrane resistance, $R_b$ is basolateral cell membrane resistance, $R_{tj}$ represent for tight junction resistance, and $R_{ic}$ expresses the intercellular resistance [28].

TEER assay was performed 21-days post seeding of normal and vinblastine-treated Caco-2 cells on filter inserts. TEER measurements were done before starting of EtOH treatment as well as 4 and 24 h after alcohol exposure to the Caco-2 monolayers. The relative changes in TEER values before and after EtOH treatments were compared to that for buffer treatment, as the control group. TEER values were calculated according to the following equation **(Eq.2)**:

$$\text{TEER} = (R_{\text{monolayer}} - R_{\text{blank}}) \times A\ (\Omega\text{cm}^2), \quad (2)$$

where, $R_{\text{monolayer}}$ is the measured resistance of cell monolayer, $R_{\text{blank}}$ represents the resistance of filter inserts without cell monolayer, and $A$ is the available filter inserts surface area.

*2.5. Transmission electron microscopy (TEM)*

Caco-2 cell monolayers, grown on Transwell filter membranes, were fixed with 1.5% glutaraldehyde in 0.15 M sodium cacodylate buffer at 4 °C for several days. Fixative, as with all reagents listed below, was always applied to both the apical and basolateral chambers of the Transwell filter units. Following fixation, cells were rinsed in buffer and post-fixed in 1% osmium tetroxide for 1 hour at 4 °C. Cultures were buffer rinsed and dehydrated through a graded ethanol series. Ten minute changes were used for each ethanol step, 35, 50, 70, 80, 90, and 95% ethanol, all at 4 °C. Six changes, 10 min each, of absolute ethanol at room temperature served to completely dehydrate the sample. Infiltration was initiated by introducing a 1:1 mixture of ethanol and Epox 812 resin to the chambers. One 10 minute change of pure Epox 812 resin was followed by a fresh change and held for 1.5 hours at 37 °C. Finally, Transwell inserts were placed in the cut-off bulb end of a disposable transfer pipette, filled with fresh resin, and polymerized for 20 hours at 60 °C. A small rectangle of resin surrounding the filter membrane was cut out using a jeweler's saw, and trimmed for cross-sectioning of the filter membrane. Semi-thin sections (1μm) were prepared using a Reichert Ultracut S microtome (Leica Biosystems, Buffalo Grove, IL) stained with methylene blue-azure II and evaluated for areas of interest.

Ultra-thin sections (60 nm) were prepared and retrieved onto 200 mesh copper grids with formvar/carbon coating. Sections were contrasted with uranyl acetate and lead citrate stains. Sections were examined at 80 kV using a CM-10 electron microscope (FEI, Hillsboro, OR). Images were collected with a model 785 Erlangshen ES1000W CCD camera, using Digital Micrograph imaging software (version 1.71.38) (Gatan, Pleasanton, CA).

*2.6. LY Permeation through Caco-2 monolayer*

Permeation of LY, a fluorescent marker, used to verify tight junction integrity in Caco-2 monolayers. Caco-2 cells were seeded onto semi-permeable PET filter inserts (Corning Costar Corporation, Corning, NY) with 6.4 mm diameter, 0.33 $cm^2$ growth area, and 0.4 μm pore size. Prior to monitoring flux through the paracellular pathway, mature Caco-2 cell monolayers (21-day seeded on filter insert) and non-mature (10-day seeded on filter insert) were washed twice with pre-warmed HBSS medium (pH 7.4). After washing, the permeation experiments were done by adding LY (0.5 mg/mL) to the apical side (AP, 200 μL) and basolateral side (BL, 600 μL) of the cell monolayer while the receiving chamber contained the corresponding volume of transport medium (HBSS-HPES). After shaking at 55 rpm for 4 h at 37 °C in incubator, samples were collected from both sides of Caco-2 cell monolayer. Aliquots (100 μL) of AP and BL were transferred to a CELLSTAR black, clear-bottom 96-well plate (Grenier, #M0562) and measured on a Molecular Device SpectraMax® M 5 plate reader. The fluorescence of LY in each compartment was measured at an excitation of 435 nm and an emission of 540 nm.

Apparent permeability coefficient ($P_{app}$) of LY was calculated according to the following equation:

$$P_{app} = \frac{dM_r}{dt} \times \frac{1}{A \times C_D(0)}, \quad (3)$$

where, $A$ stands for surface area of the cell monolayer (0.33 $cm^2$), $C_D(0)$ is the initial concentration of the drug added to the donor compartment, t is the time of transport, $M_r$ represents the mass of compound in the receiver side, and $dM_r/dt$ accounts for the flux of the drug across the cell monolayer. Uptake ratio (UR) and efflux ratio (ER) were obtained as below;

$$\text{UR} = \frac{P_{app\ (AP\text{-}BL)}}{P_{app\ (BL\text{-}AP)}} \quad (4)$$

$$\text{ER} = \frac{P_{app\ (BL\text{-}AP)}}{P_{app\ (AP\text{-}BL)}} \quad (5)$$

where, $P_{app\ (AP\text{-}BL)}$ and $P_{app\ (BL\text{-}AP)}$ stand for apparent permeability from AP to BL and BL to AP sides, respectively.

*2.7. Membrane Protein Extraction and Sample Preparation*

The expression level of junctional membrane proteins were analyzed in normal Caco-2 cells (PN = 55–65) as well as vinblastine-induced Caco-2 cells (PN = 55–65). Vinblastine-induced Caco-2 cell line was obtained by treatment of normal Caco-2 cells were with 10 nM vinblastine for 4–5 passages [29, 30]. Membrane associated proteins were extracted from normal and vinblastine-induced Caco-2 cells using the ProteoExtract™ Native Membrane Protein Extraction Kit (M-PEK, EMD Millipore, Billerica, MA). For this purpose, normal and vinblastine-induced Caco-2 cells (passage number 55–65) were seeded at the density of $6.5 \times 10^4$ cells per each 24-well

PET filter inserts for 15–21 days. By the end of time needed for cell differentiation, cells were treated with EtOH (25, 50, and 100 mM) and placed in saturated chambers filled with 95% air, 5% $CO_2$ for 4 and 24 h and kept in humid incubator at 37 °C. To obtain membrane associated proteins from filter-grown Caco-2 cells, the attached cells were scratched by cell scraper from the filter inserts. Then, the cells were incubated in 100 µl of extraction buffer I containing 0.5 µl of protease inhibitor cocktail according to the protocol supplied by the vendor. The cell suspension was gently shaken for 10 min at 4 °C and the homogenate was centrifuged at 3000 × g for 5 min to separate soluble proteins from cell pellet. To extract the membrane proteins, 100 µl of extraction buffer II containing 0.5 µl of protease inhibitor cocktail was added to the cells and shacked at 4 °C for 30 min. Finally, the enriched homogenate with membrane bounded proteins was collected from supernatant.

To digest proteins, 100 µL of 1 mg/mL of soluble and membrane bounded proteins were incubated with 15 µL of dithiothreitol (100 mM) and 50 ml of ammonium bicarbonate buffer (50 mM, pH 7.4) at 95 °C for 10 min. Afterward, 15 µL of iodoacetamide (150 mM) was added to the mixture and incubated at room temperature for 30 min in the dark. Ice-cold chloroform extraction solution (0.5 mL) which contains (MeOH 50%, $CHCl_3$ 25%, and water 25%) was added to each sample and centrifuged at 4 °C for 5 min at 16000 × g. The protein pellet was washed with ice-cold methanol (250 µL) and resuspended in 46.5 µL of sodium deoxycholate (3% w/v) solution prepared in ammonium bicarbonate buffer (50 mM, pH 7.4). Then, 3.5 µL of trypsin (1 mg/mL) was added to the latter solution and put in the Barocycler® 2320 EXT (Pressure Biosciences; West Bridgewater, MA) to digest the proteins.

Protein to trypsin ratio was 20:1 (w/w). Barocycler repeated cycles of hydrostatic pressure at 35000 psi for 90 cycles (90 min) to improve the protein digestion. Afterwards, 10 µL of 2.5% formic Acid in 1:1 (v/v) mixture of water/acetonitrile was added to the digest and centrifuged at 10,000 ×*g* for 5 minutes at 4°C. Finally, 2.5 µL of β-galactosidase (31.25 pmol), as an external control, was added to the digested protein solution before injection to LC-MS/MS.

*2.8. SWATH-MS Analysis*

The SWATH-MS proteomics analysis and data processing were accomplished based on the previously published method [31, 32]. Briefly, A SCIEX 5600 TripleTOF mass spectrometer equipped with a DuoSpray ion source (SCIEX, Concord, Canada) coupled to Acquity UHPLC HClass system (Waters Corp., Milford, MA, USA) was used. The mass spectrometer was operated in positive electrospray ionization (ESI) mode for all the experiments. Compound and source/gas parameters used in SWATH-MS method were as follows: DP = 120 V, CE = 10 V, collision energy spread (CES = 5V), TEM = 400 °C, ISVF = 5500 V, GS1 = 55 psi, and GS2 = 60 psi. TOF masses were collected from *m/z* 300 to 1500. SWATH data was acquired in the range of *m/z* 400 to 1100 over 70 SWATH windows per cycles with a window size of *m/z* 10. The total cycle time for SWATH acquisition was 3.95 sec.

The digested P-gp peptides were separated on an Acquity UHPLC Peptide BEH C18 (2.1 × 150 $mm^2$, 300 Å, 1.7 µm) equipped with Acquity VanGuard precolumn (2.1 × 5 $mm^2$ , 300 Å, 1.7 µm). Autosampler temperature was kept at 10 °C and the column temperature was maintained at 40 °C during all injections. The

chromatographic separation was performed with a runtime of 120 min at 100 µL/min with a gradient method using mobile phase A (98% water, 2% acetonitrile, 0.1% formic acid) and mobile phase B (98% acetonitrile, 2% water, 0.1% formic acid). A gradient chromatographic elusion method was performed as follows: 98% A from 0 to 3 min, 60% to 90% A from 3 to 48 min, 20% A held from 49 to 52 min to flush the column, 98% A at 53 min. The column was allowed to equilibrate at 98% A from 53 to 60 min before the start of next run. The amount of protein per injection on the column was 10 µg. In each batch, trypsin-digested β- galactosidase that is a quality control standard (1.65 pmol/injection) was injected to each sample to monitor mass calibration of the TOF detector and normalization of peptides intensity in SWATH label free quantification (LFQ) approach. The LFQ was performed using Skyline, which is an open source application for targeted proteomics quantitative data analysis.

*2.9. Protein Quantification*

Membrane Proteins and digested peptides concentrations were analyzed using Pierce™ BCA protein assay kit (Thermo Fisher Scientific, Rockford, IL, USA) and NanoDrop™ 2000 (Thermo Fisher Scientific, Wilmington, USA) by measuring UV-vis absorbance at wavelengths of 562 and 280 nm, respectively. Protease-free bovine serum albumin (BSA) solutions (125–2000 µg/mL) were used as the standard calibration line for the BCA protein quantification method.

*2.10. Statistical Analysis*

Results are reported as Mean ± Standard Error of Mean (SEM) from three independent experiments unless otherwise mentioned. The normality of data sets in each experiment was checked with Shapiro-Wilk test. Non-parametric Mann-Whitney U test was used in the case of non-normal distributions. One-way analysis of variance (ANOVA) with Dunnett's T3 post hoc test (SPSS 23, SPSS, Inc.) was used for normally distributed observations. In all analyses, probability values $<0.05$ was considered significant.

## 3. Results and discussion

### *3.1. WST-1 cytotoxicity*

**Figure 2** shows the cytotoxicity profiles of EtOH, AA, and clotrimazole on Caco-2 cell line examined by WST-1 assay. **Figure 2a** illustrates the viability percentage of Caco-2 cells after 24, 48, and 72 h treatment with EtOH. According to the graph, the EtOH and buffer exposure experiments showed that alcohol cytotoxicity was increased in a time- and EtOH concentration-dependent manner (**Figure 2a**). The viability% of Caco-2 cells was reduced by increasing EtOH treatment time from 24 to 72 h. Moreover, by increasing EtOH concentration from 0 to 1000 mM, the cell viability was decreased, accordingly. **Figure 2a** shows that after 72 h of treatment, the viability of Caco-2 cells was decreased to 85, 78, and 47% at EtOH concentrations of 250, 500, and 1000 mM, respectively. In the case of buffer treatment, cell viability was 85% in 1000 mM buffer-treated group after 72 h treatment (**Figure. 2a**). **Figure 2b** shows the cytotoxicity profile of AA (0–1000 µM**).** No significant cytotoxicity was seen at clinically relevant AA concentrations (100 µM) after 72 h treatment.

**Figure 2c** shows the viability of Caco-2 cells after treatment with clotrimazole (0-100 µM) for 24, 48, and 72 h. According to the graph, the Caco-2 viability reduced to 80.4 ± 9.0, 75.4 ± 2.3, and 17.9 ± 3.4 % after 24, 48, and 72 h of treatment, respectively.

Cytotoxicity results showed that at EtOH concentration < 500 mM, which is more clinically relevant, no significant cytotoxicity is induced by EtOH compared to the control group (buffer-treated cells). Further, AA did not show significantly reduction in cell viability even after three days of incubation at 1000 µM. Elamin and co-workers have previously shown that exposure of Caco-2 spheroids to EtOH and AA did not show any significant reduction in cell viability [33].

*3.2. TEM images*

**Figure 3** shows the effect of EtOH treatment on the organization of microvilli and paracellular barrier in Caco-2 cells. TJs are mentioned in TEM images at the apical side of lateral membrane with 1–2 nm thickness (**Figure 3a** and **c**). **Figure 3a** and **c** show the organization of TJs, AJ, and DS between two buffer-treated Caco-2 cells. According to the **Figure 3a** and **c,** the paracellular barriers between two cells are tightly formed and there is no space between cells. **Figure 3b** shows the effect of 50 mM EtOH treatment on junctional barrier between cells. According to the picture, the organization of junctional proteins is disrupted after 24 h incubation of cells with 50 mM EtOH. **Figure 3d** shows the deformation of microvilli at the top of cells in the presence of EtOH (100 mM). In addition, the organization of TJs, AJs, and DS were disrupted after 24 h treatment of cells with 100 mM EtOH. Elamin and co-workers

had shown the same effects of EtOH on the integrity of paracellular barrier in Caco-2 spheroids [34].

*3.3. EtOH and AA effects on TEER*

**Figure 4a** shows the TEER assay of normal Caco-2 cells treated with different EtOH concentrations (25, 50, and 100 mM) during 4 h and one day after removal of EtOH. Data shows a slight decrease in TEER values by the time. At the end of 4 h treatment, the medium contained EtOH was removed and cells were cultured in normal medium. One day after EtOH removal, the TEER was checked and it showed that paracellular barrier was revitalized after EtOH removal. The transient disruptive effect of single dose EtOH on intestinal permeability was previously observed by Robinson *et al* [35]. However, persistent changes may occur after prolonged chronic alcohol consumption [36].

**Figure 4b** shows the TEER changes of Caco-2 cells after 24, 48, and 72 h of treatment with buffer and EtOH (50 mM) and after removal. Results show that there is no significantly change in TEER values during buffer-treatment and one day after removal. (**Figure 4b**). After 24 h of treatment with 50 mM EtOH, a statistically significant decrease ($P = 0.002$) was observed in TEER values. The TEER values of Caco-2 cells did not significantly change during 48 and 72 h. **Figure 4b** shows that the TEER value of EtOH-treated Caco-2 cells increased to near 600 $\Omega cm^2$ that was comparable to the buffer-treated cells ($P = 0.13$). This means the effect of EtOH on the integrity of paracellular barriers are transient and it could be revitalized after alcohol removal.

The reduction in TEER value by EtOH in Caco-2 cells was reported previously.[34, 37, 38] Fisher and co-workers suggested that EtOH and its metabolite acetaldehyde are able to increase the paracellular permeability of Caco-2 cells without altering viability.[34] The proposed mechanism for EtOH-induced enhancement in paracellular permeability is disruption of TJs proteins. The proposed mechanism is activation of myosin light chain kinas (MLCK) which results in phosphorylation of MLC and occluding and subsequently destabilization of TJs [39, 40].

*3.4. Lucifer yellow permeability assay*

**Table 1** shows the permeability of LY, a fluorescent marker for paracellular pathway, across mature (highly integrate paracellular barrier) and non-mature (loose barrier) Caco-2 monolayers. As shown in the **Table 1**, the apical (AP) to basolateral (BL) permeability ($P_{app\ (AP\text{-}BL)}$) of LY drastically decreased in mature Caco-2 monolayer compared to the non-mature cells. This result confirmed the formation of tight junction proteins in mature Caco-2 cell monolayer after 21-days of seeding on filter insert.

The effect of EtOH and its metabolite, acetaldehyde (AA), on the integrity of tight junctions is shown in **Fig 5.** Results show that EtOH (100 mM) and AA (100 µM) increased the Apical to basolateral ($P_{app\ (AP\text{-}BL)}$) apparent permeability of LY (500 µM) across Caco-2 monolayer. The increased LY permeation was statistically significant in the presence of EtOH (100 mM), while it was not increased significantly in the presence of AA. This suggests that in accordance to the other published literature [34, 37], EtOH and AA are responsible for tight junction opening.

*3.5. SWATH-MS proteomics*

**Table 2** shows the abundance of TJs, AJs, and DS after 24 h treatment with 25, 50, and 100 mM EtOH versus control group. According to the results, the relative expression of JAM-A was decreased after 4 and 24 h treatment of vinblastine-induced cells with 50 mM EtOH (**Table 2**). Chopyk and co-worker have shown that EtOH decreases JAM-A protein expression level to ~ 70% of control in a concentration-and time-dependent manner in Caco-2 monolayer [41].

Cresci *et al* have shown that EtOH-exposed mice showed reduction in the expression and co-localization of zonula occludens-1 (ZO-1) and occludin in the ileum and proximal colon [42]. The reduction in occludin and ZO-3 expression level was confirmed in our study using normal and vinblastine-induced Caco-2 cells (**Table 2**). Moreover, Zhao and co-workers have shown that EtOH exposure in mice decreased the expression of occludin leading to intestinal hyper permeability [43]. They revealed that chronic consumption of EtOH results in depletion of occluding expression in mice intestine followed by increase in paracellular permeability. In a previous attempt, Ye *et al* has found that increase in microRNA122a (miR122a), enhanced by tumor necrosis factor-α (TNF-α), is responsible for occludin degradation and subsequent enhancement in paracellular permeation [44]. It could be concluded that the intestinal hyper permeability induced by chronic EtOH is mediated by increased TNF-α [45] and miR122a expression and consecutively occludin down regulation.

The expression of CAD17 and CAD23 showed insignificant decrease in expression level after 4 h treatment of normal and vinblastine-induced Caco-2 cells

with 50 mM EtOH (**Table 2**). However, normal and vinblastine-induced Caco-2 cells treatment with 50 mM did not show any decrease in expression level.

It has been mentioned that the levels of gut AJs (e.g., β-catenin and E-cadherin) and desmosome plakoglobin were clearly decreased in binge alcohol-exposed rats [46].

**Conclusion**

In this work, the effect of EtOH on paracellular integrity was examined in Caco-2 cell monolayer. WST-1 mitochondrial cytotoxicity assay was carried out on Caco-2 cells after EtOH and AA treatment. EtOH and AA did not show significant alteration in cell viability at concentrations found in GI tract. Moreover, TEER assay showed that the paracellular hyper permeability of Caco-2 cells induced by EtOH and AA was reversible after removal of reagents. LY permeation showed that paracellular transport of LY was enhanced after treatment of Caco-2 cells with EtOH. TEM images of EtOH-treated Caco-2 cells showed the disintegration of TJs, AJs, and DS. Moreover, SWATH-MS proteomics was used to analyze the effect of 50 mM EtOH on paracellular proteins in normal and vinblastine-induced Caco-2 cells for 4 and 24 h. Proteomics data showed that the abundance of TJs, AJs, and DS were diminished after treatment of Caco-2 cells with EtOH (50 mM) for 4 and 24 h. However, the reduction of junctional proteins was not statistically significant in any of the treatments. This fact confirmed that other molecular pathways are involved in paracellular opening by EtOH.

**Table III- 1.** Permeability of Lucifer yellow (LY) across mature and non-mature Caco-2 cells monolayers.

| **Caco-2 monolayer** | **$P_{app\ (AP-BL)}$ (× $10^{-6}$ cm/s)** | **$P_{app\ (BL-AP)}$ (× $10^{-6}$ cm/s)** | **UR** | **ER** |
|---|---|---|---|---|
| Non-mature | 21.55 ± 1.42 | 20.67 ± 1.17 | 1.04 ± 0.01 | 0.96 ± 0.01 |
| Mature | 0.18 ± 0.06 | 0.34 ± 0.07 | 0.53 ± 0.17 | 1.99 ± 0.56 |

Apical to basolateral ($P_{app\ (AP-BL)}$) and basolateral to apical apparent permeability ($P_{app\ (BL-AP)}$) as well as uptake ratio (UR) and efflux ratio (ER) across mature and non-mature Caco-2 cells monolayers. Data are shown as Mean ± SEM ($n$ = 3).

**Table III- 2.** Relative expression level of tight junction (TJ), Adherens junction (AJ), and desmosome (DS) proteins in EtOH-treated normal and Pgp-induced Caco-2 cells.

| Proteins | Protein class | EtOH Treatments | Normalized protein abundance (Intensity/µg total protein) | | | |
|---|---|---|---|---|---|---|
| | | | 4 h treatment | | 24 h treatment | |
| | | | Normal Caco-2 | P-gp Induced Caco-2 | Normal Caco-2 | P-gp Induced Caco-2 |
| Junctional adhesion molecule A | TJ | 0 (Control) | 0.48 | 0.80 | 0.57 | 0.58 |
| | | | 0.61 | – | 0.52 | – |
| | | 25 | 0.66 | 0.91 | 0.62 | 0.87 |
| | | | 0.39 | 0.22 | 0.34 | 0.28 |
| | | 50 | 0.60 | – | 0.68 | 0.55 |
| | | | 0.48 | 0.30 | 0.41 | 0.38 |
| | | 100 | 0.48 | 0.68 | 0.50 | – |
| | | | – | 0.36 | 0.32 | – |
| ZO-3 | | 0 (Control) | 0.02 | 0.07 | 0.04 | 0.06 |
| | | | 0.02 | – | 0.04 | – |
| | | 25 | 0.03 | 0.07 | 0.03 | 0.08 |
| | | | 0.04 | 0.10 | 0.03 | 0.08 |
| | | 50 | 0.04 | – | 0.04 | 0.02 |
| | | | 0.04 | 0.02 | 0.03 | 0.03 |
| | | 100 | 0.02 | 0.03 | 0.02 | – |
| | | | – | 0.03 | 0.01 | – |
| Cadherin-17 | AJ | 0 (Control) | 0.10 | 0.11 | 0.10 | 0.05 |
| | | | 0.03 | – | 0.02 | – |
| | | 25 | 0.12 | 0.10 | 0.12 | 0.08 |
| | | | 0.02 | 0.01 | 0.01 | 0.01 |
| | | 50 | 0.07 | – | 0.12 | 0.12 |
| | | | 0.02 | 0.01 | 0.02 | 0.01 |
| | | 100 | 0.09 | 0.08 | 0.08 | – |
| | | | – | 0.02 | 0.02 | – |
| Cadherin-23 | | 0 (Control) | 0.12 | 0.09 | 0.10 | 0.03 |
| | | | 0.12 | – | 0.05 | – |
| | | 25 | 0.17 | 0.06 | 0.12 | 0.04 |
| | | | 0.06 | 0.04 | 0.05 | 0.04 |
| | | 50 | 0.05 | – | 0.16 | 0.14 |
| | | | 0.07 | 0.03 | 0.06 | 0.03 |
| | | 100 | 0.09 | 0.03 | 0.10 | – |
| | | | – | 0.04 | 0.05 | – |

**Table III– 2.** Relative expression level of tight junction (TJ), Adherens junction (AJ), and desmosome (DS) proteins in EtOH-treated normal and P-gp-induced Caco-2 cells.

| Proteins | Protein class | EtOH Treatments | Normalized protein abundance (Intensity/µg total protein) | | | |
|---|---|---|---|---|---|---|
| | | | 4 h treatment | | 24 h treatment | |
| | | | Normal Caco-2 | P-gp Induced Caco-2 | Normal Caco-2 | P-gp Induced Caco-2 |
| Catenin alpha-2 | AJ | 0 (Control) | 0.05 | 0.08 | 0.09 | 0.03 |
| | | | 0.07 | – | 0.06 | – |
| | | 25 | 0.08 | 0.07 | 0.04 | 0.05 |
| | | | 0.03 | 0.02 | 0.04 | 0.03 |
| | | 50 | 0.04 | – | 0.06 | 0.06 |
| | | | 0.03 | 0.01 | 0.03 | 0.03 |
| | | 100 | 0.05 | 0.04 | 0.05 | – |
| | | | – | 0.02 | 0.02 | – |
| Catenin beta-1 | | 0 (Control) | 0.07 | 0.09 | 0.07 | 0.04 |
| | | | 0.08 | – | 0.08 | – |
| | | 25 | 0.11 | 0.08 | 0.09 | 0.04 |
| | | | 0.05 | 0.02 | 0.05 | 0.02 |
| | | 50 | 0.04 | – | 0.10 | 0.09 |
| | | | 0.06 | 0.03 | 0.05 | 0.03 |
| | | 100 | 0.08 | 0.06 | 0.07 | – |
| | | | – | 0.04 | 0.04 | – |
| Desmoplakin | DS | 0 (Control) | 0.26 | 0.80 | 0.28 | 0.47 |
| | | | 0.22 | – | 0.11 | – |
| | | 25 | 0.40 | 0.58 | 0.39 | 0.61 |
| | | | 0.07 | 0.11 | 0.06 | 0.03 |
| | | 50 | 0.48 | – | 0.42 | 0.27 |
| | | | 0.08 | 0.10 | 0.09 | 0.05 |
| | | 100 | 0.18 | 0.19 | 0.16 | – |
| | | | – | 0.08 | 0.06 | – |
| Desmoglein-3 | | 0 (Control) | 0.17 | 0.78 | 0.25 | 0.39 |
| | | | 0.25 | – | 0.27 | – |
| | | 25 | 0.21 | 0.42 | 0.14 | 0.37 |
| | | | 0.08 | 0.25 | 0.21 | 0.05 |
| | | 50 | 0.35 | – | 0.21 | 0.14 |
| | | | 0.09 | 0.12 | 0.11 | 0.10 |
| | | 100 | 0.14 | 0.11 | 0.10 | – |
| | | | – | 0.10 | 0.15 | – |

**Figure III– 1**

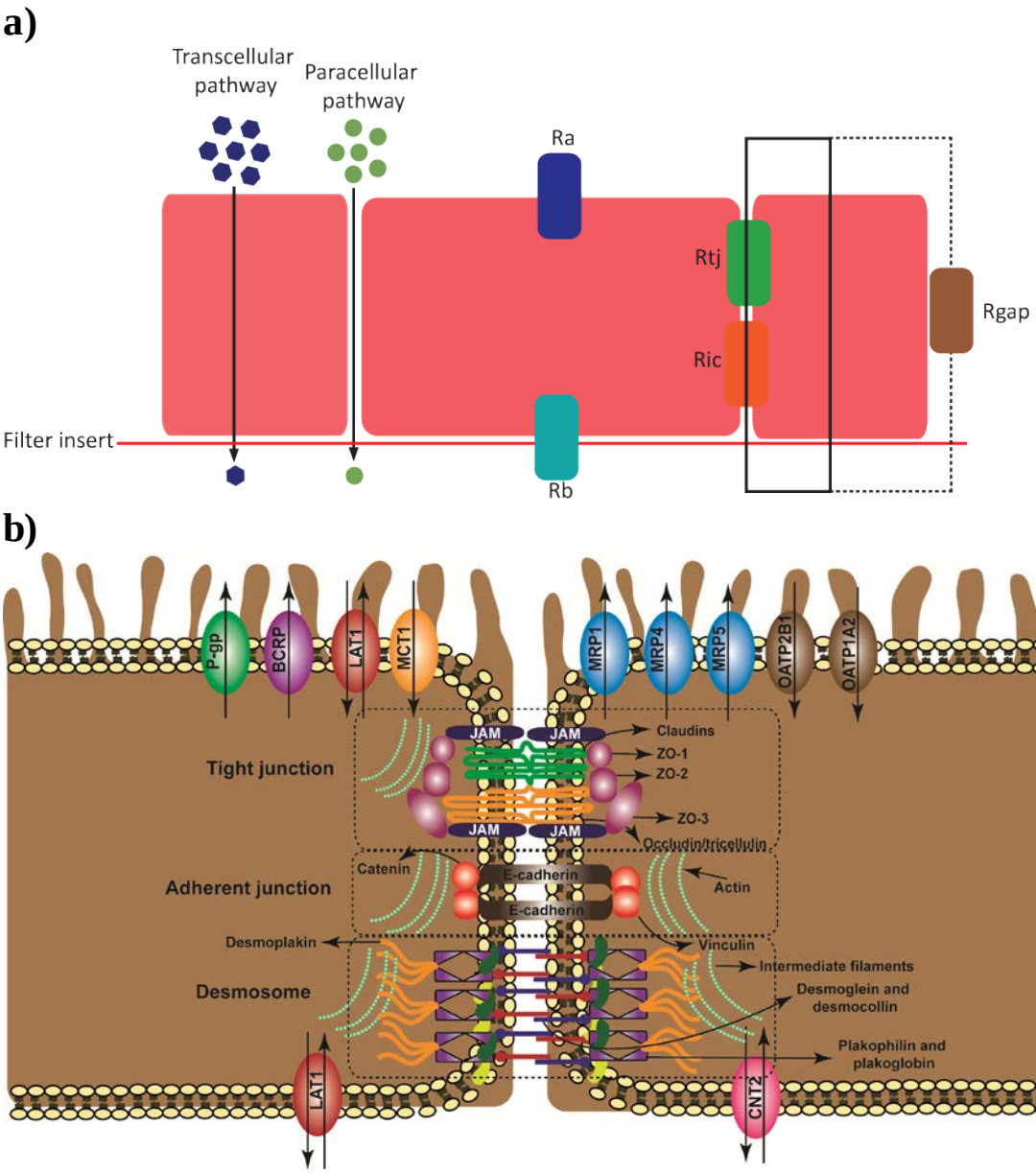


**Figure III- 1**. Schematic illustration of human epithelial cells demonstrating the involved proteins in paracellular and transcellular routes.
**a)** Two main routes of drug transport across epithelial cell monolayer are paracellular and transcellular pathways. Transcellular pathway ($R_{trc}$) is the sum of $R_a$ and $R_b$ (apical and basolateral resistance). The paracellular pathway ($R_{pc}$) equals to tight junction resistance ($R_{tj}$) plus intercellular resistance ($R_{ic}$). $R_{gap}$ indicates the partial cell coverage of the cell support. **b)** A schematic illustration of human epithelial cells. The uptake and efflux transporters on apical (AP) and basolateral (BL) sides of cells are indicated. Moreover, paracellular proteins including tight junctions (TJs), desmosomes (DS), and adherens junctions (ADs) are depicted.

**Figure III- 2**

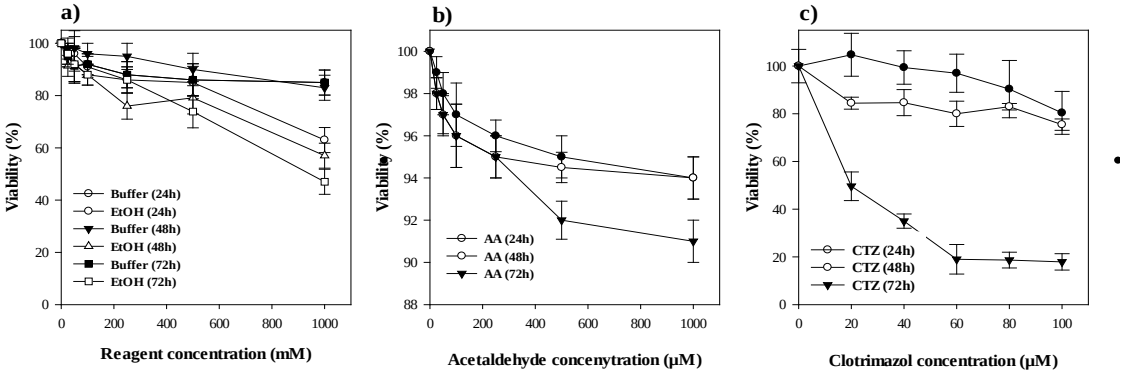


**Figure III- 2**. The water-soluble tetrazolium salt (WST-1) cytotoxicity assay conducted for Caco-2 cells treated with ethanol (EtOH), acetaldehyde (AA), and clotrimazole (CTZ).

WST-1 cytotoxicity profile for **a)** EtOH (0–1000 mM), **b)** AA (0–1000 µM), and **c)** CTZ (0–100 µM) for 24, 48, and 72 h are illustrated. No significant cytotoxicity was observed at clinically relevant EtOH and AA concentrations (<400 mM and 100 µM, respectively) after 72 h treatment. However, viability (%) for Caco-2 cells treatment with 60 µM CTZ (positive control) was 20% after 3 days treatment. Data are shown as Mean ± Standard Error of Mean (Mean ± SEM, *n*=3).

**Figure III- 3**

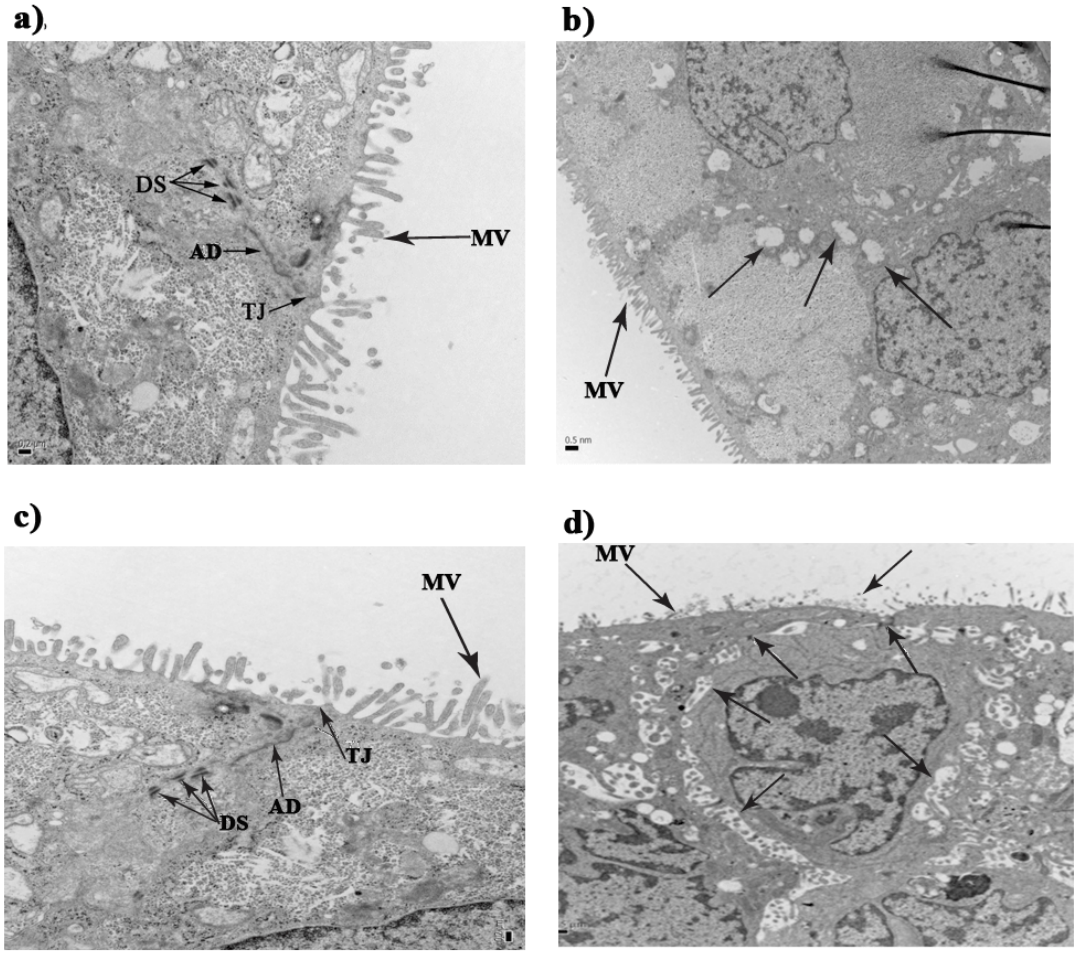


**Figure III- 3**. Transmission electron microscopy (TEM) images of buffer- and EtOH-treated Caco-2 cells for 24 h.
Panels **a** and **c)** show the TEM images of buffer-treated (50 and 100 mM) Caco-2 cells after 24 h. **b and d)** illustrate the images of EtOH-treated (50 and 100 mM) Caco-2 cells for 24 h. Deformation of MV at the top of cells was observed in after treatment with 100 mM EtOH (**Figure 3d**). However, Caco-2 treatment with 50 mM EtOH (**Figure 3b**) did not affect the MV and the structure of MV after 24 h treatment with 50 mM EtOH was comparable to the control groups (**Figure 3a** and **c**). The organization of tight junctions (TJs), adherens junctions (ADs), and desmosomes (DS) are disrupted after 24 h treatment of cells with 50 and 100 mM EtOH (**Figure 3b** and **d**) compare to the control groups (**Figure 3a** and **c**).

**Figure III- 4**

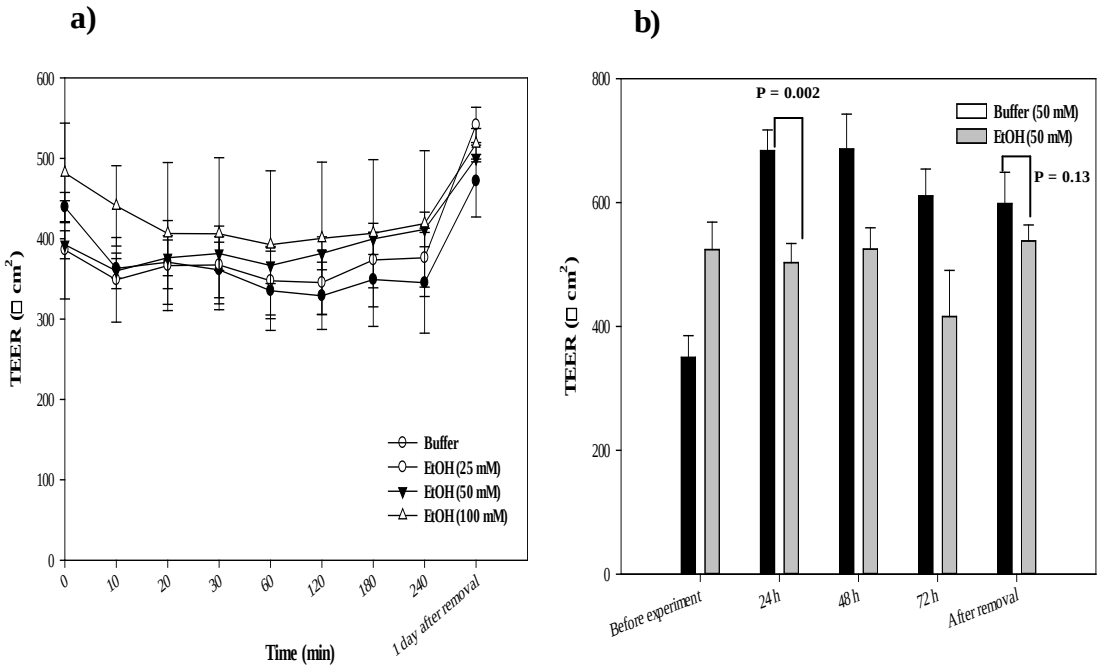


**Figure III- 4** Transepithelial electrical resistance (TEER) assay of normal Caco-2 cells treated with different EtOH concentrations and treatment time.
**a)** TEER assay of normal Caco-2 cells treated with different EtOH concentrations (25, 50, and 100 mM) during 4 h and one day after removal of EtOH. Data shows a slight decrease in TEER values during the time and while it revitalized after EtOH removal.
**b)** TEER assay of normal Caco-2 cells treated with 50 mM EtOH during 24, 48, and 72 h and one day after removal of EtOH. Data show that there is no significant difference in TEER values one day after removal of EtOH and buffer. Date are shown as Mean ± Standard Error of Mean (Mean ± SEM, $n$ = 3) and P-value <0.05 considered significant.

**Figure III-5**

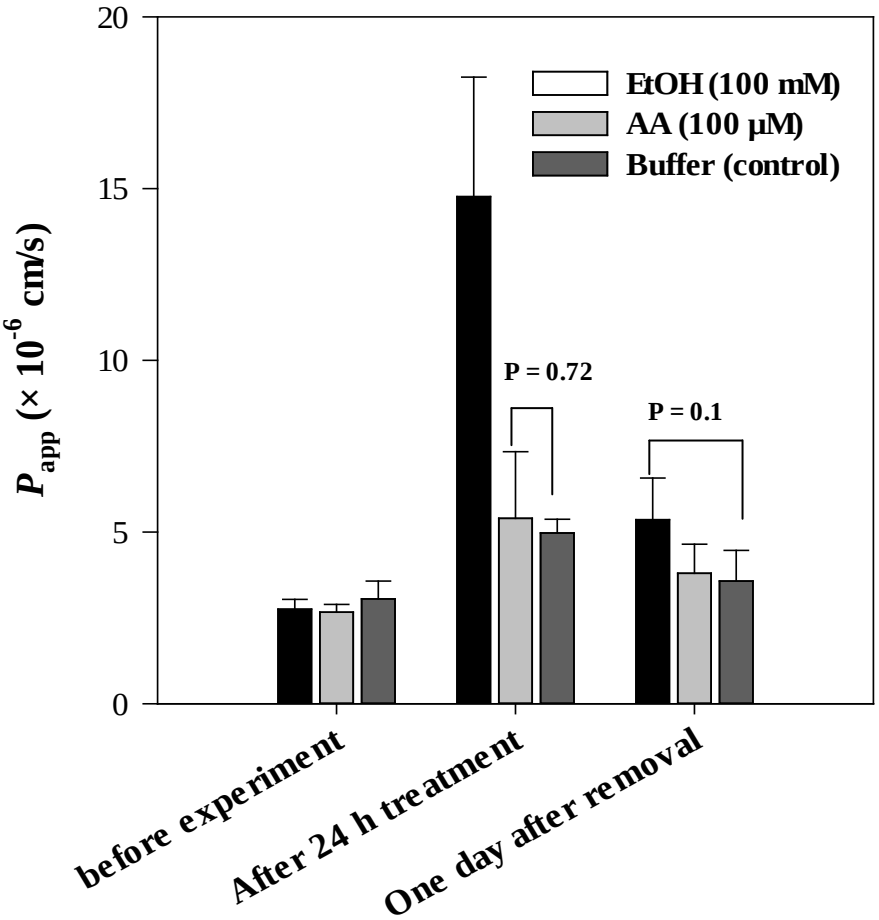


**Figure III- 5**. The effect of ethanol (EtOH), acetaldehyde (AA), and buffer (control) on the permeation of Lucifer yellow (LY) across Caco-2 cell monolayer.
Caco-2 cells treatment with EtOH (100 mM) and AA (100 µM) for 24 h increased the LY permeation compare to buffer as control. No significant difference was observed one day after reagents removal compared to the control. Date are shown as Mean ± Standard Error of Mean (Mean ± SEM, $n$ = 3) and P-value <0.05 considered significant.

**References**


1. Bishehsari, F.; Magno, E.; Swanson, G.; Desai, V.; Voigt, R. M.; Forsyth, C. B.; Keshavarzian, A. Alcohol and Gut-Derived Inflammation. *Alcohol research : current reviews* **2017,** *38*, (2), 163-171.
2. Zakhari, S. Overview: how is alcohol metabolized by the body? *Alcohol Research* **2006,** *29*, (4), 245.
3. Bishehsari, F.; Magno, E.; Swanson, G.; Desai, V.; Voigt, R. M.; Forsyth, C. B.; Keshavarzian, A. Alcohol and gut-derived inflammation. *Alcohol research: current reviews* **2017,** *38*, (2), 163.
4. Bischoff, S. C.; Barbara, G.; Buurman, W.; Ockhuizen, T.; Schulzke, J.-D.; Serino, M.; Tilg, H.; Watson, A.; Wells, J. M. Intestinal permeability–a new target for disease prevention and therapy. *BMC gastroenterology* **2014,** *14*, (1), 189.
5. Borrelli, A.; Bonelli, P.; Tuccillo, F. M.; Goldfine, I. D.; Evans, J. L.; Buonaguro, F. M.; Mancini, A. Role of gut microbiota and oxidative stress in the progression of non-alcoholic fatty liver disease to hepatocarcinoma: Current and innovative therapeutic approaches. *Redox biology* **2018,** *15*, 467-479.
6. Llorente, C.; Schnabl, B. The gut microbiota and liver disease. *Cellular and molecular gastroenterology and hepatology* **2015,** *1*, (3), 275-284.
7. Schnabl, B.; Brenner, D. A. Interactions between the intestinal microbiome and liver diseases. *Gastroenterology* **2014,** *146*, (6), 1513-1524.
8. Wang, H. J.; Zakhari, S.; Jung, M. K. Alcohol, inflammation, and gut-liver-brain interactions in tissue damage and disease development. *World journal of gastroenterology: WJG* **2010,** *16*, (11), 1304.
9. Leclercq, S.; de Timary, P.; Delzenne, N. M.; Stärkel, P. The link between inflammation, bugs, the intestine and the brain in alcohol dependence. *Translational psychiatry* **2017,** *7*, (2), e1048.
10. Banan, A.; Choudhary, S.; Zhang, Y.; Fields, J.; Keshavarzian, A. Ethanol-induced barrier dysfunction and its prevention by growth factors in human intestinal monolayers: evidence for oxidative and cytoskeletal mechanisms. *Journal of Pharmacology and Experimental Therapeutics* **1999,** *291*, (3), 1075-1085.
11. Ma, T. Y.; Nguyen, D.; Bui, V.; Nguyen, H.; Hoa, N. Ethanol modulation of intestinal epithelial tight junction barrier. *The American journal of physiology* **1999,** *276*, (4 Pt 1), G965-74.
12. Wang, Y.; Tong, J.; Chang, B.; Wang, B.; Zhang, D.; Wang, B. Effects of alcohol on intestinal epithelial barrier permeability and expression of tight junction-associated proteins. *Molecular medicine reports* **2014,** *9*, (6), 2352-2356.
13. Artursson, P.; Palm, K.; Luthman, K. Caco-2 monolayers in experimental and theoretical predictions of drug transport1PII of original article: S0169-409X(96)00415-2. The article was originally published in Advanced Drug Delivery Reviews 22 (1996) 67–84.1. *Advanced Drug Delivery Reviews* **2001,** *46*, (1), 27-43.
14. Hidalgo, I. J.; Raub, T. J.; Borchardt, R. T. Characterization of the human colon carcinoma cell line (Caco-2) as a model system for intestinal epithelial permeability. *Gastroenterology* **1989,** *96*, (3), 736-749.
15. Groschwitz, K. R.; Hogan, S. P. Intestinal barrier function: molecular regulation and disease pathogenesis. *The Journal of allergy and clinical immunology* **2009,** *124*, (1), 3-22.

16. Yu, Q. H.; Yang, Q. Diversity of tight junctions (TJs) between gastrointestinal epithelial cells and their function in maintaining the mucosal barrier. *Cell biology international* **2009,** *33*, (1), 78-82.
17. Hartsock, A.; Nelson, W. J. Adherens and tight junctions: structure, function and connections to the actin cytoskeleton. *Biochimica et Biophysica Acta (BBA)-Biomembranes* **2008,** *1778*, (3), 660-669.
18. Kowalczyk, A. P.; Green, K. J., Structure, function, and regulation of desmosomes. In *Progress in molecular biology and translational science*, Elsevier: 2013; Vol. 116, pp 95-118.
19. Garrod, D.; Chidgey, M. Desmosome structure, composition and function. *Biochimica et Biophysica Acta (BBA) - Biomembranes* **2008,** *1778*, (3), 572-587.
20. Delva, E.; Tucker, D. K.; Kowalczyk, A. P. The desmosome. *Cold Spring Harbor perspectives in biology* **2009,** *1*, (2), a002543.
21. Zhang, J.-C.; Xie, F.; Yu, X.-H.; Deng, Z.-Y.; Wang, Y.; Liang, P.; Sun, L.; Zhang, F.-X. Expression levels of P-glycoprotein in peripheral blood CD8+ T lymphocytes from HIV-1-infected patients on antiretroviral therapy. *International journal of molecular medicine* **2014,** *33*, (2), 431-440.
22. Hogg, K.; Thomas, J.; Ashford, D.; Cartwright, J.; Coldwell, R.; Weston, D. J.; Pillmoor, J.; Surry, D.; O'Toole, P. Quantification of proteins by flow cytometry: quantification of human hepatic transporter P-gp and OATP1B1 using flow cytometry and mass spectrometry. *Methods* **2015,** *82*, 38-46.
23. Greiner, B.; Eichelbaum, M.; Fritz, P.; Kreichgauer, H.-P.; von Richter, O.; Zundler, J.; Kroemer, H. K. The role of intestinal P-glycoprotein in the interaction of digoxin and rifampin. *The Journal of Clinical Investigation* **1999,** *104*, (2), 147-153.
24. Ong, S.-E.; Mann, M. Mass spectrometry–based proteomics turns quantitative. *Nature chemical biology* **2005,** *1*, (5), 252.
25. Bantscheff, M.; Schirle, M.; Sweetman, G.; Rick, J.; Kuster, B. Quantitative mass spectrometry in proteomics: a critical review. *Analytical and bioanalytical chemistry* **2007,** *389*, (4), 1017-1031.
26. Han, X.; Aslanian, A.; Yates, J. R. Mass Spectrometry for Proteomics. *Current opinion in chemical biology* **2008,** *12*, (5), 483-490.
27. Zhu, F.-Y.; Chen, M.-X.; Su, Y.-W.; Xu, X.; Ye, N.-H.; Cao, Y.-Y.; Lin, S.; Liu, T.-Y.; Li, H.-X.; Wang, G.-Q.; Jin, Y.; Gu, Y.-H.; Chan, W.-L.; Lo, C.; Peng, X.; Zhu, G.; Zhang, J. SWATH-MS Quantitative Analysis of Proteins in the Rice Inferior and Superior Spikelets during Grain Filling. *Frontiers in Plant Science* **2016,** *7*, 1926.
28. Odijk, M.; van der Meer, A. D.; Levner, D.; Kim, H. J.; van der Helm, M. W.; Segerink, L. I.; Frimat, J.-P.; Hamilton, G. A.; Ingber, D. E.; van den Berg, A. Measuring direct current trans-epithelial electrical resistance in organ-on-a-chip microsystems. *Lab on a Chip* **2015,** *15*, (3), 745-752.
29. Anderle, P.; Niederer, E.; Rubas, W.; Hilgendorf, C.; Spahn-Langguth, H.; Wunderli-Allenspach, H.; Merkle, H. P.; Langguth, P. P-Glycoprotein (P-gp) Mediated Efflux in Caco-2 Cell Monolayers: The Influence of Culturing Conditions and Drug Exposure on P-gp Expression Levels. *Journal of Pharmaceutical Sciences* **1998,** *87*, (6), 757-762.

30. Chen, Q.; Bian, Y.; Zeng, S. Involvement of AP-1 and NF-kappaB in the up-regulation of P-gp in vinblastine resistant Caco-2 cells. *Drug metabolism and pharmacokinetics* **2014,** *29*, (2), 223-6.
31. Jamwal, R.; de la Monte, S. M.; Ogasawara, K.; Adusumalli, S.; Barlock, B. B.; Akhlaghi, F. Nonalcoholic fatty liver disease and diabetes is associated with decreased CYP3A4 protein expression and activity in human liver. *Molecular pharmaceutics* **2018**.
32. Jamwal, R.; Barlock, B. J.; Adusumalli, S.; Ogasawara, K.; Simons, B. L.; Akhlaghi, F. Multiplex and Label-Free Relative Quantification Approach for Studying Protein Abundance of Drug Metabolizing Enzymes in Human Liver Microsomes Using SWATH-MS. *Journal of proteome research* **2017,** *16*, (11), 4134-4143.
33. Elamin, E.; Jonkers, D.; Juuti-Uusitalo, K.; van Ijzendoorn, S.; Troost, F.; Duimel, H.; Broers, J.; Verheyen, F.; Dekker, J.; Masclee, A. Effects of ethanol and acetaldehyde on tight junction integrity: in vitro study in a three dimensional intestinal epithelial cell culture model. *PloS one* **2012,** *7*, (4), e35008-e35008.
34. Elamin, E.; Jonkers, D.; Juuti-Uusitalo, K.; van Ijzendoorn, S.; Troost, F.; Duimel, H.; Broers, J.; Verheyen, F.; Dekker, J.; Masclee, A. Effects of Ethanol and Acetaldehyde on Tight Junction Integrity: In Vitro Study in a Three Dimensional Intestinal Epithelial Cell Culture Model. *PLoS ONE* **2012,** *7*, (4), e35008.
35. Robinson, G.; Orrego, H.; Israel, Y.; Devenyi, P.; Kapur, B. Low-molecular-weight polyethylene glycol as a probe of gastrointestinal permeability after alcohol ingestion. *Digestive diseases and sciences* **1981,** *26*, (11), 971-977.
36. Elamin, E.; Masclee, A.; Troost, F.; Pieters, H.-J.; Keszthelyi, D.; Aleksa, K.; Dekker, J.; Jonkers, D. Ethanol impairs intestinal barrier function in humans through mitogen activated protein kinase signaling: a combined in vivo and in vitro approach. *PloS one* **2014,** *9*, (9), e107421-e107421.
37. Dunagan, M.; Chaudhry, K.; Samak, G.; Rao, R. K. Acetaldehyde disrupts tight junctions in Caco-2 cell monolayers by a protein phosphatase 2A-dependent mechanism. *American Journal of Physiology-Gastrointestinal and Liver Physiology* **2012,** *303*, (12), G1356-G1364.
38. Fisher, S. J.; Swaan, P. W.; Eddington, N. D. The ethanol metabolite acetaldehyde increases paracellular drug permeability in vitro and oral bioavailability in vivo. *Journal of Pharmacology and Experimental Therapeutics* **2010,** *332*, (1), 326-333.
39. Rao, R. K. Acetaldehyde-induced barrier disruption and paracellular permeability in Caco-2 cell monolayer. *Methods in molecular biology (Clifton, N.J.)* **2008,** *447*, 171-83.
40. Samak, G.; Rao, R. M1687 Ethanol Synergizes Acetaldehyde-Induced Tight Junction (TJ) Disruption in CACO-2 Cell Monolayers By SRC Kinase and Myosin Light Chain Kinase (MLCK)-Dependent Mechanism. *Gastroenterology* **2009,** *136*, (5), A-410.
41. Chopyk, D. M.; Kumar, P.; Raeman, R.; Liu, Y.; Smith, T.; Anania, F. A. Dysregulation of junctional adhesion molecule-A contributes to ethanol-induced barrier disruption in intestinal epithelial cell monolayers. *Physiological reports* **2017,** *5*, (23), e13541.

42. Cresci, G. A.; Bush, K.; Nagy, L. E. Tributyrin supplementation protects mice from acute ethanol-induced gut injury. *Alcoholism, clinical and experimental research* **2014,** *38*, (6), 1489-501.
43. Zhao, H.; Zhao, C.; Dong, Y.; Zhang, M.; Wang, Y.; Li, F.; Li, X.; McClain, C.; Yang, S.; Feng, W. Inhibition of miR122a by Lactobacillus rhamnosus GG culture supernatant increases intestinal occludin expression and protects mice from alcoholic liver disease. *Toxicology Letters* **2015,** *234*, (3), 194-200.
44. Ye, D.; Guo, S.; Al-Sadi, R.; Ma, T. Y. MicroRNA regulation of intestinal epithelial tight junction permeability. *Gastroenterology* **2011,** *141*, (4), 1323-33.
45. Ceron, C. S.; do Vale, G. T.; Simplicio, J. A.; Ricci, S. T.; De Martinis, B. S.; de Freitas, A.; Tirapelli, C. R. Chronic ethanol consumption increases vascular oxidative stress and the mortality induced by sub-lethal sepsis: Potential role of iNOS. *European journal of pharmacology* **2018,** *825*, 39-47.
46. Cho, Y.-E.; Song, B.-J. Pomegranate prevents binge alcohol-induced gut leakiness and hepatic inflammation by suppressing oxidative and nitrative stress. *Redox Biology* **2018,** *18*, 266-278.

## MANUSCRIPT IV

This manuscript has been prepared for submission to the *"Proteomics-Clinical Applications"*

# SWATH-MS Proteomic Analysis of Gastrointestinal Tract in Alcoholic Rat Model and Human Subjects

Armin Sadighi[a], Suzanne M. de la Monte, [b], Ali Keshavarzian[c], Lorenzo Leggio[d, e], Fatemeh Akhlaghi[a*]

[a]Clinical Pharmacokinetics Research Laboratory, Department of Biomedical and Pharmaceutical Sciences, College of Pharmacy, University of Rhode Island, Kingston, RI, USA

[b]Departments of Neurology, Pathology (Neuropathology), Neurosurgery, and Medicine, Rhode Island Hospital and The Alpert Medical School of Brown University, Providence, RI, USA

[c]Department of Internal Medicine, Division of Gastroenterology, Rush University Medical Center, Chicago, IL 60637, USA

[d]Section on Clinical Psychoneuroendocrinology and Neuropsychopharmacology, Laboratory of Clinical and Translational Studies, National Institute on Alcohol Abuse and Alcoholism, Bethesda, MD, USA

[e]Center for Alcohol and Addiction Studies, Department of Behavioral and Social Sciences, Brown University, Providence, RI 02903, USA

[*]**Corresponding author:** Fatemeh Akhlaghi; Clinical Pharmacokinetics Research Laboratory; University of Rhode Island; Office 495 A; 7 Greenhouse Road; Kingston; RI 02881, USA. **Tel:** (401) 874 9205; **Fax:** (401) 874 5787; **Email:** fatemeh@uri.edu

**Abstract**

In this study, SWATH-MS proteomics was successfully used for quantitative analysis of proteins obtained from limited biopsy samples. Accordingly, the proteome of healthy human sigmoid was compared to alcoholic subjects with and without liver disease. Moreover, proteome of different parts of gastrointestinal (GI) tract from chronic-binge rat models was compared to control group. Results showed that the expression level of aldehyde dehydrogenase2 (ALDH2) in alcoholic human subjects without liver disease "low quartile sucralose" (AWLDLQ) was significantly ($P = 0.02$) higher than that in healthy control (HC). Interestingly, the expression of ALDH2 in AWLDLQ was higher than that in AWLDHQ. Moreover, filamin A expression in AWLDLQ human subjects was significantly lower than that in HC. Glutathione S-transferase A1 (GSTA1) expression in AWLDLQ was higher than that in HC. Higher expression of GSTA1 in AWLDLQ may explain the insignificant antioxidant role of GSTA in human colon compared to liver. Furthermore, the expression of vimentin (Vim), a cytoskeletal protein, was increased in proximal colon (pCol) of chronic-binge rat models. Thus, SWATH-MS proteomics was capable to analyze very limited quantity of biopsy tissue. This technique might be helpful in identification of alcoholism biomarkers and developing new drugs to cure different stages of alcoholism.

**Keywords:** SWATH-MS Proteomics, Sigmoid colon, Chronic-binge rat model

**Abbreviations:**
**ALD:** Alcoholic Liver Disease
**ALDH2:** Aldehyde dehydrogenase2
**AWLDLQ:** Alcoholic without Liver Disease Low Quartile Sucralose

**AWLDHQ:** Alcoholic without Liver Disease High Quartile Sucralose
**dCol:** Distal Colon
**GSTA1**: Glutathione S-transferase A1
**HC:** Healthy Control
**pCol:** Proximal Colon
**PCT-Micropestle:** Pressure-cycling technology- MicroPestle
**SWATH-MS:** Sequential Windowed data independent Acquisition of the Total High-resolution Mass Spectra
**Vim:** Vimentin

## 1. Introduction

Alcohol abuse or alcohol use disorder (AUD) is considered as an untreated epidemic health concern in modern societies [1]. According to the 2014 report of World Health Organization (WHO), alcoholism causes approximately 6% of all cases of death every year.[2, 3] While, moderate alcohol drinking (≤1 drink/day for women and ≤2 drink/day for men) does not show clinical problems and even is beneficial for health[4], heavy chronic drinking (binge drinking) increases the risk of organ damage.[5]

Alcohol affects the gastrointestinal (GI) epithelium by altering the intestinal epithelial function. Chronic ethanol (EtOH) exposure results in intestinal hyper permeability (leaky gut) which has been implicated in inflammatory bowel disorders (IBDs). Moreover, chronic alcohol consumption leads to liver damage[6]. Studies show that the risk of cirrhosis is enhanced by increasing the amount of drinking alcohol. Alcoholic liver disease (ALD) comprises a wide spectrum of liver disorders ranging from alcoholic steatosis to alcoholic steatohepatitis (ASH), alcoholic hepatitis, progressive fibrosis, cirrhosis, and hepatocellular carcinoma.[5, 7] Reports show that while a majority portion of heavy alcohol drinkers develop steatosis, only a minority of patients with steatosis progresses to ASH and subsequently cirrhosis and carcinoma [8, 9]. There is evidence suggesting that EtOH is not the only reason in progression of liver diseases but also the existence of a gut-liver-brain axis needs to be considered as another player. Consequently, many pathophysiological mechanisms that are affected by EtOH exposure and implicated in disease development remained unknown. Hence, analyzing proteome of alcoholic patients would be beneficial to explore protein biomarkers for early detection and treatment of alcohol-related diseases in liver and GI

tract [5]. It has been evident that the paracellular permeability in GI tract could be considered as a practical indicator to determine the severity of EtOH damage.

The artificial sweetener sucralose (a chlorinated derivative of sucrose) is considered as a useful GI tract permeability probe[10]. Resistance of sucralose to bacterial fermentation makes it as a suitable marker for whole GI tract permeability. The higher urinary excretion of sucralose indicates the higher gut leakiness.[11] The usefulness of sucralose permeation in determining gut leakiness has been investigated in alcoholic steatohepatitis.[12] The alcoholic subjects without liver disease can be categorized into low quartile and high quartile sucralose permeation groups. This categorization might be helpful to show the level of damage induced by EtOH in GI tract.

Various proteomics approaches have been used to determine the effect of EtOH at the cellular level. Mass spectrometry (MS) with LC-MS/MS has gained a great demand in proteomics and protein studies.[13-15] Among all MS approaches, the Sequential Windowed data independent Acquisition of the Total High-resolution Mass Spectra (SWATH-MS) offers superior advantages, like high accuracy and reproducibility over the other MS methods. SWATH-MS is a data-independent acquisition (DIA) method that acquires all MS/MS fragments by recording all theoretical fragment spectra produced from the precursor ions.

In this study, the proteome of sigmoid colon obtained from healthy human subjects was compared with that in ALD patients. Furthermore, alcoholic patients with no liver disease and different intestinal permeability were also examined.

Moreover, the proteome of GI tract of chronic-binge rat model was investigated and compared with that in control rats.

## 2. Experimental Section

### 2.1. Human intestinal Tissue

Human sigmoid colon samples were generously provided by Dr. A. Keshavarzian from Rush University Medical Center (RUMC, Chicago, IL). Briefly, mucosal biopsies from healthy control (HC), alcoholic liver disease (ALD), alcoholic without liver disease low quartile sucralose permeation (AWLDLQ), and alcoholic without liver disease high quartile sucralose permeation (AWLDHQ) volunteers were obtained. These samples were collected via endoscopy at the RUMC Endoscopy Lab obtained from six HC (three females, three males; 25−63 years old), six ALD (five female, one male; 48−63 years old), six AWLDLQ (three female, three male; 43−56 years old), and six AWLDHQ (two female, four males; 40−68 years old). The urinary concentration of excreted sucralose was used to categorize the groups of alcoholic patients without liver disease into low and high quartile sucralose.[11, 16] Samples were snap frozen in liquid nitrogen in the endoscopy room. Then, sigmoid biopsies were stored at -80°C until the time of tissue lysis for proteomics analysis. The details of procedure method and inclusion/exclusion criteria for selecting subjects were fully described in Ref.[17]

### 2.2. Rat experimental models

Four-week old male and female Long Evans rats were fed isocaloric liquid diets containing 0% or 26% ethanol for 8 weeks (n = 12 per group). During the last three weeks of the experiment, EtOH exposed rats were binged with 2 g/kg EtOH via oral gavage on Tuesdays, Thursdays, and Saturdays; controls were treated with saline. At the end of the experiment, rats were deeply anesthetized with isofluorane and exsanguinated by cardiac puncture. All experiments were performed following protocols approved by Institutional Animal Care and Use Committee at the Lifespan-Rhode Island Hospital, and conformed to guidelines established by the National Institutes of Health.

**2.3. Human and rat tissue lysis and digestion**

Rat and human tissue lysis and digestion method was carried out according to the procedure described by Shao *et al* [18]. Sample lysis and protein digestion were performed in the Barocycler® 2320 EXT (Pressure Biosciences; West Bridgewater, MA). Tissue samples were prepared with a PCT MicroPestle. Briefly, tissue pieces including rat stomach, ileum, proximal colon (pCol), and distal colon (dCol) as well as human sigmoids (1–5 mg) were placed in microTubes (Pressure BioSciences) with a PCT-MicroPestle (Pressure BioSciences) in 25 µL of lysis buffer. The lysis buffer for all samples contained 8 M urea in 100 mM ammonium bicarbonate. Samples were sonicated on ice in the microTubes three times for 10 s. After sonication, sample lysis and protein extraction were performed with a PCT-MicroPestle using 60 pressure cycles, each consisting of 50 s of 45,000 psi (high pressure) and 10 s of atmospheric pressure at 33 °C in the Barocycler. The supernatant was collected for BCA protein

assay (Section 2.5). Thereafter, proteins were ready for digestion step. For protein reduction and alkylation, TCEP (tris(2-carboxyethyl)phosphine) (10 mM) and iodoacetamide (40 mM) were added to the solution for 30 min of incubation in the dark at room temperature. After the replacement of the PCT-MicroPestle with a PCT-MicroCap (150 µL size), samples were diluted with 100mM ammonium bicarbonate to (75 µL) to reduce the urea concentration to 2 M prior to digestion with trypsin (10 µL, 1 mg/mL). Digestion was performed in the Barocycler at 33 °C using 45 cycles, each consisting of 50 s at 20 000 psi (high pressure) and 10 s at atmospheric pressure. Subsequently, second trypsin (10 µL, 1 mg/mL) digestion was carried out in the Barocycler with a PCT-MicroCap (size 150 µL) under the condition of 90 cycles, each consisting of 50 s at 20 000 psi (high pressure) and 10 s at atmospheric pressure at 33 °C. Thereafter, digestion was stopped by 12% formic acid (Optima™ LC-MS/MS grade, Fisher Scientific). The peptides were stored in −80 °C before SWATH-MS analysis. **Figure 1** shows a schematic illustration of the experimental procedure from tissue lysis and protein digestion to injection of samples to LC-MS/MS and data analysis.

### 2.4. Protein and peptide concentration measurement

Protein concentration was determined using Pierce™ Micro BCA protein assay kit (Thermo Fisher Scientific, Rockford, IL, USA) with a Molecular Device SpectraMax® M 5 plate reader (Molecular Devices, Sunnyvale, CA) by measuring UV-vis absorbance at wavelength of 562 nm. A protease-free bovine serum albumin (BSA) solution (2–40 µg/mL) was used as the standard calibration line for the BCA

protein quantification method. MS-ready peptides were dissolved in deionized water with 0.4% formic acid and measured with a NanoDrop 1000 spectrophotometer (Thermo Scientific) at 280 nm (1 Ab = 1 mg/mL).

### 2.5. Triple-TOF MS analysis in SWATH mode

The SWATH-MS proteomics analysis and data processing were accomplished based on the previously published method.[19, 20] Briefly, A SCIEX 5600 TripleTOF mass spectrometer equipped with a DuoSpray ion source (SCIEX, Concord, Canada) coupled to Acquity UHPLC HClass system (Waters Corp., Milford, MA, USA) was used. The mass spectrometer was operated in positive electrospray ionization (ESI) mode for all the experiments. Compound and source/gas parameters used in SWATH-MS method were as follows: DP = 120 V, CE = 10 V, collision energy spread (CES = 5V), TEM = 400 °C, ISVF = 5500 V, GS1 = 55 psi, and GS2 = 60 psi. TOF masses were collected from *m/z* 300 to 1500. SWATH data was acquired in the range of *m/z* 400 to 1100 over 70 SWATH windows per cycles with a window size of *m/z* 10. The total cycle time for SWATH acquisition was 3.95 sec.

The digested P-gp peptides were separated on an Acquity UHPLC Peptide BEH C18 (2.1 × 150 $mm^2$, 300 Å, 1.7 µm) equipped with Acquity VanGuard precolumn (2.1 × 5 $mm^2$ , 300 Å, 1.7 µm). Autosampler temperature was kept at 10 °C and the column temperature was maintained at 40 °C during all injections. The chromatographic separation was performed with a runtime of 120 min at 100 µL/min with a gradient method using mobile phase A (98% water, 2% acetonitrile, 0.1% formic acid) and mobile phase B (98% acetonitrile, 2% water, 0.1% formic acid). A

gradient chromatographic elusion method was performed as follows: 98% A from 0 to 3 min, 60% to 90% A from 3 to 48 min, 20% A held from 49 to 52 min to flush the column, 98% A at 53 min. The column was equilibrated at 98% A from 53 to 60 min before the start of next run. The amount of protein per injection on the column was 10 μg. In each batch, trypsin-digested β- galactosidase that is a quality control standard (1.65 pmol/injection) was injected to each sample to monitor mass calibration of the TOF detector and normalization of peptides intensity in SWATH label free quantification (LFQ) approach. The LFQ was performed using Skyline, which is an open source application for targeted proteomics quantitative data analysis.

### 2.6. Statistical Analysis

The normality of data sets in each experiment was checked with Shapiro-Wilk test. One-way analysis of variance (ANOVA) with Dunnett's T3 post hoc test (SPSS 23, SPSS, Inc.) was used for normally distributed observations. Kruskal-Wallis (KW) one-way ANOVA (non-parametric ANOVA) with Dunn's multiple comparison post hoc test was used in non-normally distributed data. In all analyses, probability values $<0.05$ was considered significant.

## 3. Results and discussion

### 3.1. EtOH affects the expression of ALDH2 in human sigmoid colon

The expression level of proteins in sigmoid samples of ALD, AWLDLQ, AWLDHQ, and HC subjects has been investigated by SWATH-MS proteomics. The fold changes in proteins expression are mentioned in **Table 1.** According to the results, the expression of the most proteins was not significantly altered in alcoholic

subjects versus HC. However, aldehyde dehydrogenase2 (ALDH2), filamin A, and glutathione S-transferase A1 (GSTA1) showed significant differences across groups.

ALDH2 detoxifies acetaldehyde (major EtOH metabolite) into acetate. The role of ALDH2 in metabolism of EtOH inside the cells has been illustrated in **Figure 2.**[21] Many studies on mice models have shown that ALDH2 overexpression in liver cells ameliorates the pathological damages induced by chronic EtOH intake.[22] Moreover, Chaudhry and co-workers have shown that ALDH2 deficiency enhances EtOH-induced disruption of paracellular barriers in alcohol-fed mice models.[23] In our proteomics results, expression of ALDH2 in ALD and AWLDHQ was insignificantly lower than that in HC group (**Table 1**). Progression of alcoholism to liver disease in ALD subjects as well as higher paracellular damage in AWLDHQ group might be induced due to the lower ALDH2 expression. In contrast, AWLDLQ subjects showed significantly higher expression of ALDH2 compared to the HC. More expression of ALDH2 in AWLDLQ patients might be the reason for retaining paracellular integrity in these subjects.

**Figure 3a** shows a Box-plot illustrating the relative abundance of ALDH2 across four groups of subjects. KW with Dunn's post hoc test showed that there is statistically significant difference in expression of ALDH2 across AWLDHQ versus AWLDLQ subjects (P-value = 0.005). Higher expression of ALDH2 in AWLDLQ subjects may explain why paracellular barrier in these subjects is more integrated than that in AWLDHQ.

### 3.2. EtOH affects the expression of GSTA1 in human sigmoid

**Figure 3b** shows a Box-plot illustrating the relative abundance of GSATA1 across four groups of subjects. KW with Dunn's post hoc test showed that there is statistically significant difference in expression of GSTA1 across ALD versus AWLDLQ subjects (P-value = 0.02). According to the **Table 1**, the GSTA1 expression in ALD subjects was insignificantly lower than that in HC (P = 0.23). It was previously indicated by Ma and co-workers that GSTA1 is downregulated in EtOH-induced in mice model.[24] In that study, the protective role of GSTA1 in scavenging the free radicals generated by EtOH was suggested to justify the GSTA1 release from liver. The lower expression of GSTA1 in sigmoid samples of ALD subjects was confirmed in our proteomics study. However, the expression level of GSTA1 in AWLDLQ was higher than that in HC (**Table 1**). Sigmoid colon in AWLDLQ subjects is possibly less affected by reactive oxygen species generated by EtOH consumption. Enhanced expression of GSTA1 in AWLDLQ may suggest the different role of this enzyme in EtOH-induced injury in GI tract compared to liver.

### 3.3. EtOH affects the expression of filamins in human sigmoid colon

**Figure 4** shows the role of filamin A in relation to other cytoskeletal components. The expression of filamin A is decreased in ALD, AWLDLQ, and AWLDHQ subjects compares to the HC (**Table 1**). However, the reduction of filamin A expression was statistically significant in AWLDLQ subjects (P-value = 0.05). Tobin and co-workers have hypothesized that clinically relevant EtOH concentration (20–40 mM) disrupts the mu-opioid receptor (MOP)-filamin A interaction [25]. Our results showed alteration in the expression level of filamin A in alcoholic subjects compared to the HC group.

According to our results, it could be suggested that diminished expression of filamin A in alcoholic patients is probably the reason for disrupting MOP-filamin A interaction.

No significant difference was observed in the expression of any investigated protein in ALD patients compared to the HC. The reason is the organ of analysis. While, the site of EtOH-induced damage in these subjects is liver, proteomics analysis of liver samples from ALD patients might be more relevant.

### 3.4. EtOH affects the expression of proteins in rat GI tract

The fold changes in proteins expression in stomach, ileum, pcolon, and d-Col of EtOH-treated versus control rat groups are mentioned in **Table 2**. Results showed the significant increase of vimentin in pCol region of alcoholic rat models (P-value = 0.05). Vimentin is an intermediate filament protein involved in cellular structure and integrity. Induction of vimentin was not statistically significant in dCol (**Table 2**). Results show expression of vimentin was not observed in stomach samples of control and binge rats. Moreover, the vimentin expression was slightly decreased in ileum but not statistically significant (P-value = 0.8).

Kelso *et al* have shown that vimentin is upregulated in binge rat models with neurodegeration.[26] They found that a prominent increase in vimentin expression happened 4 and 7 days after the last EtOH dose. Duly and co-workers has shown that binge alcohol rat models induced liver fibrogenesis by increasing the expression of vimentin.[27] in another study on alcohol-fed mice, Ambade *et al* have shown that chronic EtOH exposure leads to vimentin upregulation.[28] Although, these works had

been done in brain and liver tissues, our pCol proteomics result is in agreement with their findings.

## 4. Conclusion

SWATH-MS proteomics exhibits as a prominent technique in quantitative analysis of proteins from limited biopsy samples. In this work, the proteome of human sigmoid colon biopsies as well as alcoholic rat GI tracts were studied. Results show that the expression level of some proteins in sigmoidal colon samples of alcoholic patients was altered compared to the healthy subjects. Significant differences were observed in expression of proteins in AWLDLQ subjects compare to the HC. No significant difference was observed in the expression of any investigated protein in ALD patients. Moreover, the effect of chronic EtOH consumption on proteins of different parts of GI tracts was examined in rat models. Vimentin and desmin showed a significant induction in pCol of binge-chronic rat models compare to the control group. The power of SWATH-MS proteomics in analysis of clinical biopsies might be helpful in identification of biomarkers to cure different stages of alcoholism.

**Table IV- 1.** Ratio of proteins expression in sigmoid colon of ALD, AWLDLQ, and AWLDHQ versus HC of human subjects.

| | Abundance ratio | | | | | |
|---|---|---|---|---|---|---|
| **Protein name** | **ALD/HC** | **P-value** | **AWLDLQ/HC** | **P-value** | **ANLDHQ/HC** | **P-value** |
| Short-chain specific acyl-CoA dehydrogenase | 0.72 | 0.91 | 2.11 | 0.16 | 0.27 | 0.16 |
| Very long-chain specific acyl-CoA dehydrogenase | 0.81 | 1 | 5.62 | 0.07 | 0.74 | 0.74 |
| β-Actin | 0.83 | 0.83 | 1.22 | 0.52 | 1.03 | 0.63 |
| Beta-actin-like protein 2 | 0.82 | 1 | 0.97 | 0.91 | 1.60 | 0.26 |
| Actin-2 | 0.82 | 0.83 | 1.12 | 0.67 | 1.16 | 0.42 |
| Alcohol dehydrogenase 1B | 0.95 | 0.13 | 1.15 | 0.13 | 0.09 | 0.15 |
| Aldehyde dehydrogenase (mitochondrial) | 0.85 | 0.59 | 5.21 | 0.02* | 0.41 | 0.22 |
| Sodium/potassium-transporting ATPase subunit α-1 | 0.84 | 0.82 | 0.56 | 0.91 | 0.46 | 0.74 |
| Cadherin-17 | 0.98 | 0.91 | 1.85 | 0.58 | 1.29 | 0.49 |
| Catenin β-1 | 0.86 | 0.91 | 1.06 | 0.39 | 0.93 | 0.29 |
| Desmin | 0.98 | 0.83 | 0.30 | 0.13 | 0.88 | 0.52 |
| Desmoplakin | 0.73 | 0.66 | 0.90 | 0.18 | 0.72 | 0.22 |
| Fibronectin | 0.77 | 0.52 | 2.93 | 0.09 | 1.88 | 0.52 |
| Filamin-A | 0.84 | 1 | 0.20 | 0.05* | 0.81 | 0.75 |
| Glutathione S-transferase A1 | 0.41 | 0.23 | 5.70 | 0.03* | 0.84 | 0.63 |
| Lamin-B1 | 0.88 | 0.66 | 1.77 | 0.28 | 0.93 | 1 |
| Myosin-9 | 0.46 | 0.45 | 0.27 | 0.13 | 1.54 | 0.81 |
| Spectrin β-chain | 0.36 | 0.74 | 1.56 | 0.33 | 0.59 | 0.62 |
| Spectrin α-chain | 0.71 | 0.74 | 1.46 | 0.45 | 0.74 | 0.81 |
| Tubulin alpha-1A | 0.71 | 0.83 | 0.53 | 0.83 | 0.97 | 0.42 |
| Tubulin alpha-1B | 0.68 | 1 | 0.58 | 0.67 | 0.92 | 0.52 |
| Villin-1 | 0.75 | 0.66 | 0.15 | 0.13 | 1.55 | 0.09 |
| Vinculin | 1.04 | 1 | 0.65 | 0.67 | 0.78 | 0.87 |

**Abbreviation: HC:** Healthy Control, **AWLDLQ:** Alcoholic Without Liver Disease Low Quartile Sucralose, and **AWLDHQ:** Alcoholic Without Liver Disease High Quartile Sucralose.

Non-parametric Mann–Whitney U test was used to determine the significance of difference between ALD, AWLDLQ, and AWLDHQ groups versus healthy control (HC) group, respectively. *Statistically significant decrease was observed in expression of FLNA in AWLDLQ versus HC group. The expression of GSTA1, and ALDH2 were significantly higher in AWLDLQ subjects compared to the HC group.

**Table IV- 2.** Ratio of proteins expression in different gastrointestinal (GI) parts of EtOH- versus control- treated rats.

| | Abundance ratio | | | | | | | |
|---|---|---|---|---|---|---|---|---|
| **Protein name** | **E-Stom/C-Stom** | **P-value** | **E-Ile/C-Ile** | **P-value** | **E-dCol/C-dColon** | **P-value** | **E-pCol/C-pCol** | **P-value** |
| Sodium/potassium-transporting ATPase subunit alpha-1 | 0.95 | 0.56 | 0.52 | 0.82 | 0.33 | 0.25 | 0.38 | 0.27 |
| Cadherin-1 | 0.55 | 0.56 | 0.61 | 0.51 | 0.91 | 0.56 | 0.50 | 0.44 |
| Cadherin-17 | – | – | 0.59 | 1.00 | 0.35 | 0.56 | 0.37 | 0.24 |
| Aldehyde dehydrogenase, mitochondrial | 0.59 | 0.56 | 1.27 | 0.56 | 1.16 | 1.00 | 0.79 | 0.51 |
| 4-trimethylaminobutyraldehyde dehydrogenase | 0.81 | 0.56 | 0.91 | 0.82 | 0.91 | 1.00 | 0.54 | 0.27 |
| Junction plakoglobin | 0.50 | 0.56 | 1.11 | 0.51 | – | – | – | – |
| Filamin-C | 0.47 | 0.25 | 1.08 | 0.82 | – | – | 1.58 | 0.27 |
| Vimentin | – | – | 0.85 | 0.82 | 2.25 | 0.25 | 2.77 | 0.05***** |
| Actin, cytoplasmic 1 | 0.48 | 0.56 | 1.17 | 0.82 | 2.48 | 0.56 | 1.31 | 0.27 |
| Annexin A2 | 0.63 | 0.56 | 0.86 | 0.51 | 0.75 | 0.56 | 0.49 | 0.27 |
| Vinculin | 0.43 | 0.56 | 1.11 | 0.82 | 2.45 | 0.25 | 1.58 | 0.27 |
| Actin, cytoplasmic 2 | 0.49 | 0.56 | 0.80 | 0.82 | 2.41 | 0.56 | 1.38 | 0.27 |
| Tubulin alpha-1A chain | 0.49 | 0.56 | 0.72 | 0.82 | 0.91 | 1.00 | 0.70 | 0.51 |
| Tubulin alpha-1B chain | 0.49 | 0.56 | 0.72 | 0.82 | 0.89 | 0.56 | 0.69 | 0.51 |

**Abbreviations: E-stom:** stomach of EtOH-treated rats, **C-Stom**: stomach of control rats, **E-Ile:** ileum of EtOH-treated rats, **C-Ile:** ileum of control rats, **E-dCol:** distal colon of EtOH-treated rats, **C-dColon:** distal colon of control rats, **E-pCol:** proximal colon of EtOH-treated rats, **C-pColon:** proximal colon of control rats.

E-stom/C-Stom shows the fold change observed in the proteins abundance in stomach of EtOH-treated versus stomach of control rat group. Likewise, E-Ile/C-Ile, E-dCol/C-dCol, and E-pCol/C-pCol show the fold change observed in the protein abundance of Ile, dCol, and pCol from EtOH-treated versus control rat groups. Non-parametric Mann–Whitney U test was used to determine the significance of difference between EtOH-treated groups versus control group in each part of GI tract.

*****Statistically significant difference was observed in expression of Vim in alcohol-treated rats versus control groups.

**Figure IV-1**

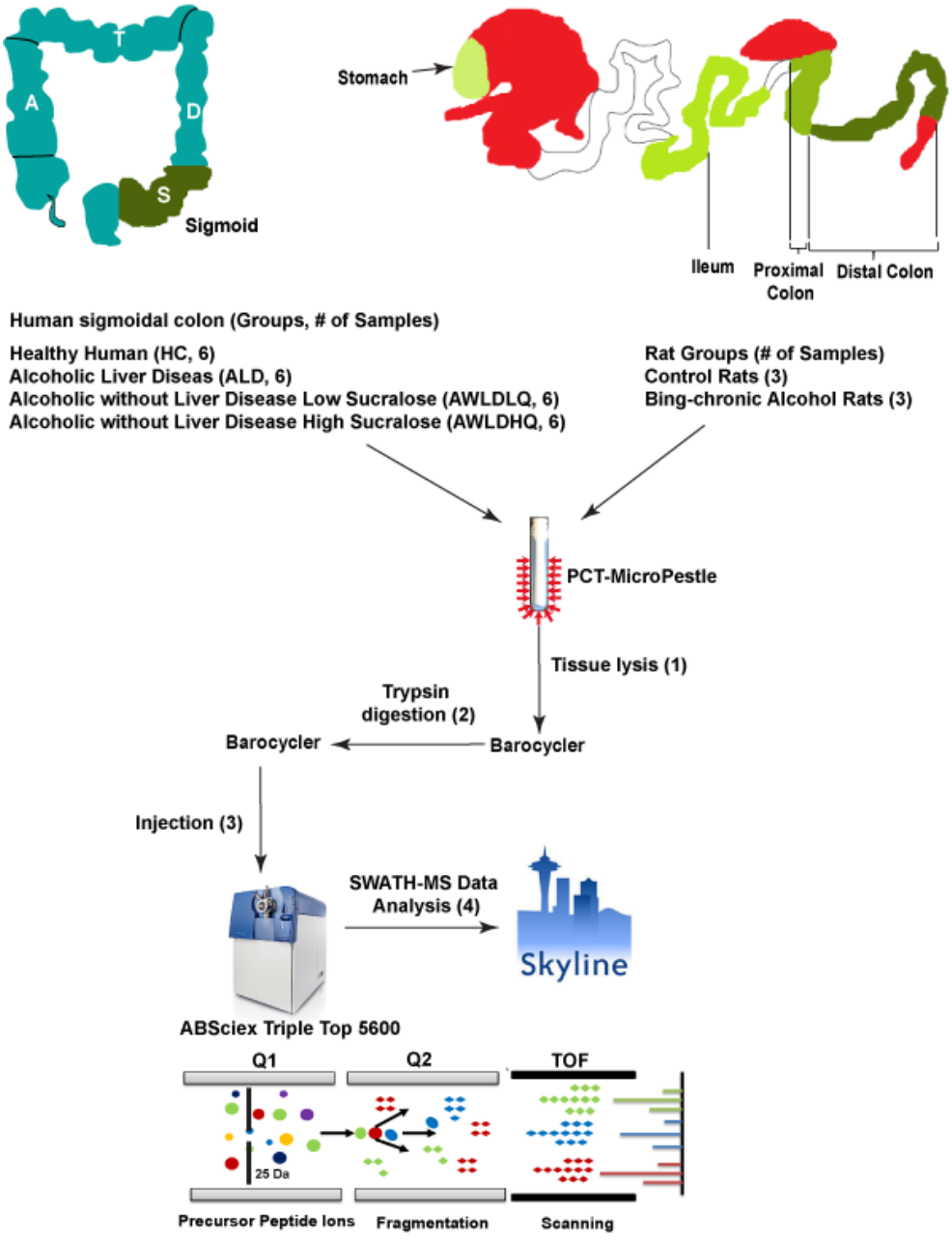


**Figure IV- 1.** Schematic illustration of the experimental procedure to study rat and human gastrointestinal (GI) tract samples by SWATH-MS approach.
Overview of the experimental procedure to study variable protein levels via SWATH-MS proteomics over four different rat gastrointestinal segments (stomach, ileum, proximal, and distal colon) as well as human sigmoid colon. Abbreviation: A: ascending colon, T: transverse colon, D: descending colon, SWATH-MS: Sequential Windowed data independent Acquisition of the Total High-resolution Mass Spectra, PCT-MicroPestle: Pressure-cycling technology- MicroPestle.

**Figure IV-2**

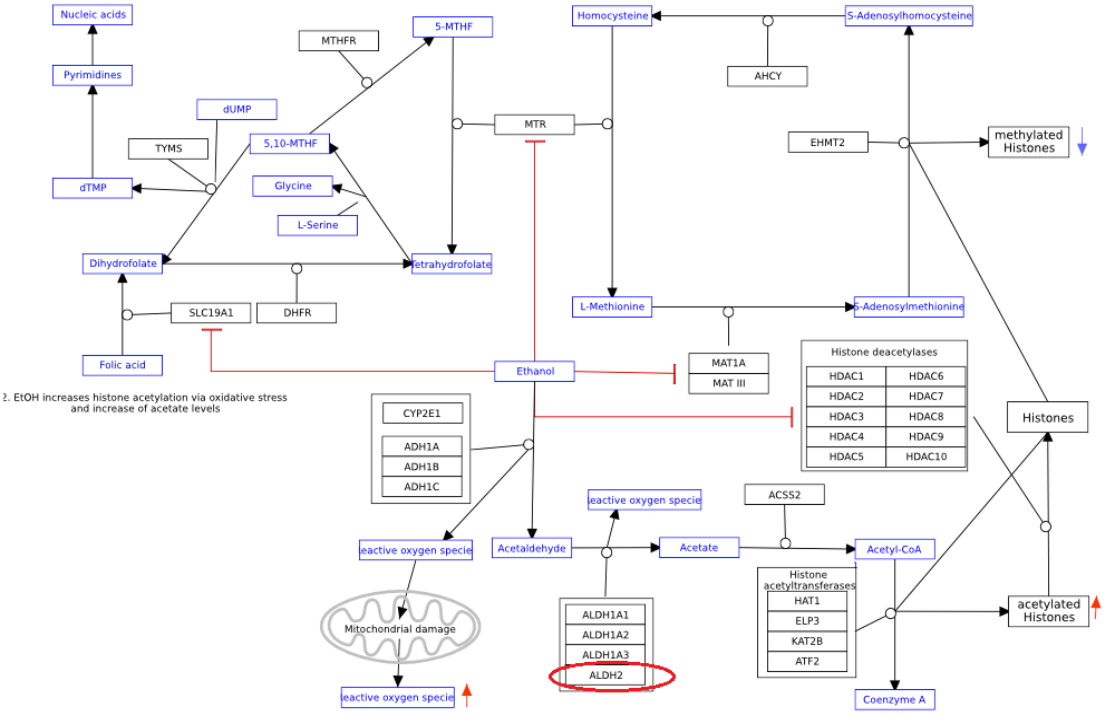


**Figure IV- 2** Schematic illustration of ALDH2 in EtOH effects on different molecular pathways.
The enzyme ALDH2 has been mentioned by a red line. The pathway is obtained from Wikipathways (https://www.wikipathways.org).

**Figure IV- 3**

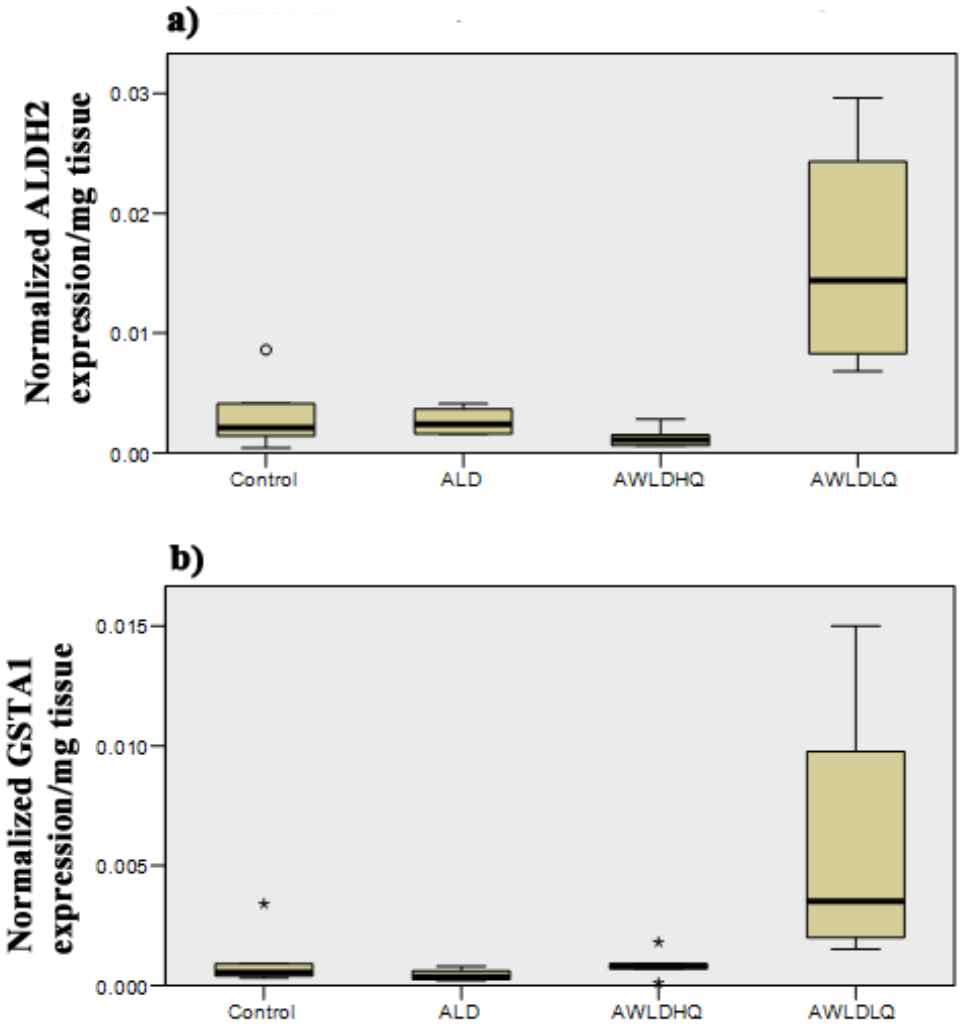


**Figure IV- 3a)** Box-plot of normalized aldehyde dehydrogenase2 (ALDH2) and **b)** glutathione S-transferase A1 (GSTA1).
Protein abundance across control (HC), alcoholic with liver disease (ALD), alcoholic without liver disease low quartile sucralose permeation (AWLDLQ), and alcoholic without liver disease high quartile sucralose permeation (AWLDHQ) groups was illustrated. Kruskal-Wallis H-test with post hoc Dunn's was conducted to find out the significance level among groups. The P-value of difference between AWLDLQ and AWLDHQ subjects was 0.005. Furthermore, the P-value between AWLDLQ and ALD was 0.02 for GSTA1.

**Figure IV-4**

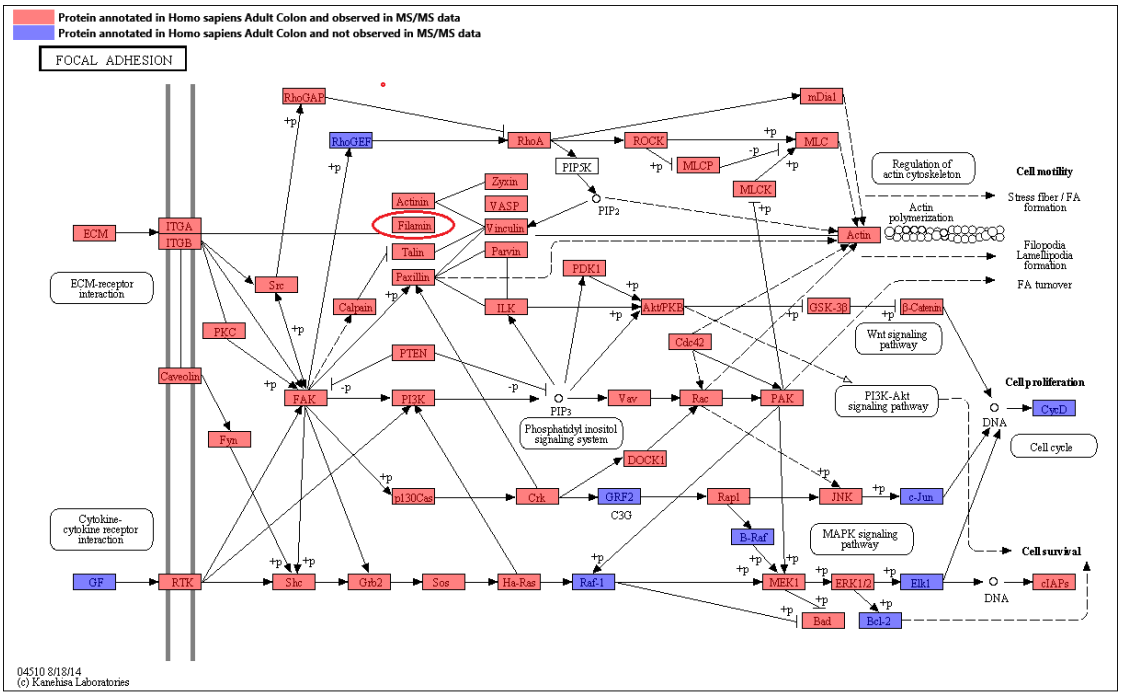


**Figure IV- 4.** Graphical representation of the Kyoto Encyclopedia of Genes and Genomes (KEGG) for adherens junction pathway.
The role of filamin proteins in relation to other proteins has been illustrated. Filamin A protein is shown by a red line.

**References**


1. Forouzanfar, M. H.; Afshin, A.; Alexander, L. T.; Anderson, H. R.; Bhutta, Z. A.; Biryukov, S.; Brauer, M.; Burnett, R.; Cercy, K.; Charlson, F. J. Global, regional, and national comparative risk assessment of 79 behavioural, environmental and occupational, and metabolic risks or clusters of risks, 1990–2015: a systematic analysis for the Global Burden of Disease Study 2015. *The Lancet* **2016,** *388*, (10053), 1659-1724.
2. Thursz, M.; Gual, A.; Lackner, C.; Mathurin, P.; Moreno, C.; Spahr, L.; Sterneck, M.; Cortez-Pinto, H. EASL Clinical Practice Guidelines: Management of alcohol-related liver disease. *Journal of hepatology* **2018,** *69*, (1), 154-181.
3. Organization, W. H.; Unit, W. H. O. M. o. S. A., *Global status report on alcohol and health, 2014*. World Health Organization: 2014.
4. Gunzerath, L.; Faden, V.; Zakhari, S.; Warren, K. National Institute on Alcohol Abuse and Alcoholism report on moderate drinking. *Alcoholism: Clinical and Experimental Research* **2004,** *28*, (6), 829-847.
5. Stärkel, P.; Leclercq, S.; de Timary, P.; Schnabl, B. Intestinal dysbiosis and permeability: the yin and yang in alcohol dependence and alcoholic liver disease. *Clinical Science* **2018,** *132*, (2), 199-212.
6. Farhadi, A.; Banan, A.; Fields, J.; Keshavarzian, A. Intestinal barrier: an interface between health and disease. *Journal of gastroenterology and hepatology* **2003,** *18*, (5), 479-497.
7. Singal, A. K.; Bataller, R.; Ahn, J.; Kamath, P. S.; Shah, V. H. ACG Clinical Guideline: alcoholic liver disease. *The American journal of gastroenterology* **2018,** *113*, (2), 175.
8. Lefkowitch, J. H. Morphology of Alcoholic Liver Disease. *Clinics in Liver Disease* **2005,** *9*, (1), 37-53.
9. Teli, M. R.; Day, C. P.; James, O. F. W.; Burt, A. D.; Bennett, M. K. Determinants of progression to cirrhosis or fibrosis in pure alcoholic fatty liver. *The Lancet* **1995,** *346*, (8981), 987-990.
10. Meddings, J. B.; Gibbons, I. Discrimination of site-specific alterations in gastrointestinal permeability in the rat. *Gastroenterology* **1998,** *114*, (1), 83-92.
11. Forsyth, C. B.; Shannon, K. M.; Kordower, J. H.; Voigt, R. M.; Shaikh, M.; Jaglin, J. A.; Estes, J. D.; Dodiya, H. B.; Keshavarzian, A. Increased intestinal permeability correlates with sigmoid mucosa alpha-synuclein staining and endotoxin exposure markers in early Parkinson's disease. *PloS one* **2011,** *6*, (12), e28032.
12. Keshavarzian, A.; Farhadi, A.; Forsyth, C. B.; Rangan, J.; Jakate, S.; Shaikh, M.; Banan, A.; Fields, J. Z. Evidence that chronic alcohol exposure promotes intestinal oxidative stress, intestinal hyperpermeability and endotoxemia prior to development of alcoholic steatohepatitis in rats. *Journal of hepatology* **2009,** *50*, (3), 538-547.
13. Ong, S.-E.; Mann, M. Mass spectrometry–based proteomics turns quantitative. *Nature chemical biology* **2005,** *1*, (5), 252.
14. Bantscheff, M.; Schirle, M.; Sweetman, G.; Rick, J.; Kuster, B. Quantitative mass spectrometry in proteomics: a critical review. *Analytical and bioanalytical chemistry* **2007,** *389*, (4), 1017-1031.

15. Han, X.; Aslanian, A.; Yates, J. R. Mass Spectrometry for Proteomics. *Current opinion in chemical biology* **2008,** *12*, (5), 483-490.
16. Shaikh, M.; Rajan, K.; Forsyth, C. B.; Voigt, R. M.; Keshavarzian, A. Simultaneous gas-chromatographic urinary measurement of sugar probes to assess intestinal permeability: Use of time course analysis to optimize its use to assess regional gut permeability. *Clinica Chimica Acta* **2015,** *442*, 24-32.
17. Miller, G. E.; Engen, P. A.; Gillevet, P. M.; Shaikh, M.; Sikaroodi, M.; Forsyth, C. B.; Mutlu, E.; Keshavarzian, A. Lower Neighborhood Socioeconomic Status Associated with Reduced Diversity of the Colonic Microbiota in Healthy Adults. *PLOS ONE* **2016,** *11*, (2), e0148952.
18. Shao, S.; Guo, T.; Gross, V.; Lazarev, A.; Koh, C. C.; Gillessen, S.; Joerger, M.; Jochum, W.; Aebersold, R. Reproducible tissue homogenization and protein extraction for quantitative proteomics using micropestle-assisted pressure-cycling technology. *Journal of proteome research* **2016,** *15*, (6), 1821-1829.
19. Jamwal, R.; de la Monte, S. M.; Ogasawara, K.; Adusumalli, S.; Barlock, B. B.; Akhlaghi, F. Nonalcoholic fatty liver disease and diabetes is associated with decreased CYP3A4 protein expression and activity in human liver. *Molecular pharmaceutics* **2018**.
20. Jamwal, R.; Barlock, B. J.; Adusumalli, S.; Ogasawara, K.; Simons, B. L.; Akhlaghi, F. Multiplex and Label-Free Relative Quantification Approach for Studying Protein Abundance of Drug Metabolizing Enzymes in Human Liver Microsomes Using SWATH-MS. *Journal of proteome research* **2017,** *16*, (11), 4134-4143.
21. Slenter, D. N.; Kutmon, M.; Hanspers, K.; Riutta, A.; Windsor, J.; Nunes, N.; Mélius, J.; Cirillo, E.; Coort, S. L.; Digles, D. WikiPathways: a multifaceted pathway database bridging metabolomics to other omics research. *Nucleic acids research* **2017,** *46*, (D1), D661-D667.
22. Guo, R.; Xu, X.; Babcock, S. A.; Zhang, Y.; Ren, J. Aldehyde dedydrogenase-2 plays a beneficial role in ameliorating chronic alcohol-induced hepatic steatosis and inflammation through regulation of autophagy. *Journal of hepatology* **2015,** *62*, (3), 647-656.
23. Chaudhry, K. K.; Samak, G.; Shukla, P. K.; Mir, H.; Gangwar, R.; Manda, B.; Isse, T.; Kawamoto, T.; Salaspuro, M.; Kaihovaara, P.; Dietrich, P.; Dragatsis, I.; Nagy, L. E.; Rao, R. K. ALDH2 Deficiency Promotes Ethanol-Induced Gut Barrier Dysfunction and Fatty Liver in Mice. *Alcoholism, clinical and experimental research* **2015,** *39*, (8), 1465-1475.
24. Ma, X.; Liu, F.; Li, M.; Li, Z.; Lin, Y.; Li, R.; Li, C.; Chang, Y.; Zhao, C.; Han, Q.; Zhou, Q.; Zhao, Y.; Wang, D.; Liu, J. Expression of glutathione S-transferase A1, a phase II drug-metabolizing enzyme in acute hepatic injury on mice. *Experimental and therapeutic medicine* **2017,** *14*, (4), 3798-3804.
25. Tobin, S. J.; Cacao, E. E.; Hong, D. W. W.; Terenius, L.; Vukojevic, V.; Jovanovic-Talisman, T. Nanoscale Effects of Ethanol and Naltrexone on Protein Organization in the Plasma Membrane Studied by Photoactivated Localization Microscopy (PALM). *PLOS ONE* **2014,** *9*, (2), e87225.

26. Kelso, M. L.; Liput, D. J.; Eaves, D. W.; Nixon, K. Upregulated vimentin suggests new areas of neurodegeneration in a model of an alcohol use disorder. *Neuroscience* **2011,** *197*, 381-93.
27. Duly, A. M. P.; Alani, B.; Huang, E. Y. W.; Yee, C.; Haber, P. S.; McLennan, S. V.; Seth, D. Effect of multiple binge alcohol on diet-induced liver injury in a mouse model of obesity. *Nutrition &Amp; Diabetes* **2015,** *5*, e154.
28. Ambade, A.; Satishchandran, A.; Szabo, G. Alcoholic hepatitis accelerates early hepatobiliary cancer by increasing stemness and miR-122-mediated HIF-1α activation. *Scientific Reports* **2016,** *6*, 21340.